

University of Massachusetts Medical School
eScholarship@UMMS

GSBS Dissertations and Theses

Graduate School of Biomedical Sciences

2013-03-29

Role of Autophagy in Post-Mitotic Midbody Fate and Function: A Dissertation

Tse-Chun Kuo
University of Massachusetts Medical School

Let us know how access to this document benefits you.

Follow this and additional works at: https://escholarship.umassmed.edu/gsbs_diss

 Part of the [Cell Biology Commons](#), and the [Cellular and Molecular Physiology Commons](#)

Repository Citation

Kuo T. (2013). Role of Autophagy in Post-Mitotic Midbody Fate and Function: A Dissertation. GSBS Dissertations and Theses. <https://doi.org/10.13028/M2MC75>. Retrieved from https://escholarship.umassmed.edu/gsbs_diss/670

This material is brought to you by eScholarship@UMMS. It has been accepted for inclusion in GSBS Dissertations and Theses by an authorized administrator of eScholarship@UMMS. For more information, please contact Lisa.Palmer@umassmed.edu.

**ROLE OF AUTOPHAGY IN POST-MITOTIC MIDBODY FATE
AND FUNCTION**

A Dissertation Presented

By

TSE-CHUN KUO

Submitted to the Faculty of the
University of Massachusetts Graduate School of Biomedical Sciences,
Worcester
in partial fulfillment of the requirements for the degree of

DOCTOR OF PHILOSOPHY

MARCH 29, 2013

INTERDISCIPLINARY GRADUATE PROGRAM

**ROLE OF AUTOPHAGY IN POST-MITOTIC MIDBODY FATE AND
FUNCTION**

A Dissertation Presented By

Tse-Chun Kuo

The signatures of the Dissertation Committee signify completion and approval
as to style and content of the Dissertation

Stephen Doxsey, Ph.D., Thesis Advisor

Eric Baehrecke, Ph.D., Member of Committee

Kirsten Hagstrom, Ph.D., Member of Committee

Rytis Prekeris, Ph.D., Member of Committee

William Theurkauf, Ph.D., Member of Committee

The signature of the Chair of the Committee signifies that the written
dissertation meets the requirements of the Dissertation Committee

Dannel McCollum, Ph.D., Chair of Committee

The signature of the Dean of the Graduate School of Biomedical Sciences
signifies that the student has met all graduation requirements of the school.

Anthony Carruthers, Ph.D.,
Dean of the Graduate School of Biomedical Sciences

Interdisciplinary Graduate Program

March 29, 2013

Copyright Information

Chapter II has appeared in a separate publication.

Kuo, T.-C., Chen, C.-T., Baron, D., Onder, T. T., Loewer, S., Almeida, S., Weismann, C. M., Xu, P., Houghton, J.-M., Gao, F.-B., Daley, G. Q., Doxsey, S. (2011). Midbody accumulation through evasion of autophagy contributes to cellular reprogramming and tumorigenicity. *Nature cell biology*, 13(10), 1214–1223. doi:10.1038/ncb2332

Acknowledgements

I would like to express my very great appreciation to my thesis advisor Dr. Steve Doxsey. His enlightenment, guidance, support, and caring have made this a wonderful journey. This study was once partially scooped. However, his guidance and support have eventually made this project come to fruition.

I would also like to thank my committee members, Dr. Dan McCollum, Dr. Eric Baehrecke, Dr. William Theurkauf, and Dr. Kirsten Hagstrom for their suggestions and encouragement over past years as the study grows from an idea to a completed story. In particular, I am indebted to Dr. Eric Baehrecke for his constant caring feedback, support, and important career advices. Also thanks to Dr. Rytis Prekeris for participating as an outside reader in my thesis defense and his thoughts and fun discussions.

My grateful thanks are also extended to all the members of the Doxsey lab, both past and present, for their contributions to this thesis research, especially to Dr. Chun-Ting Chen for his discovery of post-mitotic midbody accumulation and to Dr. Desiree Baron for her help in several autophagy assays. I would also like to thank our collaborators Dr. Tamer Onder, Dr. Sabine Loewer, Dr. Thorsten Schlaeger, Dr. George Daley, Dr. Sandra Almeida, Dr. Fen-Biao Gao, Dr. Janel McLean, Dr. Jun-Song Chen, and Dr. Kathy Gould for generously sharing their time and insights that enable this study. In addition, special thanks to Dr. Heidi Hehnly-Chang and Alison Bright for spending countless hours helping me improve my talks and writing.

Finally, I'd like to thank my family and friends for their moral support and encouragement during these years, especially to my wonderful husband, Chih-Fei Kao, for his endless patience, consideration, and love.

Abstract

The midbody (MB) is a proteinaceous complex formed between the two daughter cells during cell division and is required for the final cell separation event in late cytokinesis. After cell division, the post-mitotic midbody, or midbody derivative (MB^d), can be retained and accumulated in a subpopulation of cancer cells and stem cells, but not in normal diploid differentiated cells. However, the mechanisms by which MB^ds accumulate and function are unclear. Based on this, I hypothesize that the MB^d is degraded by autophagy after cell division in normal diploid differentiated cells, whereas non-differentiated cells have low autophagic activity and would accumulate MB^ds. Indeed, I found this to be the case. MB^d degradation occurred soon after cytokinesis in differentiated cells that possess high autophagic activity. Specifically, I found MB^d degradation to be mediated by binding of the autophagy receptor, NBR1, to the MB protein Cep55. Moreover, by performing proteomic analysis of NBR1 interactions I found additional MB-localized proteins that are potential substrates for NBR1. In contrast to differentiated cells, stem and cancer cells have low autophagic activity thus MB^ds evade autophagosome encapsulation and accumulate. To examine whether MB^ds can define the differentiation status of a cell, we depleted NBR1 from differentiated fibroblasts causing an increase in MB^d number. Strikingly, under these conditions, reprogramming of fibroblasts to pluripotent stem cells is increased. Equally interestingly, cancer cells with increased MB^ds have increased *in vitro* tumorigenicity. In conclusion, this study gives an insight into the fates of post-mitotic midbodies and also suggests a

non-cytokinetic role of midbodies in enhancing pluripotency in stem cells and cancer stem cells.

Table of Contents

Title page	i
Approval pages	ii
Copyright	iii
Acknowledgements	iv
Abstract	v
Table of Contents	vii
List of Figures	viii
List of Tables	x
Chapter I: General Introduction	1
Chapter II: Midbody accumulation through evasion of autophagy contributes to cellular reprogramming and tumorigenicity.	11
Chapter III: Identification of cell cycle phase-specific interactors and phosphorylation sites of autophagy receptor protein NBR1.	48
Chapter IV: General Discussion	66
Appendix A: Supplemental Figures	76
Appendix B: Materials and Methods	88
Appendix C: References	98

List of Figures

- 1-1** Regulation of autophagy.
- 2-1** MB^ds accumulate within cells.
- 2-2** MB^ds are preferentially inherited by the cell with the older centrosome.
- 2-3** MB^ds accumulate in stem cells *in vivo* and *in vitro*.
- 2-4** MB^d-accumulation is high in stem cells and subpopulations of cancer cells and does not correlate with cell doubling time.
- 2-5** MB^ds in stem and cancer cells evade membrane encapsulation and lysosomal degradation.
- 2-6** Autophagy controls intracellular MB^d levels.
- 2-7** NBR1 is a receptor for targeting MB^ds to the autophagy pathway.
- 2-8** MB^d enrichment increases reprogramming efficiency and enhances *in vitro* tumorigenicity.
- 2-S1** Different-aged centrosomes in dividing cells show differential labeling for the components and modification of centrosomes.
- 2-S2** Multiple planes of confocal images demonstrate that the MB^d in the ventricle-facing daughter of the dividing neural progenitor is intracellular.
- 2-S3** Organelles respond to digitonin treatment as expected.
- 2-S4** Effects of lysosomal inhibition.
- 2-S5** NBR1 depletion impedes autophagosome capturing of MB^d.
- 2-S6** p62 depletion does not affect MB^ds in U2OS cells.
- 2-S7** An unidentified lysosomal degradation pathway compensates for autophagy deficiency.
- 2-S8** The proteasome does not play a role in MB^d degradation.
- 2-S9** Full scan data of immunoblots in Fig. 2-7d.

- 3-1** Exogenously expressed NBR1, but not p62, promotes MB^d degradation.

- 3-2** Alfy overexpression does not promote MB^d degradation.
- 3-3** Plk1 and Myh9 are localized to both mitotic MB and the MB^d.
- 3-4** NBR1 is hyperphosphorylated in mitosis.
- 3-5** Schematic figure of NBR1 showing its domain structures and phosphorylation sites mapped in mitotic cells and asynchronous cells.
- 3-6** Overlap of interacting proteins found between NBR1 and p62 by LC-MS/MS.

List of Tables

- Table 2-S1** Reprogramming is more efficient following an increase in MB^d levels by NBR1 depletion.
- Table 2-S2** MB proteins contain CMA-targeting motif.
- Table 3-1** Identification of cell cycle phase-specific interactors by LC-MS/MS in NBR1-MAP isolates.
- Table 3-2** NBR1 interacting partners detected in mitotic MB proteome.

Chapter I

General Introduction

Cytokinesis, an essential step at the termination of cell division, requires the midbody, a proteinaceous organelle-like structure. The midbody contains proteins indispensable for cytokinesis completion, chromosome segregation, and vesicle trafficking (Skop et al., 2004). Some of the midbody proteins have been implicated in stem cell maintenance and cancer progression (Strebhardt and Ullrich, 2006; Chen et al., 2007; O'Brien et al., 2010); however, whether the midbody itself regulates these processes is unknown. Here, I focused on understanding the role of autophagy in regulating post-mitotic midbody fate thus revealing its non-mitotic functions. Our results demonstrated a role of selective autophagy in the removal of the post-mitotic midbody (or midbody derivative, MB^d), and also suggested potential functions of these organelles in stem and cancer cells.

Midbody formation and its function in cytokinesis

The midbody was first described by Walther Flemming more than a century ago as a chromophilic structure between two dividing daughter cells (a.k.a. Flemming body). Since then, with the aid of microscopy, studies have provided more details into midbody

structure and dynamics. The midbody is derived from the midzone, an area assembled during anaphase in the center of the spindle where the spindle microtubules from opposite poles overlap. Assembly of the midzone involves primarily the centralspindlin complex composed of MKLP1, a kinesin-like protein, and MgcRacGAP, a Rho GTPase activating protein (Mishima et al., 2002; Pavicic-Kaltenbrunner et al., 2007). As cytokinesis initiates, centralspindlin promotes the activation of RhoA, leading to cleavage furrow formation and ingression at the cell equator (reviewed in Fededa & Gerlich, 2012; Green et al., 2012). This constriction proceeds until the spindle midzone is compacted into a single large microtubule bundle with an electron-dense structure in the center. Together, the microtubule bundle and the electron-dense structure form the midbody.

Studies over the years have revealed a function for the midbody in localizing factors and coordinating events required for faithful abscission, a membrane remodeling and fusion event that separates the daughter cells. Abscission requires selective transport of endocytic and secretory vesicles as well as the association of the ESCRT complex to the midbody. Depletion of proteins essential for tethering these vesicles at the midbody, such as centriolin and Cep55 for secretory vesicles, or FIP protein family and ARF6 for Rab11-containing endosomes, causes abscission failure (Gromley et al., 2005; Wilson et al., 2005; Fielding et al., 2005; Zhao et al., 2006). ESCRT complex recruitment to the midbody also requires Cep55 (Morita et al., 2007; Carlton et al., 2007; Lee et al., 2008). While the aforementioned findings suggest that the midbody directs the location of the cleavage site within the intercellular bridge, there is also compelling evidence that the midbody must interact with the cleavage furrow through centralspindlin to ensure

completion of cytokinesis (Lekomtsev et al., 2012). Because of these diverse functions, the midbody lies at the heart of the cytokinetic mechanism.

Fates of post-mitotic midbodies

Previous work showed that after cell division, midbodies (MBs) appeared to be jettisoned from cells (Mullins et al., 1977; Dubreuil et al., 2007) or retained within cancer cells (Gromley et al., 2005; Goss et al., 2008; Pohl and Jentsch, 2009). Due to these observations and that MB^d fates were not systematically tested in cells of different origins, colleagues in Doxsey laboratory and I examined (in chapter II) over fifteen cultured cell lines and several human and mouse stem cell niches (mouse neocortex, seminiferous tubules, human hair follicles) and found that MB^d fates are distinct in different cell types (Fig. 2-3 and 2-4a). In stem cells, induced pluripotent stem cells (iPSCs) and cancer cells, MB^ds were retained and accumulated. By contrast, normal proliferating non-cancer, non-stem cells did not accumulate MB^ds. Most interesting, MB^ds were higher in cancer stem cells and cancer cells with higher tumorigenic potential. When MB^d-rich human embryonic stem cells were induced to differentiate, MB^ds were significantly decreased. When differentiated cells were induced to become pluripotent, MB^ds were significantly increased. These findings thus suggested a relationship between the accumulation of MB^ds and the pluripotency and tumorigenic potential of cells. MB^ds can be degraded by autophagy (Pohl and Jentsch, 2009); however, how autophagy interfaces with MB^d degradation upon different cell physiological states has not been illuminated.

Autophagy function and regulation

Autophagy is an evolutionarily conserved degradative mechanism that involves the formation of autophagic vacuoles (autophagosome) around cargoes to ensure their delivery to lysosomes for degradation. In virtually all cells autophagy is constitutively active at a low basal level in the absence of stress to degrade and recycle unwanted cellular components contributing to cellular homeostasis. Upon stress conditions, autophagy can be activated to serve as a survival response. Known stimuli that induce autophagy include: nutrient starvation, endoplasmic reticulum stress, and pathogen invasion. Autophagy also contributes to cell makeover or tissue remodeling, as in oocyte fertilization (Tsukamoto et al., 2008; Sato & Sato 2011) or during *Drosophila* morphogenesis (Berry et al., 2007). Because of its wide spectrum of targets, autophagy participates in many physiological processes, including embryogenesis, innate and adaptive immunity, cancer progression, neurodegeneration, and aging (reviewed in Cecconi and Levine, 2008; Levine and Kroemer, 2008).

Recent studies have revealed the molecular mechanisms of autophagy in yeast and other eukaryotes, and most of these mechanisms are conserved (reviewed in Yang and Klionsky, 2010; Mizushima et al., 2011; Fig. 1-1). In mammals, the formation of the autophagosome requires membrane targeting of Atg8 homologues (LC3, gate16,

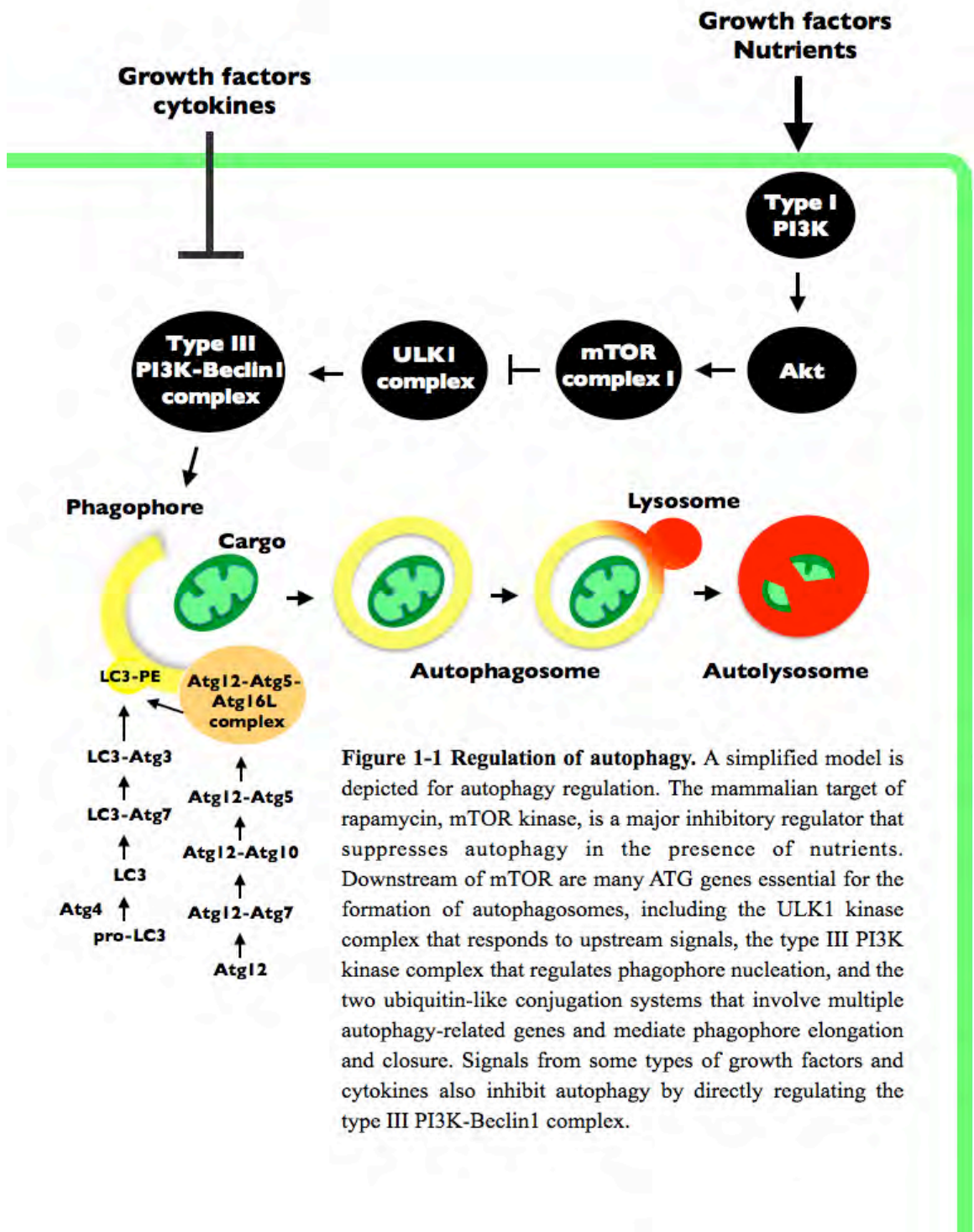


Figure 1-1 Regulation of autophagy. A simplified model is depicted for autophagy regulation. The mammalian target of rapamycin, mTOR kinase, is a major inhibitory regulator that suppresses autophagy in the presence of nutrients. Downstream of mTOR are many ATG genes essential for the formation of autophagosomes, including the ULK1 kinase complex that responds to upstream signals, the type III PI3K kinase complex that regulates phagophore nucleation, and the two ubiquitin-like conjugation systems that involve multiple autophagy-related genes and mediate phagophore elongation and closure. Signals from some types of growth factors and cytokines also inhibit autophagy by directly regulating the type III PI3K-Beclin1 complex.

gabarap), which is mediated by two ubiquitin-like conjugations involving Atg3, Atg4, Atg5, Atg7, Atg10, Atg12, and Atg16. Upstream, signaling complexes PI3K III and ULK1 positively regulate autophagy. Type III PI3K complex contains the Vps34 lipid kinase, p150, Beclin 1, and ATG14, and is essential for the nucleation of pre-autophagosomal membrane. The ULK1 complex, which comprises the kinase ULK1, Atg13, FIP200/RB1CC1, and Atg101, is repressed by mTOR kinase under nutrient-rich conditions but becomes activated to direct translocation of the PI3K III complex to the nucleation site (Itakura, 2010; Matsunaga et al., 2010). Other signaling pathways that control autophagy also exist, some of them inhibit autophagy through PI3K III complex and their inhibition activates autophagy under normal nutrient-rich conditions (Lipinski et al., 2010).

Selective autophagy and its players

Autophagy was first described as a non-selective, bulk cytoplasmic degradation system. However, recent studies have demonstrated autophagy to be a highly organized specific degradation system given that the degradation of autophagic cargo happens selectively under nutrient-deficient conditions (Kristensen et al., 2008; Kraft et al., 2008; Gao et al., 2010). For instance, a mass spectrometry-based quantitative proteomics indicates that autophagic cargoes are degraded in an orderly manner- the degradation of cytosolic proteins occurs more rapidly than the protein complexes and organelles (Kristensen et al., 2008). Also, mature ribosomes are selectively modified by the

Ubp3p/Bre5p ubiquitin protease and removed by autophagy upon nutrient starvation in *Saccharomyces cerevisiae* (Kraft et al., 2008). Moreover, autophagy receptors that confer cargo specificity have been identified.

Selective autophagy receptors identified in mammals to date include p62/SQSTM1, NBR1, NDP52, optineurin, and c-CBL (Bjorkoy et al., 2005; Pankiv et al., 2007; Kirkin et al., 2009a; Thurston et al., 2009; Sandilands et al., 2011; Wild et al., 2011). Owing to their ubiquitin-binding domain and LC3-interacting motif, autophagy cargo receptors are able to bring selected ubiquitin-positive substrates into close vicinity of the autophagy machinery. Among these receptors, p62 is the most studied and is known to be involved in various selective forms of autophagy, including the degradation of mitochondria, peroxisome, misfolded protein aggregates, and invading pathogens (Kirkin et al., 2009b). p62 often acts in concert with other receptors. For instance, both p62 and NBR1 localize to ubiquitinated protein aggregates and depletion of either protein affects aggregate clearance (Kirkin et al., 2009a). Similarly, p62, NDP52, and optineurin are independently recruited to ubiquitinated *Salmonella typhimurium* and all three receptors are required for restricting the intracellular growth of the bacteria (Thurston et al., 2009; Zheng et al., 2009; Cemma et al., 2011; Wild et al., 2011). However, it is not clear why multiple receptors are required and how the receptors are chosen/involved in a given form of selective autophagy.

In addition to autophagy receptors, several adaptor proteins have been implicated in selective autophagy (Gamerding et al., 2009; Filimonenko et al., 2010; Ogawa et al.,

2011). These proteins, although not directly associated with the ubiquitin or Atg8/LC3-homologues, are able to bind other autophagy-related proteins and may thus bridge substrates to autophagosomes. One example is Alfy, the autophagy-linked FYVE protein that binds to both p62 and Atg5 and participates in the clearance of mutant Huntingtin, an aggregation-prone protein implicated in neurodegeneration (Filimonenko et al., 2010). It was found that the sub-cellular distribution of Alfy to ubiquitinated aggregates relies on its binding to p62 (Clausen et al., 2010), whereas Alfy's ability to accelerate aggregate removal depends on its Atg5 interaction (Filimonenko et al., 2010). It is proposed that Alfy functions as a scaffold to bring the Atg5-Atg12-Atg16L complex and LC3 together to ubiquitinated substrates, hence promoting aggregate degradation (Filimonenko et al., 2010). For other adaptor proteins, BAG3 (BCL-2-associated athanogene 3) acts in conjunction with p62 to degrade protein aggregates while Tecpr1 (Tachylectin-II-like beta-propeller domain 1) targets *Shigella* in an Atg5-dependent manner (Gamerding et al., 2009; Ogawa et al., 2011).

Selective autophagy regulation by post-translational modification

As mentioned in the last section, ubiquitination of the substrates can provide specificity to an autophagy receptor. Indeed, ubiquitin is often co-localized with autophagy substrates before substrate degradation (Pankiv, et al., 2007; Clausen et al., 2010). Ubiquitin attachment or co-expression appears to be sufficient to target small substrate like long-lived cytosolic proteins and large substrates like peroxisomes or protein inclusions for autophagic degradation (Kim et al., 2008; Tan et al., 2008). However, although diverse types of substrates are targeted by ubiquitination, substrate

selection does not always require ubiquitination. Degradation of mutant superoxide dismutase 1 (SOD1), mutant STAT5A, Sindbis viral capsid, and P granules of *Caenorhabditis elegans* are examples of ubiquitin-independent autophagic degradation (Gal et al., 2009; Zhang et al., 2009; Orvedah et al., 2010; Ogawa et al., 2011; Watanabe and Tanaka, 2011).

Recently, protein phosphorylation has been linked to selective autophagy. For instance, the autophagy receptor, Optineurin, displays higher binding affinity to LC3 and promotes autophagy of *Salmonella* when a residue adjacent to its LC3-interacting motif is phosphorylated (Wild et al., 2011). Similarly, phosphorylation of the ubiquitin-binding domain of p62 increases its affinity to polyubiquitin and promotes degradation of polyubiquitinated proteins (Matsumoto et al., 2011). These studies thus indicate a general role for phosphorylation in controlling the function of autophagy receptors. Moreover, they reveal another layer of spatiotemporal regulation in controlling the autophagy signaling networks. As LC3-interacting motifs and ubiquitin-binding domains are common features of the autophagy receptors, it would be tempting to speculate a broader effect of phosphorylation on the process of selective autophagy.

Intrigued by the phenomenon of MB^d accumulation and considering its potential importance, we have set out to study the fate and function of these organelles after cytokinesis. In chapter II, we will describe how the fates of post-mitotic midbodies are regulated differentially by NBR receptor-mediated autophagy, leading to their accumulation in cells with differentiating potential. We will also describe the potential

functions of post-mitotic midbodies as suggested by the results of NBR1 depletion. In chapter III, we will present the first proteomics study on the NBR1-interaction network, which reveals several new potential MB^d substrates for NBR1, as well as modification events that may regulate NBR1's function in autophagy.

CHAPTER II

MIDBODY ACCUMULATION THROUGH EVASION OF AUTOPHAGY CONTRIBUTES TO CELLULAR REPROGRAMMING AND TUMORIGENICITY

Fig. 2-1a-d, f, and g, Fig. 2-2, Fig. 2-3 (except d and h), part of Fig. 2-4a, Fig. 2-4b-d, Fig. 2-5b, and 5e (H1, H9, and HeLa), Fig. 2-7e, Fig. 2-S1, and Fig. 2-S3 were contributed by Dr. Chun-Ting Chen.

Fig. 2-1e, Fig. 2-3d, Fig. 2-6e-g, Fig. 2-8d and e, Fig. 2-S2, and Fig. 2-S4 were contributed by Dr. Desiree Baron.

Cara Weismann contributed to part of Fig. 4a.

Dr. Tamer Onder and Dr. Sabine Loewer contributed to Fig. 2-8a-b, and Table 2-S1.

Tse-Chun Kuo contributed to Fig. 2-3h, Fig. 2-4a (RPE, DLD-1 and MCF-7), Fig. 2-5c-e (RPE-1, MCF-7, and HeLa), Fig. 2-6a-d, Fig. 2-7a-d, Fig. 2-8a-c, and f, Fig. 2-S5-8, Table 2-S1, and Table 2-S2.

ABSTRACT

The midbody (MB) is a singular organelle formed between daughter cells during cytokinesis and required for their final separation. MBs persist in cells long after division as midbody derivatives (MB^ds), but their fate is unclear. Here we show that MB^ds are inherited asymmetrically by the daughter cell with the older centrosome. They selectively accumulate in stem cells, induced pluripotent stem cells (iPSCs) and potential cancer ‘stem cells’ (CSCs) *in vivo* and *in vitro*. MB^d loss accompanies stem cell differentiation, and involves autophagic degradation mediated by binding of the autophagic receptor, NBR1, to the MB protein Cep55. Differentiating cells and normal dividing cells do not accumulate MB^ds and possess high autophagic activity. Stem cells and cancer cells accumulate MB^ds by evading autophagosome encapsulation and exhibit low autophagic activity. MB^d enrichment enhances reprogramming to iPSCs and increases *in vitro* tumorigenicity of cancer cells. These results suggest unexpected roles for MB^ds in stem cells and CSCs.

INTRODUCTION

Cell division culminates in the separation of two genetically identical daughter cells (Eggert et al., 2006). During division, cell fate determinants segregate asymmetrically to stem cell progeny (Neumüller and Knoblich, 2009). The two spindle poles organized by differentially-aged centrosomes contribute to this asymmetry (Doxsey et al., 2005; Neumüller and Knoblich, 2009) in that the older centrosome is inherited by the daughter cell that retains the stem cell fate (Yamashita et al., 2003, 2007; Wang et al., 2009).

Abscission completes cell division by severing the intercellular bridge between the two future daughter cells (Eggert et al., 2006; Barr and Gruneberg, 2007). Within the intercellular bridge lies the midbody (MB), a large proteinaceous organelle (Mullins, J.M. and Biesele, 1977; Gromley et al., 2005; Barr and Gruneberg, 2007; Steigemann et al., 2009) that was previously thought to detach from cells and disintegrate extracellularly as a remnant (Mullins, J.M. and Biesele, 1977; Barr and Gruneberg, 2007). Recent studies show that post-abscission MBs or MB derivatives (MB^ds) can be retained by daughter cells, suggesting alternative fates for these organelles (Gromley et al., 2005, Goss and Toomre, 2008; Pohl and Jentsch, 2009).

The fate and function of MB^ds is unclear. In neural progenitors, MB^ds possess the putative stem cell marker CD133/prominin-1 and are proposed to participate in intercellular signaling during neural development (Marzesco et al., 2005; Dubreuil et al., 2007). MB^ds can be degraded by autophagy (see below, Pohl and Jentsch, 2009), but the relationship between MB^d loss or retention and the physiological state of cells is

unknown.

During autophagy (macroautophagy), double membrane-bound autophagosomes assemble, engulf cytoplasmic material, and fuse with lysosomes for degradation (Mizushima and Klionsky, 2007; Yorimitsu and Klionsky, 2007; Mizushima et al., 2008; Levine, B. and Kroemer, 2008). Autophagy is required for cellular homeostasis, eliminating defective ubiquitin-tagged proteins and organelles (Kuma et al., 2004, Mizushima and Klionsky, 2007; Yorimitsu and Klionsky, 2007; Levine and Kroemer, 2008), clearing cell fate determinants and cell remodeling (Fimia et al., 2007; Tsukamoto et al., 2008; Cecconi and Levine, 2008). Defects in autophagy contribute to many disorders, including neurodegeneration (Hara et al., 2006), hepatomegaly (Komatsu et al., 2005) and aging (Mizushima et al., 2008, Levine and Kroemer, 2008).

Here we show that MB^ds accumulate in stem cells and are lost upon differentiation. They are selectively degraded by linking the NBR1 autophagic receptor to the Cep55 MB protein. MB^ds accumulate by evasion of autophagosome encapsulation, asymmetric inheritance, and maintenance of low autophagic activity. Reprogramming efficiency and *in vitro* tumorigenicity are increased following experimental elevation of MB^d levels suggesting non-mitotic roles for these organelles in stem and cancer cells.

RESULTS

Post-mitotic midbodies accumulate within cells

Multiple MB^ds were observed in subpopulations of cells by immunofluorescence (IF), but their precise location was unclear (up to 20; Fig. 2-1a, b). Three-dimensional reconstruction of immunofluorescent images revealed multiple MB^ds inside polarized and nonpolarized cells (Fig. 2-1c, d). Immuno-electron microscopy confirmed this localization and revealed ultrastructural features characteristic of MB^ds (Fig. 2-1e, Mullins and Biesele, 1977; Dubreuil et al., 2007). About 70% of cell-associated MB^ds were trypsin-resistant, suggesting that they were intracellular (Fig. 2-1f). This intracellular localization of MB^ds suggested that they might accumulate in cells through successive divisions (below).

MB^ds were also released from cells. In 2-day co-cultures of HeLa cells stably expressing either monomeric RFP (cytoplasmic marker) or MKLP1-GFP (MB marker), about 7% of MKLP1-GFP⁺ MB^ds associated with RFP⁺ cells (Fig. 2-1g). Such free MB^ds were also generated by other cell types (e.g., human adult fibroblasts, HeLa; 1-10%). These observations resolve the conflict of previous studies suggesting that MB^ds are either retained and degraded (Gromley et al., 2005; Goss and Toomre, 2008; Pohl and Jentsch, 2009) or released as remnants after abscission (Mullins and Biesele, 1977). We show that MB^ds accumulate in some cells (Fig. 2-1a-d) but not others, and it is this cell type-specific difference in MB^d-accumulation that is the focus of this study.

Figure 2-1

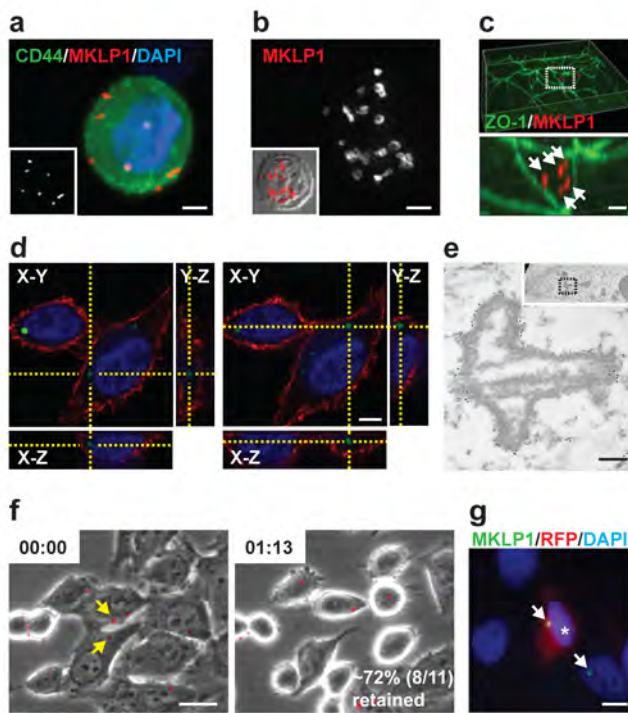


Figure 2-1 MB^ds accumulate within cells. (a, b) Multiple MB^ds associate with a PC3 cell (a) and a B-lymphoblast (b). Insets (a) MB^d labeling and (b) merged phase-contrast image with MB^d labeling to show cell boundaries. MKLP1, MB^d marker (a, b; red); CD44, membrane (a; green); DAPI, DNA (a; blue). Bar, 5 μm (a) and 2 μm (b). (c, d) Three-dimensional reconstruction of polarized cells in a monolayer (c) and a HeLa cell (d) show intracellular MB^ds. (c) ZO-1, tight junction; MKLP1, MB^ds. Bar, 2 μm . Enlargement (c, bottom) of box (c, top) shows five MB^ds (arrows). (d) Wheat germ agglutinin, plasma membrane (red); MKLP1-GFP, MB^ds (green); DAPI, DNA (blue). Bar, 5 μm . (e) Electron micrograph of a MB^d in a permeabilized MCF-7 cell showing immunogold labeling with MKLP1 antibodies. Inset, lower magnification of the MB^d (boxed) in cell; nucleus, right. Bar, 200 nm. (f) Time-lapse images during extracellular trypsin treatment of HeLa cells show retention of most MB^ds (MKLP1-GFP, red). Two MB^ds (yellow arrows) are lost upon treatment, suggesting digestion and/or dissociation. Time (hr:min) post-trypsin. Bar, 5 μm . (g) Two-day co-cultures of HeLa cell expressing either MKLP1-GFP (MB^d marker) or cytosolic RFP. Green MB^ds (arrows) associated with red cells (asterisk) indicate post-mitotic transfer of MB^ds between cells. Bar, 10 μm .

MB^ds are inherited by the cell with the older centrosome

Multiple MB^ds often clustered around the centrosome or spindle pole (Gromley et al., 2005 and data not shown), reminiscent of MB^d-sized aggresomes, which segregate to one daughter cell under control of centrosomes (Johnston et al., 2002; Rujano et al., 2006). Moreover, centrosome age-dependent differences in signaling were observed late in cytokinesis (Anderson and Stearns, 2007). These centrosome age-related differences led us to examine the relationship between centrosomes and MB^d inheritance.

In G1, the centrosome contains one mother centriole (MC) and one daughter centriole (DC; reviewed in Doxsey et al., 2005). After centriole duplication, three generations of centrioles are present: an older mother, a younger mother and two new daughters (Doxsey et al., 2005; Anderson and Stearns, 2007). The centrosome with the older MC is termed the older centrosome (Yamashita et al., 2007; Wang et al., 2009). GFP-tagged centrin1 (CETN1-GFP; Piel, et al., 2000) expressed in mitotic HeLa cells was brightest at one of the four centrioles (92.2% of cells, n=116; Fig. 2-2a) and turned over very slowly (FRAP $t_{1/2}$ ~4 hours and Wang et al., 2009). The brightest centriole remained so from metaphase to late cytokinesis (91.3% of cells, n=46; supplementary information, Fig. 2-S1a), suggesting that it was the older MC. This was confirmed by staining with the older centrosome marker, hCenexin1 (~90% of HeLa and MCF-7 cells, n=143 and n=347, respectively; Fig. 2-2b; Anderson and Stearns, 2007). Several other centriole antigens also showed intrinsic age-related differences in labeling (supplementary information, Fig. 2-S1b).

Figure 2-2 MB^ds are preferentially inherited by the cell with the older centrosome. (a) CETN1-GFP signal is brighter in upper centrosome/spindle pole of a mitotic spindle. The merged DIC image with CETN1-GFP labeling at two centrosomes shows metaphase chromosome. Insets (lower left, upper right), enlargement and semi-quantitative integrated intensity profile of centrioles. Bar, 5 μm . (b) The brighter CETN1-GFP signal represents the older centrosome as it co-stains more intensely for hCenexin1 and remains more intense throughout cell division (supplementary information, Fig. 2-S1a). Bar, 5 μm . Lower left, merge. (c, d) Time-lapse images show that the mitotic MB is preferentially inherited by the daughter cell with the older centrosome in HeLa cells (c) and hESCs (d). Cells were imaged at the indicated times (hr:min) from telophase by phase-contrast microscopy (c) and from metaphase by DIC microscopy (d). Middle panel of (c) and left panel of (d), CETN1-GFP at centrosomes; enlargements and integrated intensity profiles show the daughter cell having the older centrosome (c, upper; d, lower) inherits the MB^d (Time-lapse images: 9:59 in c; lower right image in d). Mitotic MB and MB^ds (c, d; arrows). MKLP1, MB^d marker (red); α -tubulin, mitotic MB and cell boundary marker (green); DAPI, DNA (blue). Bars, 10 μm (c, d).

Using CETN1-GFP to identify the older MC; bright-field imaging to follow MB dynamics in living cells; and immunofluorescence to confirm MB^d inheritance, we determined that MB^ds were preferentially inherited by the cell with the older centrosome. This was observed in pluripotent human embryonic stem cells (hESCs; 83.3% of H9, n=18; Fig. 2-2d), immortalized somatic cells (91.3% of hRPE-1, n=23) and cancer cells (U2OS: 84.6%, n=13; HeLa: 75.0%, n=24; Fig. 2-2c). We conclude that most inherited MB^ds are asymmetrically transferred to the daughter cell with the older centrosome in several cell types.

MB^ds accumulate in stem cells *in vivo*

Other studies have shown that the older centrosome is asymmetrically inherited by the stem cell during asymmetric divisions in the *Drosophila* male germline (Yamashita, et al., 2007) and the mouse neocortex (Wang et al., 2009). The association of the older centrosome with both MB^ds and stem cell divisions led us to ask whether MB^ds were found in stem cell niches. To address this, we determined the localization of MB^ds in human and mouse tissues. In seminiferous tubules of testes, MB^ds were confined to the basal compartment, the site of germline stem cells and their mitotic progeny (both capable of self-renewal; Fig. 2-3a, up to 8 puncta/cell, 5-mm section; Oatley and Brinster, 2008; Barroca et al., 2009). Electron microscopy also revealed multiple cytoplasmic structures with features characteristic of MB^ds within these cells (Fig. 2-3b, c).

In the ventricular zone (VZ, Sox2+31) of embryonic mouse brains, CD133-labeled MB^ds were associated with neural progenitors (Fig. 2-3d and supplementary information, Fig. 2-S2; Marzesco, et al., 2005; Dubreuil et al., 2007). During asymmetric divisions, intracellular MB^ds were usually found in ventricle-facing daughter cells (progenitors; 75%, n=8) and not in daughters with presumed committed fates (Wang et al., 2009). MB^ds in the human hair follicle were also confined to a subpopulation of cells in the stem cell niche, the bulge (Morris et al., 2004), suggesting distinct properties of this subpopulation (Fig. 2-3e, f). MB^ds were also enriched in b1-integrin+ (Conboy et al., 2010) mouse skeletal muscle progenitors (SMPs; 4-fold) over non-SMP cells. These observations suggested that MB^ds were selectively retained and accumulated during successive stem cell divisions *in vivo*.

Figure 2-3

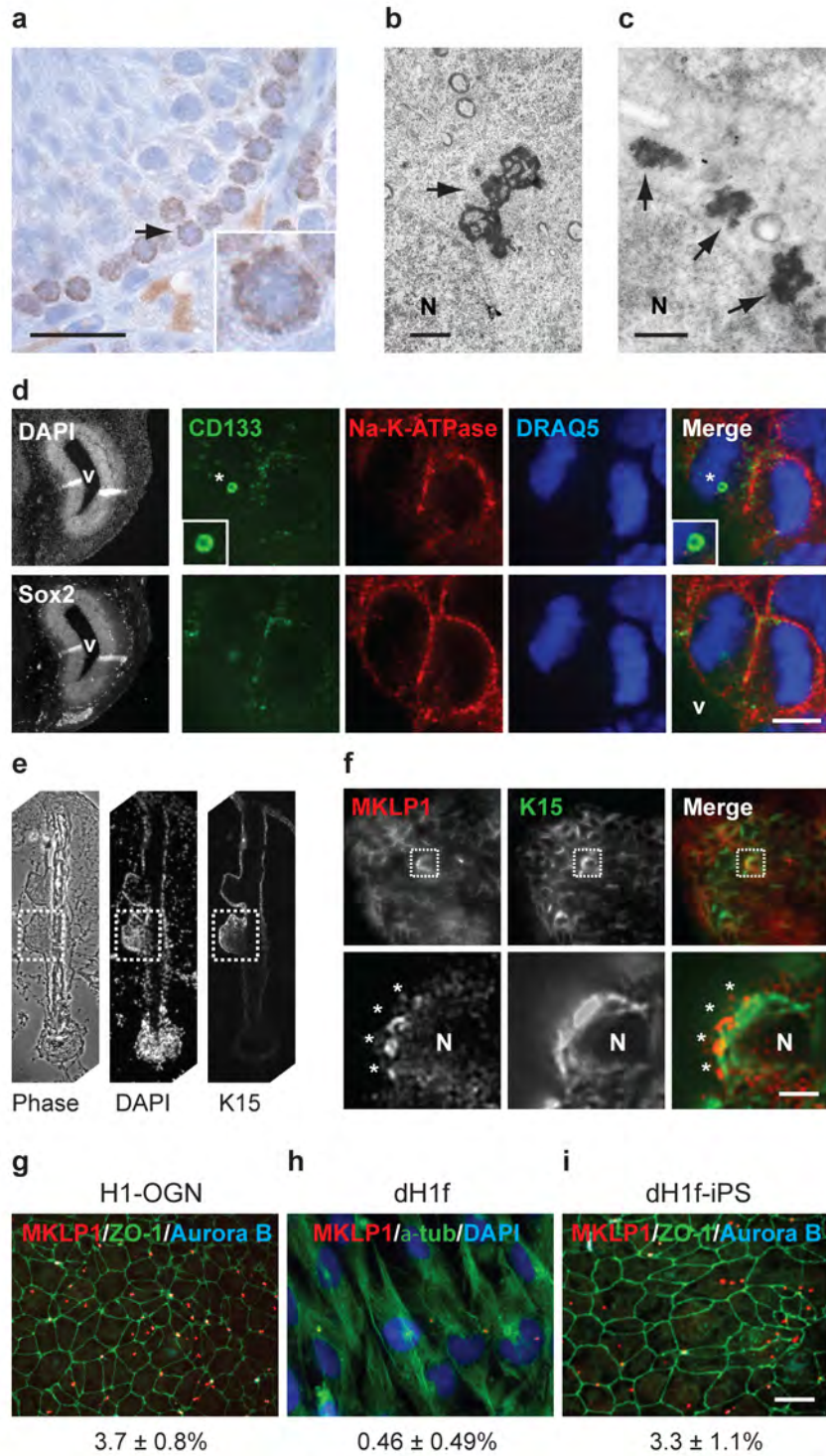


Figure 2-3 MB^ds accumulate in stem cells *in vivo* and *in vitro*. (a) Histological section through mouse seminiferous tubules labeled for MKLP1 shows several MKLP1+ puncta in cells of the basal layer where stem cells reside. Bar, 20 μ m. Inset, enlargement of the cell (arrow) (b, c) Electron micrographs of mitotic MB (b, arrow) and multiple MB-like structures in interphase cells with similar shape and size in a juxtannuclear position (c, arrows) in basal cells of mouse seminiferous tubules. N, nucleus. Bars, 1 μ m. (d) Representative planes of a neural progenitor cell in the ventricular zone (Sox2+, left-bottom panel) of an E13.5 mouse brain show that an intracellular MB^d (asterisk) is associated with the ventricle-facing daughter in the asymmetrically dividing cell (top row). The bottom row emphasizes the position of paired chromosomes in a dividing anaphase cell. CD133, MB/MB^d marker (green); Na-K-ATPase, cell-border marker (red); DRAQ5, DNA (blue); DAPI, DNA. Ventricle (V). Bar, 5 μ m. Note that abscission occurs apically in these cells. (e) A histological section through a hair follicle (left, phase-contrast microscopy) stained for the stem cell marker keratin 15 to identify the bulge region (dotted box), the stem cell niche. DNA stain (DAPI) and the phase-contrast image show full follicle architecture. (f) Upper panels show MB^d-accumulating cells in the bulge region (boxed) colabeled with K15 and MKLP1. Enlargements (lower panels) of the boxed region highlight a cell with four MB^ds (asterisks). N, nucleus. Bar, 5 μ m. (g-i) Quantitative analysis and representative images show a decrease in MB^d-accumulating cells upon the differentiation of pluripotent stem cells (g, H1-OGN) to fibroblast-like cells (h, dH1f), and an increase in MB^d-accumulating cells after reprogramming differentiated cells (h) to induced pluripotent stem cells (i, dH1f-iPS). (g-i) numbers refer to mean \pm s.d., $n=3$. MKLP1, MB^ds; ZO-1, tight junctions; α -tubulin, microtubules; Aurora B, MBs. Bar, 10 μ m.

MB^ds accumulate in stem cells *in vitro*

To rigorously test the idea that MB^ds are selectively inherited by stem cells, we examined MB^d fate during stem cell differentiation and somatic cell reprogramming. MB^d ‘accumulation’ was assessed by counting cells with >1 MB^d, as all cells can transiently acquire one MB^d after abscission (below). MB^d-accumulation decreased ~8-fold upon differentiation of hESCs (H1-OGN) to fibroblast-like cells (dH1f; Fig. 2-3g, h). Differentiation was judged by loss of embryonic stem cell markers (Oct4, Sox2, Klf4, Nanog) and gain of the CD13 differentiation marker (Park et al., 2008; Chan et al., 2009). In contrast, MB^d-accumulation increased ~7-fold after reprogramming dH1f cells to iPSCs (dH1f-iPS; Fig. 2-3h, I; Zwaka and Thomson, 2003; Park et al., 2008). We conclude that MB^d-accumulation *in vitro* reflects that observed *in vivo*, and can be manipulated by altering the potency status of cells.

MB^d-accumulation is enhanced in tumor-derived cells

We next examined differences in MB^d-accumulation among cell lines derived from stem cells, normal dividing cells and cancer cells (Fig. 2-4a). MB^d-accumulation was low in primary and telomerase-immortalized normal cells and significantly higher in hESCs and iPSCs (~7-fold on average; Fig. 2-4a). Most cancer cells exhibited even higher levels of MB^d-accumulation. For example, MB^d-accumulation in tumorigenic MCF-10AT and MCF-10CA1a cells was much higher than in the normal MCF-10A parental line. The common ability of stem cells and cancer cells to accumulate MB^ds, express stem cell

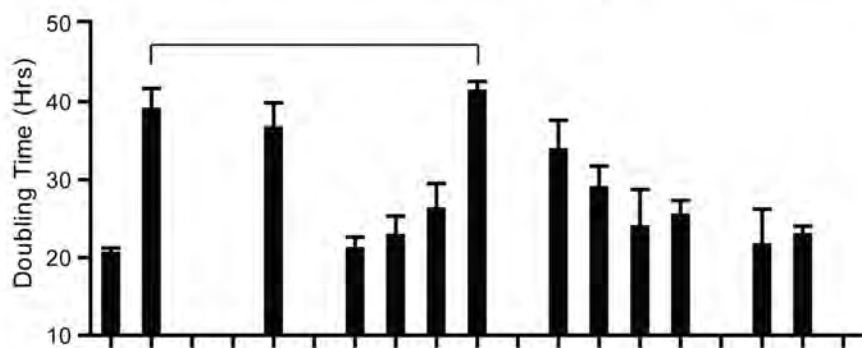
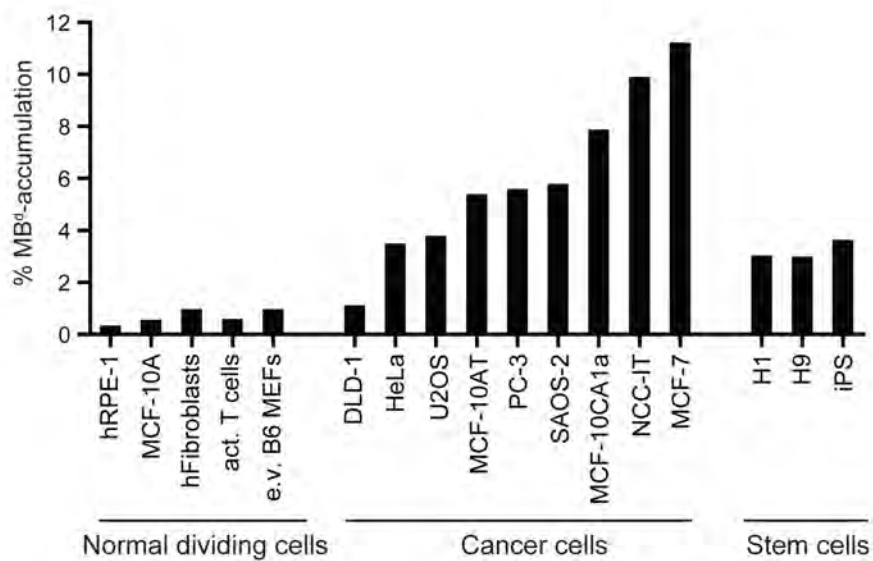
markers (Visvader and Lindeman, 2008) and possess stem cell properties (O'Brien et al., 2007; Pece et al., 2010) suggests a relationship between MB^d-accumulation, tumorigenicity and cancer 'initiating' or 'stem' cells defined by the CSC theory (Pardal et al., 2003).

MB^d-accumulation does not correlate with cell proliferation rate

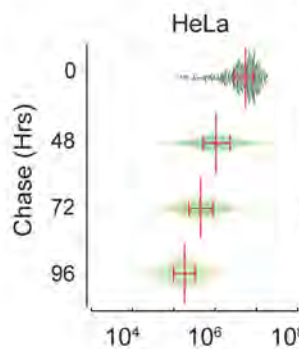
A simple explanation for cell type-specific differences in MB^d-accumulation is variability in proliferation rates. Slower division rates could allow more time for MB^d degradation, as recently proposed (Pohl and Jentsch, 2009). However, we observed no correlation between population doubling-time and MB^d-accumulation (Fig. 2-4a). It was still possible that MB^d-accumulating cells cycled faster than the bulk population. However, a cohort of cells pulse-labeled with EdU (Salic and Mitchison, 2008) showed a proportional decrease in EdU intensity, reflecting dilution of dye after successive divisions (Fig. 2-4b) and indicating that MB^d-accumulating and non-accumulating subpopulations had similar cycling rates (Fig. 2-4c, d).

Figure 2-4

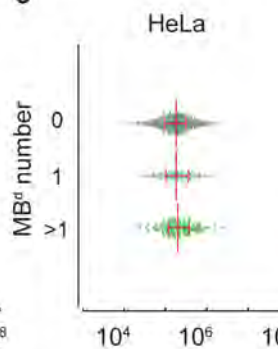
a



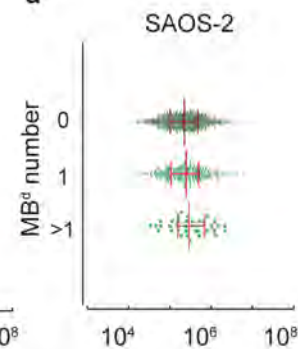
b



c



d



EdU intensity in DAPI+ nuclei (A.U.)

Figure 2-4 MB^d-accumulation is high in stem cells and subpopulations of cancer cells and does not correlate with cell doubling time. (a) Percent of cells that accumulate MB^ds (>1) in a range of different cell types, as indicated. Below, doubling-times of representative cell lines aligned with MB^d-accumulation data. Data are presented as mean \pm s.d.; Cell lines are examined in triplicate (MCF-10A, DLD-1, MCF-10AT, MCF-7, H1, and H9), or quadruplicate (e.v. B6 MEFs, HeLa, SAOS-2, and MCF-10CA1a), except hRPE-1 ($n=6$), U2OS ($n=7$) and NCC-IT ($n=8$). Horizontal line, cell lines with different MB^d-accumulation potential (14-fold) but similar doubling time. (b) Cells pulse-chased with EdU show a decrease in EdU intensity (x-axis) over time (y-axis), reflecting dilution of dye after cell divisions. (c, d) After a 96-hr chase period, EdU levels were compared between cells with MB^d numbers of >1, 1, and 0 (y-axis) in HeLa (c) and SAOS-2 cells (d). In both cases, no significant differences were noted (c, $p=0.2101$; d, $p=0.5609$, one-way ANOVA, with at least 800 cells analyzed for each experiment, $n=3$), indicating similar cycling rates among different subpopulations of cells. (b-d) Each graph is a representative experiment. Cells analyzed shown by green points, median depicted by vertical red lines, and horizontal red lines with ticks illustrate the interquartile range.

MB^d-accumulating cells evade membrane encapsulation of MB^ds

We next asked if MB^ds occupied different sites within MB^d-rich and MB^d-poor cells. To test this, we used the Fluorescence Protease Protection (FPP) assay (Lorenz et al., 2006) to monitor degradation of MB^ds following plasma membrane permeabilization and protease addition (Fig. 2-5a). Under these conditions, MKLP1-GFP+ MB^ds were degraded in MB^d-rich HeLa cells but not in MB^d-poor hRPE-1 cells indicating that MB^d-poor cells sequestered MB^ds in membrane-bound compartments whereas MB^d-rich cells accumulated them in the cytoplasm (Fig. 2-5b). Importantly, the integrity of intracellular organelles was maintained during the course of these experiments (supplementary information, Fig. 2-S3).

Stem cells and cancer cells evade lysosomal degradation of MB^ds

The protease resistance of MB^ds and low MB^d-accumulation in MB^d-poor hRPE-1 cells (Fig. 2-4a and 2-5b) suggested that MB^ds were delivered to a membrane-bound compartment for degradation, such as the lysosome. Indeed, MB^ds were often found within LAMP2-labeled lysosomes in MB^d-poor cells (Fig. 2-5c; Eskelinen et al., 2003). To test this further, we examined the fate of newly-formed MB^ds in synchronous populations of MB^d-poor cells (Fig. 2-5d). Three hours after release from mitosis, the percent of MB^d+ cells (MB^d levels) peaked at ~40% (50% being the maximum since half the cells were 'born' without a MB^d). This was followed by a peak in MB^d localization to lysosomes (~42% at 7 hours; Fig. 2-5d) and then a decrease of MB^ds to baseline levels

Figure 2-5

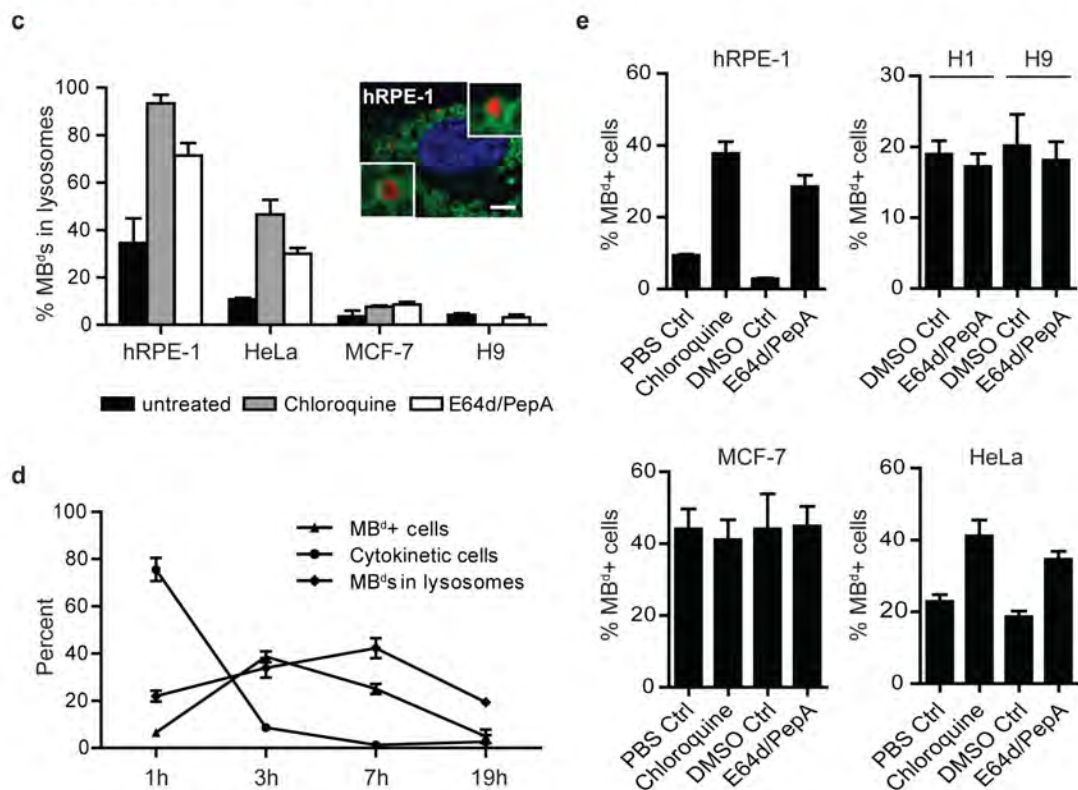
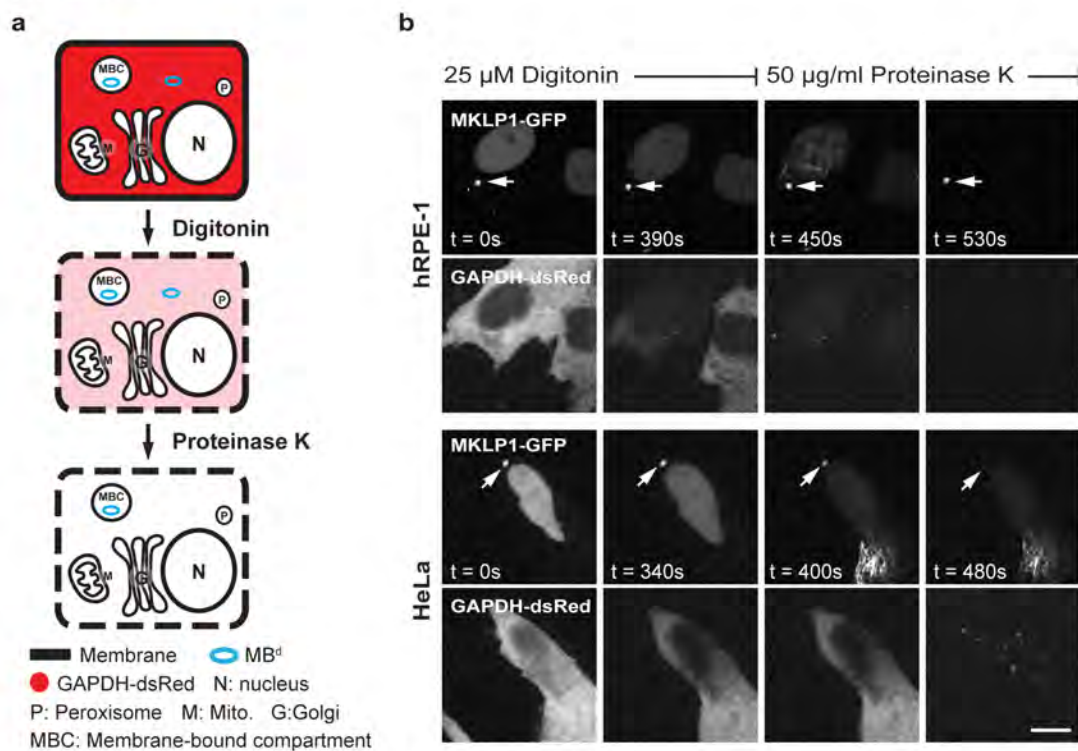


Figure 2-5 MB^ds in stem and cancer cells evade membrane encapsulation and lysosomal degradation. (a) Depiction of fluorescence protease protection (FPP) assay. Digitonin selectively permeabilizes the plasma membrane but not internal membranes. Proteinase K degrades cytoplasmic components but membranous compartments remain intact. Under these conditions, MKLP1-GFP-labeled MB^ds (blue circle) in the cytoplasm will be degraded whereas those inside membrane-bound compartments (MBCs) will not. (b) MB^ds in MB^d-poor hRPE-1 cells are largely protected (~90% in membranous compartments, cells analyzed=10), whereas most MB^ds in HeLa cells are not (~27%, cells analyzed: 11), and are thus degraded in cytoplasm. Bar, 5 μ m. (c) Graph depicting the presence of MB^ds in lysosomes upon chloroquine or E64d/pepstatin A (E64d/PepA) inhibition in hRPE-1 and HeLa cells, but not in MCF-7 and H9 hESCs. Chloroquine treatment of H9 hESCs is not included as it caused differentiation and cell death. A representative image of hRPE-1 cells inhibited by chloroquine is shown depicting two MB^ds inside lysosomes. MKLP1 and LAMP2 are used as MB^d (red) and lysosome (green) markers, respectively. DAPI, DNA (blue). $n=100$ MB^ds/treatment in each of the biological triplicates. Bar, 5 μ m. (d) Graph showing the percent of MB^{d+} cells (MB^d levels), the percent of MB^ds within lysosomes, and the percent of cells exiting cytokinesis following synchronization. MKLP1 and LAMP2 are used as markers as in (c). Note that MB^ds are transferred into only one of the two nascent daughter cells after abscission (Fig. 2-2d), so a 50% maximum will be expected for MB^{d+} cells. The peak of MB^ds transferred to cells is 3 hours after plating followed by a peak of MB^ds entering lysosomes at 7 hours. (e) Both chloroquine and E64d/PepA treatments increase the percent of MB^{d+} cells in hRPE-1 cells and HeLa cells (chloroquine: $p=0.0021$ and $p=0.0187$, respectively; E64d/PepA: $p=0.0022$ and $p=0.0043$, respectively; $n=3$ for all experiments). In contrast, lysosomal inhibition has no detectable effect on hESCs (H1, H9) and MCF-7 cancer cells. Data are presented as mean \pm s.d. (c-e), except mean \pm s.e.m. in hESCs (e).

(16-19 hours; Fig. 2-5d). These data and the FPP data suggested that MB^ds in hRPE-1 cells entered the cytoplasm, moved into lysosomes and were degraded before the next cell cycle (Fig. 2-5b, d).

If lysosomes are involved in MB^d degradation, lysosomal inhibition should increase MB^d levels. Indeed, when lysosomal activity was inhibited in MB^d-poor hRPE-1 cells with either chloroquine or E64d/PepA protease inhibitors (Klionsky et al., 2008) MB^d levels (Fig. 2-5e) and the percent of MB^ds found within lysosomes (Fig. 2-5c) were elevated. In contrast, MB^d levels and the percent of MB^ds in lysosomes in MB^d-rich cells (hESC, MCF-7; Fig. 2-5c, e) were largely unaffected by lysosomal inhibition (see supplementary information, Fig. 2-S4a). The modest increase in MB^d+ HeLa cells (Fig. 2-5e) was consistent with their modest MB^d-accumulating ability (Fig. 2-4a). We conclude that lysosomal degradation prevents MB^d-accumulation in MB^d-poor cells, but does not play a major role in MB^d-rich cells (e.g. stem cells, CSCs) thus allowing MB^ds to accumulate.

Autophagic degradation controls intracellular MB^d levels

To determine how MB^ds were directed to lysosomes, we explored pathways leading to lysosomal degradation. Reported autophagy levels in MCF-7 and DLD-1 cells (Liang et al., 1999; Sato et al., 2007) suggested a relationship between autophagy and MB^d fate. Low autophagy levels in MCF-7 cells resulting from a deficiency in the autophagy gene, *BECN1* (also known as *Atg6*; Liang et al., 1999), are consistent with high MB^d-accumulation (~26-fold over normal cells; Fig. 2-4a). High autophagy levels in DLD-1

cells (Sato et al., 2007) are consistent with low MB^d-accumulation (only ~1.8-fold over normal cells; Fig. 2-4a). In agreement with this trend was the presence of MB^ds in autophagosomes of MB^d-poor cells (Fig. 2-6a).

Experimental reduction of autophagy activity using MEFs from *Atg5*-deleted mice (Kuma et al., 2004) or by siRNA-mediated depletion of *Atg7*, increased MB^d levels (Fig. 2-6b, c). Induction of autophagy by rapamycin and lithium chloride treatment (Sarkar et al., 2005; Sarkar et al., 2008) in HeLa cells or by exogenous BECN1 expression in MCF-7 cells, decreased MB^d levels (Fig. 2-6d, e). These results demonstrated the role of autophagy in regulating MB^d levels in different cell types, and suggested an inverse relationship between autophagic activity and MB^d-accumulation. This inverse relationship was revealed in 12 cell lines by LC3-II (see Methods; Mizushima and Yoshimori, 2007; Klionsky et al., 2008) or p62 (Bjorkoy et al., 2005; Komatsu et al., 2007; Klionsky et al., 2008) -based measurements of autophagic activity (Fig. 2-6f, g and supplementary information Fig. 2-S4b). We conclude that MB^d levels are, in part, modulated by cell type/lineage-specific autophagy (Fig. 2-3g-i, 4a, 6f and 6g).

Figure 2-6

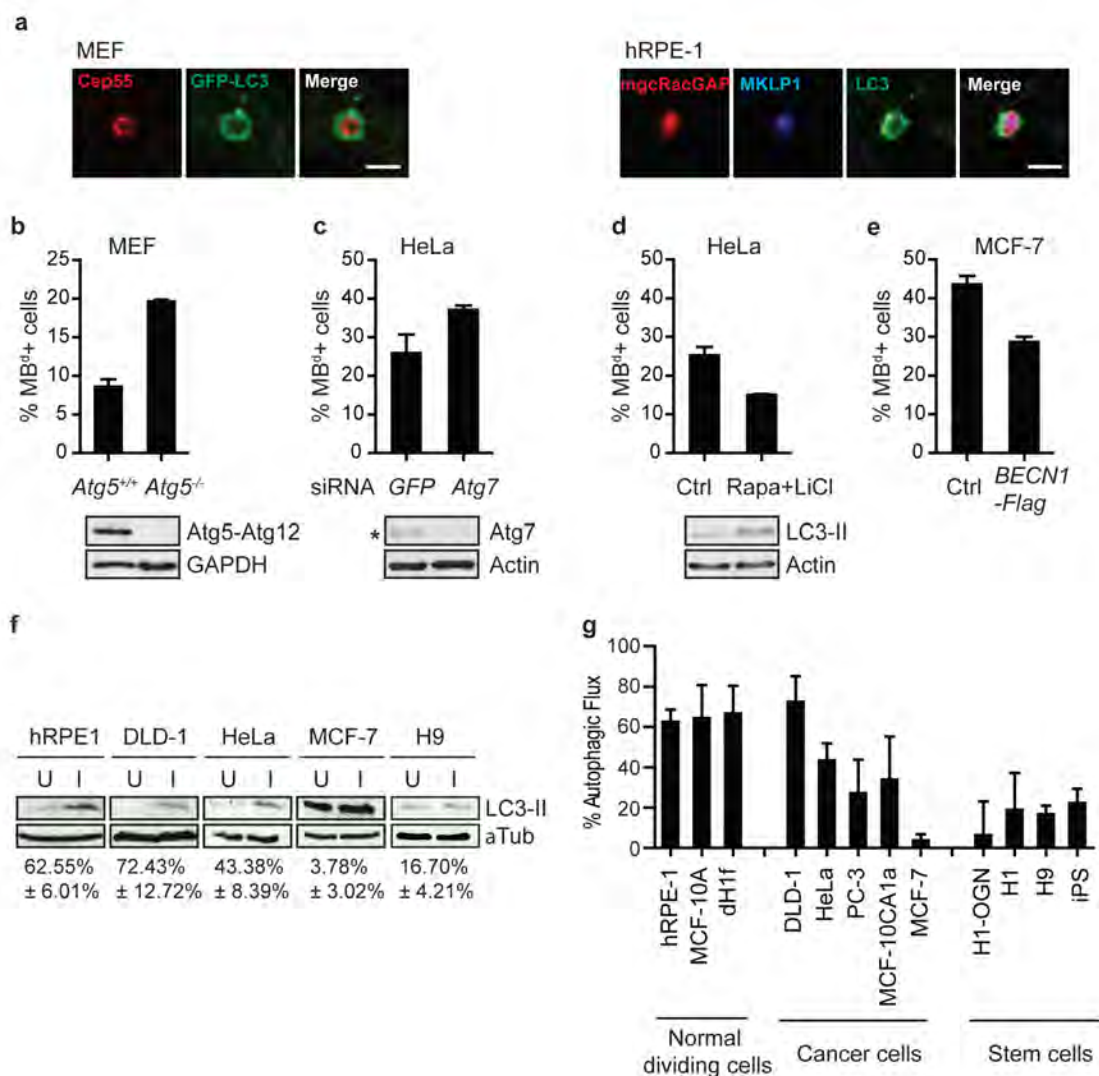


Figure 2-6 Autophagy controls intracellular MB^d levels. (a) Single-plane confocal images of MB^ds within LC3-positive autophagosomes in MEFs expressing GFP-LC3 (left) and in hRPE-1 cells stained for endogenous LC3 (right). MB^d markers: Cep55, MKLP1, or mgcRACGAP. Autophagosomes: GFP-LC3 or LC3. Note that MKLP1 (blue) and mgcRACGAP (red) are co-localized (magenta) in the autophagosome (green), suggesting that MB^ds are sorted into autophagosomes. Bars, 2 μ m. (b-c) Decreasing autophagy levels by deletion of *Atg5* gene (left, MEFs) or depletion of *Atg7* by siRNA (right, HeLa) significantly increases the percent of MB^{d+} cells ($p=0.0019$ and $p=0.021$, respectively, $n=3$). Immunoblots confirm loss of the *Atg5-Atg12* conjugation in mutant cells and depletion of *Atg7* (asterisk). (d-e) Rapamycin (Rapa) and lithium chloride (LiCl) co-treatment induces autophagy and decreases the percent of MB^{d+} cells (left, HeLa; $p=0.0056$, $n=3$). Immunoblots showing increased LC3-II levels confirm autophagy induction. Induction of autophagy by over-expression of Flag-tagged BECN1 reduces the percent of MB^{d+} cells (right, MCF-7; $p=0.0008$, $n=4$) (f) Representative immunoblots showing high autophagic activity in normal cells and low autophagic activity in stem cells and cancer cells. The activity of autophagy was determined by measuring autophagic flux: the amount of autophagic cargo that is delivered to lysosomes for degradation. Lysosomal protease inhibitors E64d and PepA were used to inhibit lysosomal degradation and autophagic cargo, lipidated LC3 (LC3-II), was used to assess autophagic flux. U, uninhibited. I, inhibited. Below, the average of the percent change in LC3-II levels after lysosomal inhibition from 3 experiments. α -tubulin, loading control. (g) Quantification of autophagic flux from 3 experiments in different cell lines. Normal dividing cells (MB^d-poor) typically have high autophagic flux, whereas stem and cancer cells (MB^d-rich) have low autophagic flux. The data are presented as mean \pm s.d. (b-g).

NBR1 is an autophagic receptor for MB^d-specific degradation

To test whether MB^d degradation involves non-specific or receptor-mediated autophagy pathways (Mizushima, et al., 2008), we investigated the mammalian autophagic receptors, p62 (Bjorkoy et al., 2005; Komatsu et al., 2007; Pankiv et al., 2007) and NBR1 (Kirkin, et al., 2009a; Waters et al., 2009). p62 is implicated in MB^d clearance (Pohl and Jentsch, 2009), whereas NBR1 is untested. NBR1 and p62 localized to mitotic MBs and MB^ds (Fig. 2-7a, top, data not shown, and Pohl and Jentsch, 2009), suggesting that MB^d degradation involves receptor-mediated autophagy. NBR1-silencing in HeLa cells impeded autophagosomal encapsulation of the MB^d (supplementary information, Fig. 2-S5) and increased MB^d levels to Atg7-silencing levels (Fig. 2-6c and 2-7b), suggesting that NBR1 is likely a major autophagic receptor for MB^d degradation. In contrast, *p62*-deletion (Komatsu et al., 2007) or siRNA-mediated p62 depletion had no detectable effect on MB^d levels (Fig. 2-7b, c, 2-S6) or NBR1 recruitment to MB^ds (Fig. 2-7a, bottom).

To date, no MB^d target(s) for autophagic degradation have been identified. Candidate-based screening revealed that endogenous NBR1 co-immunoprecipitated with the MB protein Cep55 in hRPE-1 cells (Fig. 2-7d). Cep55 over-expression increased MB^d levels (Fig. 2-7e, left) and the level of NBR1-negative MB^ds (Fig. 2-7e, middle), presumably through NBR1 sequestration in the cytoplasm (Fig. 2-7e, right). This suggested a role of Cep55 in NBR1-mediated MB^d degradation. We propose that the Cep55/NBR1 interaction couples MB^ds to the autophagic machinery to control MB^d fate.

Figure 2-7

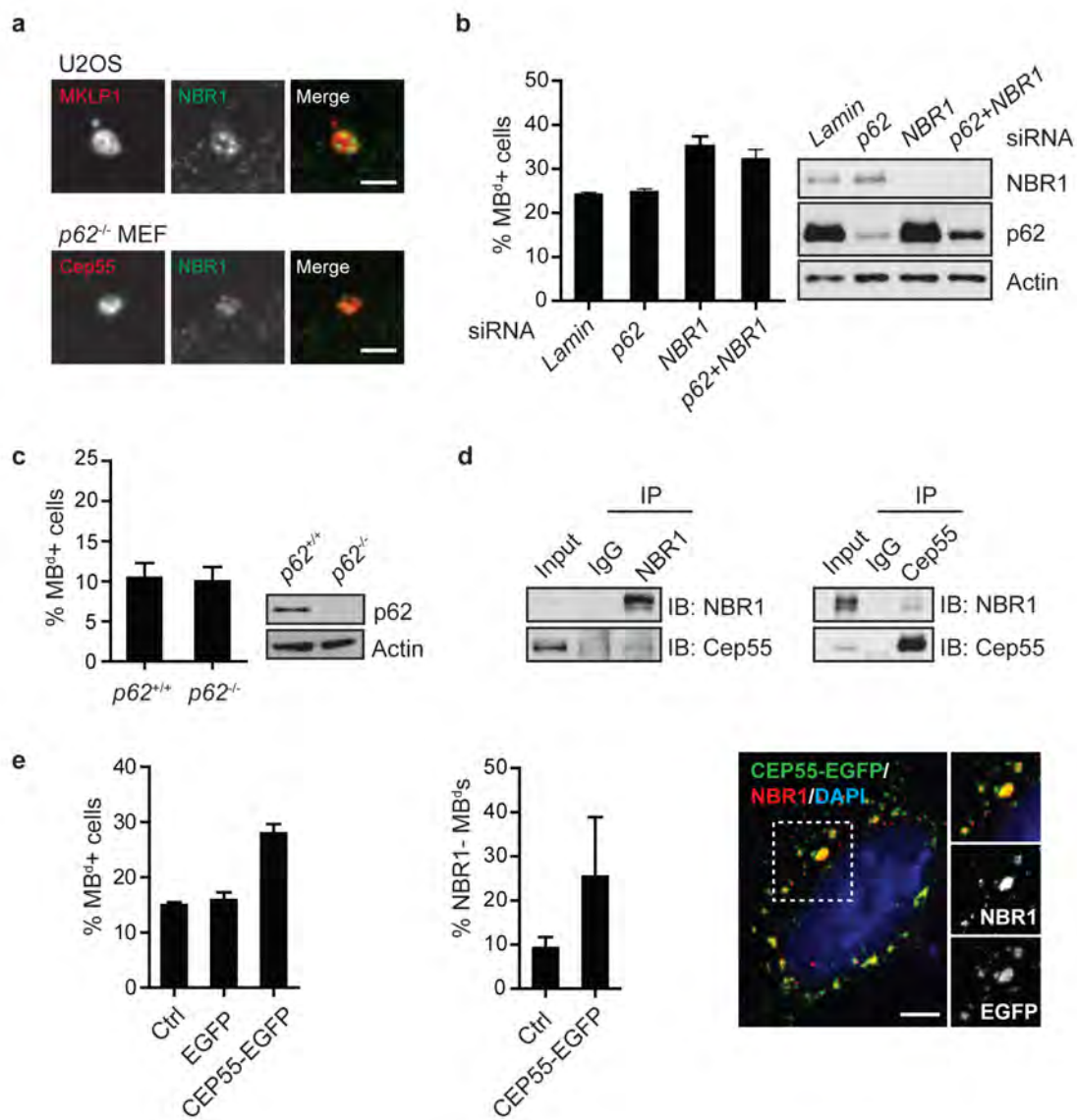


Figure 2-7 NBR1 is a receptor for targeting MB^ds to the autophagy pathway. (a) Single-plane confocal images showing co-localization of the MB^d and the autophagic receptor, NBR1, in U2OS cells and *p62*-deleted MEFs. MB^d markers: MKLP1 or Cep55. Bar, 2 μ m. (b) The percent of MB^d+ cells is significantly increased following the depletion of NBR1 ($p=0.022$, $n=3$), but not another autophagic receptor, p62. Co-depletion of NBR1 and p62 does not further increase MB^d levels over NBR1 depletion alone. (c) Deletion of the *p62* gene does not affect the percent of MB^d+ cells. For (b) and (c), immunoblots verify protein loss. (d) Co-immunoprecipitation reveals Cep55 and NBR1 form a complex. Precipitated proteins and 5% of the input material (Input) were analyzed by immunoblotting with antibodies against NBR1 or Cep55. (e) Over-expression of CEP55-EGFP increases the percent of MB^d+ cells (left; $p=0.0007$, $n=3$) and the percent of NBR1-negative MB^ds (middle; $p=0.0568$, $n=3$), presumably by sequestering NBR1 away from MB^ds in cells expressing CEP55-EGFP (right), and consequently preventing MB^d degradation. The dotted box in right panel is enlarged (top right panel), and the labeling of NBR1 and CEP55-EGFP (middle and bottom right panel) are also presented. DAPI, DNA (blue). Bar, 5 μ m. The data are presented as mean \pm s.d. (b, c, and e).

Cells enriched in MB^ds exhibit increased reprogramming efficiency

We next examined the functional consequences of manipulating MB^d levels. We first tested the role of MB^ds during reprogramming (Yu et al., 2007; Park, et al., 2008; Chan et al., 2009) in cells stably expressing NBR1-specific shRNAs (shNBR1) to increase MB^d levels over controls (shNT). MB^d levels increased ~1.8-fold in dH1f cells, ~1.5-fold in IMR90 embryonic fibroblasts (Yu et al., 2007), and ~1.9-fold in hFib2 adult fibroblasts (Park, et al., 2008). Under these conditions, iPSC colony formation increased significantly in all three cell types depleted of NBR1: dH1f cells (up to 8.7-fold, avg. 3.1 ± 0.5 -fold), IMR90 cells (up to 4.2-fold, avg. 3.4 ± 0.8 -fold; Fig. 2-8a, b and supplementary information Table. 2-S1) and adult hFib2 cells (up to 2.5-fold, avg. 1.7 ± 0.5 -fold). Similar results were obtained with different batches of viruses, different combinations of reprogramming factors, and different viral delivery systems (see Methods). Importantly, increased reprogramming following NBR1-depletion occurred without significant changes in global autophagic activity (dH1f; Fig. 2-8c) or cell proliferation rate (shNBR1: 27.3 ± 2.5 hrs; shNT: 26.8 ± 4.5 hrs; $n=6$), suggesting that NBR1 is selective for MB^d degradation.

Cancer cells enriched in MB^ds exhibit increased *in vitro* tumorigenicity

Because MB^ds selectively accumulate in stem cell niches, hESCs, and iPSCs, we reasoned that they may also accumulate in CSCs. On the basis of Hoechst 33343 extrusion, the side population (SP) of MCF-7 cells (Engelmann et al., 2008) was isolated.

These putative CSCs showed a 7-fold increase in MB^d+ cells over the non-SP population (MP; Fig. 2-8d).

To directly address the role of MB^ds in cancer cells, MKLP1-GFP-expressing HeLa populations with high or low percentages of MB^d+ cells were isolated by FACS, and tested for anchorage-independent growth. Increased colony formation was observed in the “MB^d high” versus the “MB^d low” population, and colony formation increased with increasing MB^d levels (up to 4-fold; Fig. 2-8e). An increase in colony formation was also observed in MB^d-enriched HeLa cells (Fig. 2-8f, left) and mouse hepatocarcinoma cells (134-4; Fig. 2-8f, right) following NBR1-silencing. Results of all three strategies suggest that MB^ds in cancer cell subpopulations may contribute to their tumorigenic potential.

Figure 2-8

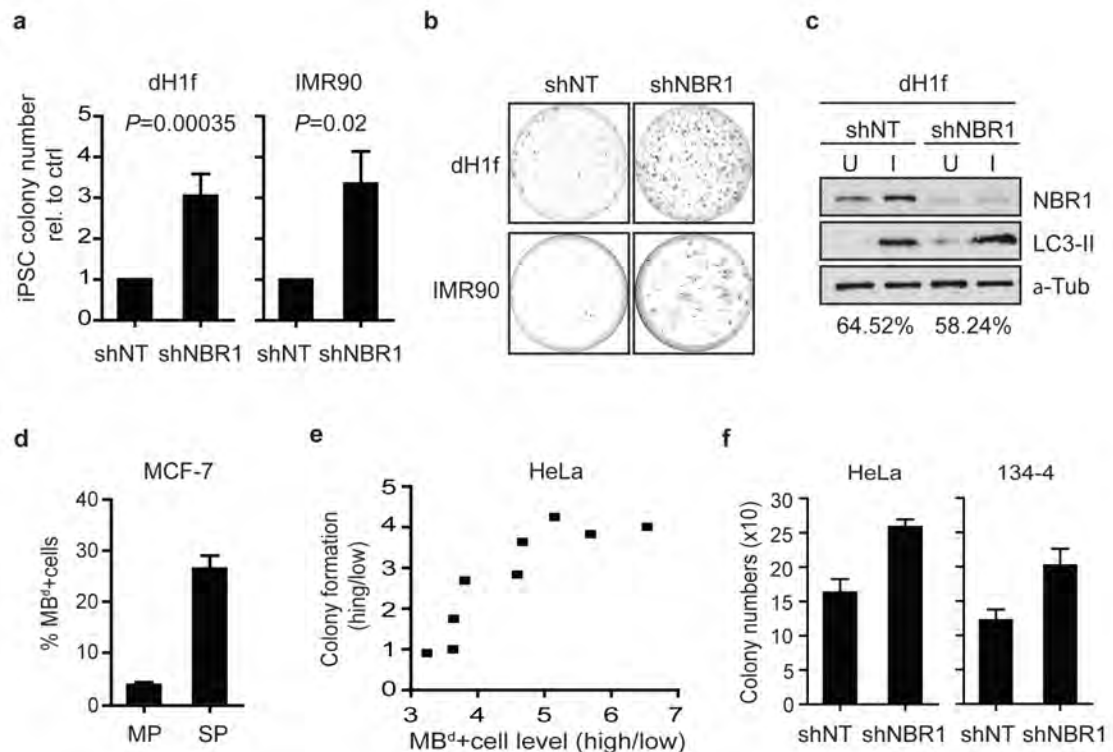


Figure 2-8 MB^d enrichment increases reprogramming efficiency and enhances *in vitro* tumorigenicity. (a-c) Reprogramming is more efficient after MB^d enrichment. Differentiated cells (dH1f) and embryonic fibroblasts (IMR90) are reprogrammed after stable expression of either NBR1-specific shRNA (shNBR1) or non-targeting shRNA (shNT). Emerging iPSC colonies are scored based on Tra-1-60 expression³⁷. (a, b) Cells depleted of NBR1 to increase MB^d levels show an increase in iPSC colony formation (a, dH1f: 3.1±0.5-fold, $n=15$, $p=0.00035$; IMR90: 3.4±0.8-fold, $n=3$, $p=0.02$; data are mean ± s.e.m.) but insignificant changes in autophagic activity (c) over shNT control. (b) Representative plates with Tra-1-60-immunostained iPSC colonies. Immunoblot (c, top) and densitometry (c, bottom; percent of autophagic flux) show representative result ($n=3$); a-tubulin, loading control. (d) MCF-7 side-population (SP) cells have a significantly higher percentage of MB^d+ cells over the non-SP population (MP; $p=0.0015$, $n=3$; data are mean ± s.d.). (e, f) MB^d enrichment in cancer cells leads to increased anchorage-independent growth. MKLP1-GFP-expressing HeLa cells are separated into “MB^d high” and “MB^d low” subpopulations. An increase in the “MB^d high” over “MB^d low” ratio is associated with an increase in soft-agar colony formation (e). No significant difference was observed when the enrichment of MB^d high subpopulation was less than 3-fold. More soft-agar colonies are formed when MB^ds are enriched by NBR1-depletion (shNBR1) in HeLa (f, left; $p=0.0012$, $n=3$) and mouse 134-4 cells (f, right; $p=0.0086$, $n=3$); control, shNT. Data are mean ± s.d., and the colony number (e, f) is the sum of INT-violet-stained colonies from 10 random fields.

DISCUSSION

We have identified new roles for MB^ds outside their canonical function in cytokinesis. This work provides the first evidence for MB^d-accumulation in stem cells, hESCs and iPSCs *in vivo* and *in vitro*, and for dramatic MB^d reduction in differentiating progeny of stem cells. MB^ds appear to function in maintaining or enhancing the pluripotency of stem cells and the tumorigenicity of cancer cells.

Our findings suggest that MB^d loss that accompanies stem cell differentiation is mediated by autophagic degradation, resulting in selective elimination of MB^ds in differentiated cells but retention in germ or stem cells. This process is intriguingly similar to clearance of P granule components in committed somatic cells of *C. elegans*, which is also mediated by autophagy (Zhang et al., 2009). Moreover, P granules contain molecules required for cell fate specification (Strome, 2005), and MB^ds contain stem cell markers (Marzesco et al., 2005, Dubreuil et al., 2007) and enhance cell fate conversion (present study). It is thus tempting to propose that MB^ds may serve as scaffolds for organizing cell fate determinants. Equally intriguing is the observation that essentially all cancer cells examined contain MB^d-accumulating subpopulations, making this a common intrinsic property of both stem cells and cancer cells. The observation that MB^d-enriched cancer subpopulations exhibit enhanced *in vitro* tumorigenicity is consistent with the CSC model for potentiation of tumorigenicity (Pardal et al., 2003; O'Brien et al., 2007; Visvader et al., 2008; Pece et al., 2010).

Our data identify two primary mechanisms for MB^d-accumulation. The first is asymmetric MB^d inheritance by the daughter cell with the older centrosome (Fig. 2-9,

top). In fly testes and mouse neocortex, the old centrosome segregates to the stem cell during asymmetric divisions and is accompanied by increased microtubule-anchoring ability (Yamashita et al., 2003, 2007; Wang et al., 2009). MB^d inheritance could be facilitated through increased anchoring of microtubules to the older centrosome, and increased microtubule binding to the MB^d in the daughter cell with the older centrosome. This would be consistent with the observed MB^d-accumulation in stem cells but not in their differentiated progeny. Despite the slower division rate of stem cells *in vivo* (Fuchs, 2009), MB^d-accumulation could still occur via this mechanism. However, our results also indicate that such asymmetry occurs in different cell types, suggesting that it may only be physiologically relevant in stem cells and CSCs.

Evasion of autophagic degradation is a second mechanism for MB^d-accumulation (Fig. 2-9, bottom). This is exemplified by the inverse relationship between MB^d levels and autophagic activity, and by changes in MB^d levels with manipulation of autophagy levels. MB^d-accumulation can also be mediated by uncoupling receptor-mediated entry into the autophagy pathway, since depletion of the NBR1 autophagic receptor or over-expression of the corresponding ligand, Cep55, increases MB^d levels. In contrast, another known autophagic receptor, p62, does not appear to be involved in MB^d clearance (Fig. 2-7b, c, 2-S6). NBR1 and p62 can form a complex (Lamark et al., 2003; Kirkin et al., 2009a); however, evidence suggests that they may act independently as autophagic receptors (Kirkin et al., 2009a). Thus, p62/NBR1 complex formation may not be a prerequisite for autophagic degradation. Since NBR1-silencing increases MB^ds to levels seen following inhibition of autophagy in HeLa cells (Fig. 2-6c and 2-7b), NBR1-

mediated autophagic degradation likely represents a major pathway for selective MB^d elimination. However, it is still possible that other autophagic receptors and MB^d ligands may exist and contribute to MB^d degradation, even though Cep55 is the sole MB ligand for the NBR1 receptor identified thus far (Fig. 2-7d). In our model, Cep55 and NBR1 and perhaps other MB^d ligands and autophagy receptors, act as switches that control MB^d fate. Ongoing proteomic analyses may identify other molecules and pathways for MB^d degradation.

MB^d levels can be further increased in autophagy-compromised *Atg5*^{-/-} MEFs when lysosome enzymes are inhibited (supplementary information, Fig. 2-S7), suggesting that other degradative pathways may contribute to MB^d degradation. Chaperone-mediated autophagy (CMA; Majeski and Dice, 2004; Mizushima et al., 2008), which targets ~30% of cytosolic proteins and is upregulated upon compromised autophagy (Kaushik et al., 2008), is a potential candidate since multiple MB proteins contain CMA-targeting motifs (KFERQ-like motifs; Majeski and Dice, 2004; supplementary information, Table 2-S2). The proteasome system is another major cellular degradation pathway (Nedelsky et al., 2008) but it doesn't appear to play a role in MB^d degradation (supplementary information, Fig. 2-S8).

Figure 2-9

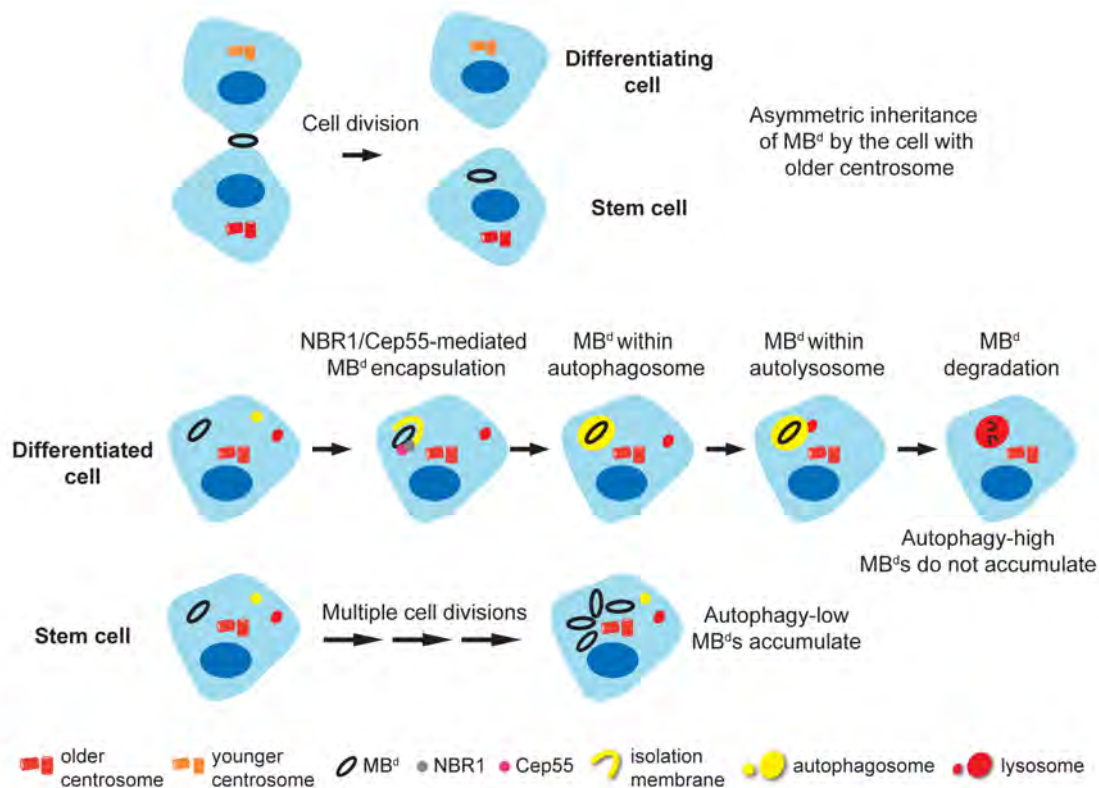


Figure 2-9 Model for MB^d fate in cells. The newly-formed MB^d is preferentially inherited by the daughter cell with the older centrosome (top panel). The inherited MB^d (black ring) is recognized by binding of the NBR1 autophagic receptor (grey circle) with the MB protein Cep55 (magenta). The MB^d is then encapsulated by the autophagosome (yellow circle), and degraded after fusion of autophagosome and lysosome (red circle) in differentiated cells. This pathway prevents MB^d-accumulation. In contrast, stem cells efficiently accumulate MB^ds through successive divisions and evasion of NBR1-mediated autophagy. Additionally, differentiated and stem cells possess overall high and low autophagic activity, respectively.

Other non-degradative processes may also regulate MB^d levels. Even though elevated proliferation rate has been proposed as a factor hindering autophagic MB^d degradation and causing MB^d-accumulation in cancer and normal cells (Pohl and Jentsch, 2009), we didn't observe such a correlation (Fig. 2-4a). Additional work is required to determine if MB^d-accumulation also requires selective sequestration of previously inherited (pre-existing) MB^ds, as suggested by selective accumulation of MB^ds in stem cells of the testes and lateral ventricle of the brain (Fig. 2-3a-d). Release of MB^ds has also been observed in chicken and mouse neural progenitors (Marzesco et al., 2005; Dubreuil et al., 2007) and in human cells (Mullins and Biesele, 1977; and Fig. 2-1g), and may be another, possibly minor pathway for eliminating MB^ds (or for intercellular signaling, Dubreuil et al., 2007). Finally, ongoing work is addressing whether MB^ds are distributed to both daughters of stem cells during symmetric divisions as might be expected if MB^ds are essential for stem cell function.

In summary, our results demonstrate that MB^ds are more than the remnants of cytokinesis. Their fate is differentially controlled in different cell types and mediated by diverse pathways. The shared ability to accumulate MB^ds by stem cells and putative CSCs, and the striking impact on cellular phenotypes following manipulation of MB^d levels suggest that MB^ds perform important cell type-specific functions that remain to be discovered.

ACKNOWLEDGEMENTS

We thank E. Baehrecke for critical reading of the manuscript, T. Schlaeger and colleagues for assistance with H1-OGN and associated cell lines, the UMMS Flow Facility for assistance with MB^d-enrichment, P. Furcinitti of UMMS Digital Light Microscopy Core Facility for assistance with imaging, the UMMS DERC Morphology Core for assistance with immunohistochemistry, D. Guertin and C. Sparks for assistance with SMP preparation, S. Lyle and C. Powers for sample preparation, and H-L. Liu for assistance with clone construction. We thank N. Mizushima for GFP-LC3 expressing, *Atg5*^{-/-}, and matched wild-type MEFs, M. Komatsu and T. Ishii for *p62*^{-/-} and matched wild-type MEFs, S. Jones for *ex vivo* C57BL/6 MEFs, B. Lewis for mouse hepatocellular cancer lines, S. Pino for *in vitro* activated T cells, W. Jiang for MKLP1-GFP plasmid, K. Khanna for CEP55-EGFP plasmid, J. Lippincott-Schwartz and G. Gaietta for plasmids for FPP assay, B. Levine (UT Southwestern) for Flag-tagged BECN1 expressing plasmid, A. Khodjakov for CETN1-GFP expressing plasmids, K. Lee for hCenexin1 antibody and the Progeria Society for cell lines. The a6F antibody to Na-K-ATPase developed by D.M. Fambrough, and H4B4 antibody to LAMP2 developed by J.T. August and J.E.K. Hildreth were obtained from the Developmental Studies Hybridoma Bank developed under the auspices of the NICHD and maintained by The University of Iowa, Department of Biology, Iowa City, IA 52242. This work was supported by funding from the National Institutes of Health (GM051994) to S.J.D and (F32 GM084660-02) to D.M.B, the W.M. Keck Foundation to S.J.D., the Ellison Foundation (AG-SS-1918-07) to S.J.D., the Department of Defense (W81XWH-08-1-0457) to S.J.D. and (W81XWH-06-1-0140) to

C-T. Chen, and the Diabetes and Endocrine Resource Center (5P30DK3252025). Core resources supported by the Diabetes Endocrinology Research Center grant DK32520 were also used (DK32520).

CHAPTER III

**IDENTIFICATION OF CELL CYCLE PHASE-SPECIFIC INTERACTORS AND
PHOSPHORYLATION SITES OF THE AUTOPHAGY RECEPTOR PROTEIN
NBR1**

INTRODUCTION

Autophagy is a catabolic degradative process that involves the formation of a double-membrane structure known as the autophagosome. This structure forms around and encapsulates cellular cargoes, such as protein aggregates, organelles, or invading bacteria. Following encapsulation of cargoes, the autophagosome fuses with the lysosome, resulting in cargo degradation and nutrient recycling. Autophagy was first described as a non-selective, bulk cytoplasmic degradation system; however, with the identification of autophagy receptors conferring cargo specificity, the selectivity of autophagy is being unraveled.

Several autophagy receptors have been identified in mammals, including: p62/SQSTM1, NBR1, NDP52 and optineurin (Bjorkoy et al., 2005; Pankiv et al., 2007; Kirkin et al., 2009a; Thurston et al., 2009; Wild et al., 2011). These receptors interact with both cargos and Atg8/LC3-homologues on the autophagosomal membrane, bringing selected substrates into close proximity with autophagy machinery. Of the known selective autophagy receptors, NBR1 and p62 share very similar domain structures (Fig. 3-1) that include: a PB1 domain (PB1), a zinc finger binding domain (ZnF), an LC3-interacting region (LIR), and an ubiquitin-associated motif (UBA). NBR1 and p62 were originally thought to act cooperatively based on their ability to interact through the PB1 domain and colocalize at cytoplasmic puncta (Lamark et al., 2003; Kirkin et al., 2009a). In addition, both NBR1 and p62 contribute to ubiquitinated substrate removal

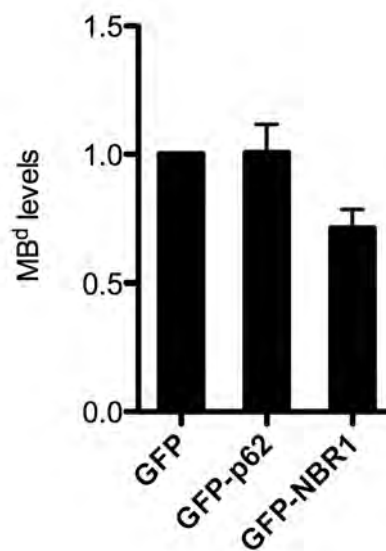
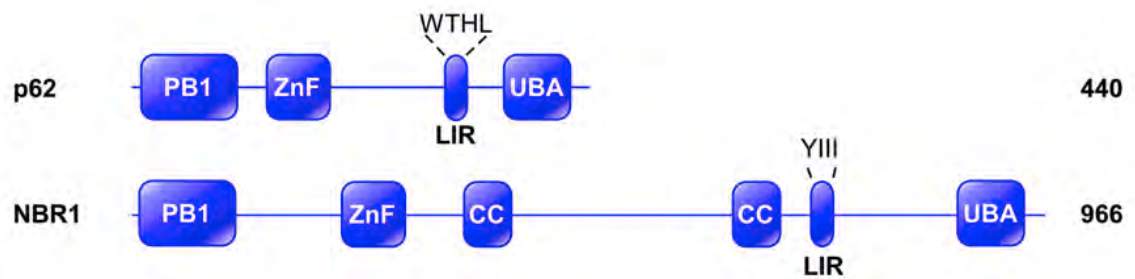


Figure 3-1 Exogenously expressed NBR1, but not p62, promotes MB^d degradation.

Upper: schematic figures of p62 and NBR1. Numbers indicate length of proteins in amino acids. PB1, Phox and Bem1p domain; ZnF, Zinc finger domain, CC, coiled-coil domain; LIR, LC3-interacting region; UBA, Ub-associated domain. The figure is adapted from Kirkin et al., 2009b. **Lower:** HeLa cells were transfected with GFP, GFP-p62, or GFP-NBR1 as indicated for 48hrs. Cells were fixed and immunostained for GFP, MB marker MKLP1, and α -tubulin, mitotic MB and cell boundary marker. MB^d levels (the % of MB^d_s⁺ cells were only quantified in cells showing GFP expression. The averaged MB^d level for each condition was normalized against the control. MB^d levels are significantly decreased following overexpression of NBR1 (0.7-fold, p=0.01, n=3).

(Kirkin et al., 2009a). However, there is evidence suggesting that NBR1 and p62 act independently on different substrates. For example, NBR1 and p62 degradation by autophagy is independent of each other (Kirkin et al., 2009a). Also, following *Salmonella enterica* invasion, p62 is required for autophagosomal engulfment of the bacteria, while NBR1 has no effect (Zheng et al., 2009). Moreover, my findings provide evidence that NBR1, not p62, is the cargo receptor for the post-mitotic midbody (midbody derivative, MB^d) through the MB protein Cep55. Depletion of NBR1 impeded MB^d autophagosome encapsulation, thereby increasing MB^d levels (Fig. 2-7b and 2-S5), whereas NBR1 overexpression promoted MB^d clearance (Fig. 3-1). By contrast, loss of p62 or p62 overexpression had no detectable effect on MB^d levels (Fig. 2-7b, c, 2-S6, and 3-1) or NBR1 recruitment to MB^ds (Fig. 2-7a, bottom). Thus NBR1-mediated MB^d degradation is an autophagy pathway that does not require p62.

MB^d degradation appears to be distinct from the degradation of protein aggregates. The MB^d resembles protein aggregates and/or inclusions because of its large size. However, we found MB^d degradation was not promoted by the autophagy-linked FYVE protein Alfy, a key factor involved in aggregate degradation (Fig. 3-2). Therefore, NBR1-mediated autophagic degradation of MB^ds likely represents a unique form of selective autophagy.

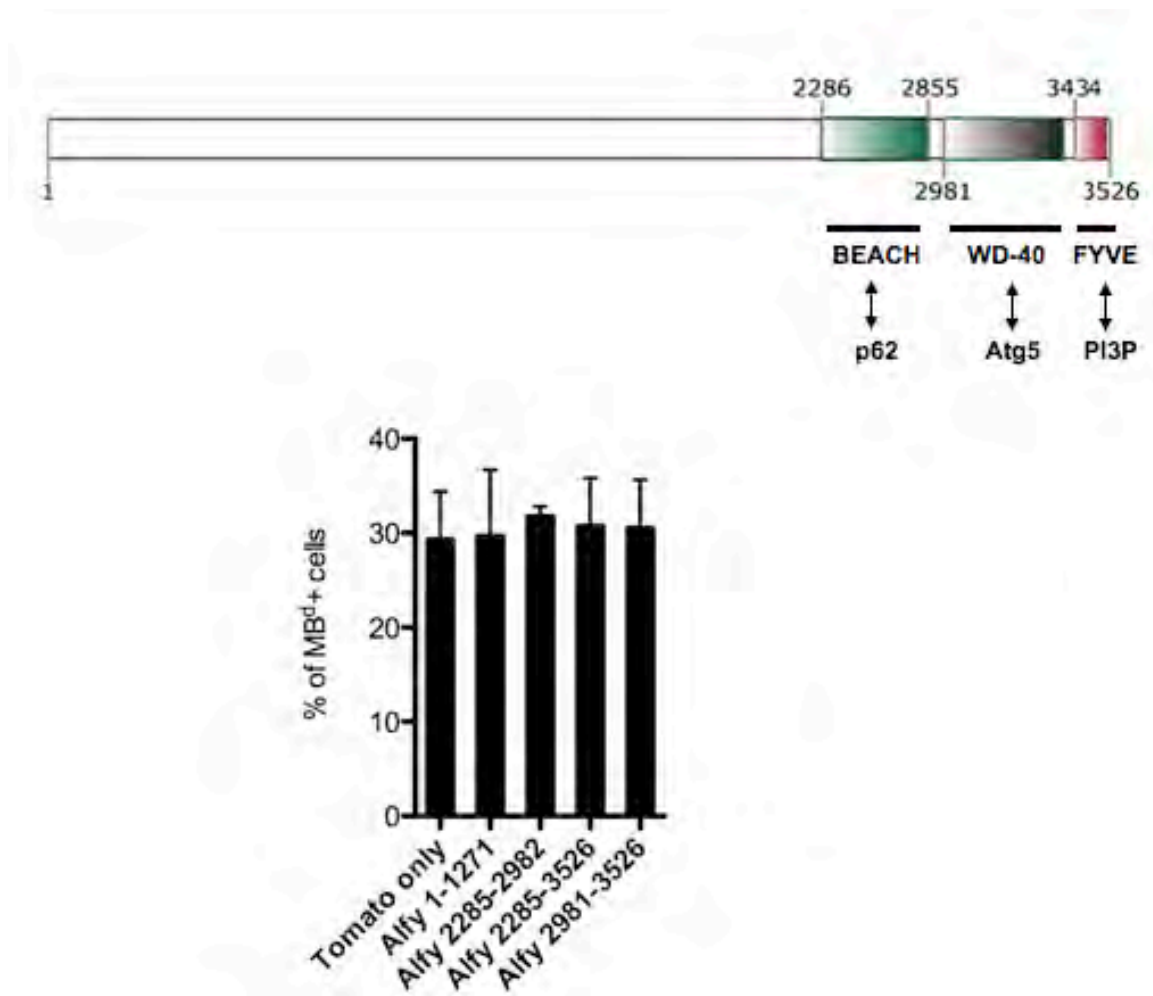


Figure 3-2 Alfy overexpression does not promote MB^d degradation. *Upper:* schematic figure of Alfy showing the location of its BEACH domain, WD-40 repeats, and FYVE domain, which mediates its interaction with p62, Atg5, PI3P, respectively. Alfy truncations containing WD-40 repeats and FYVE domain (aa 2981-3526) are capable of promoting aggregate clearance when overexpressed (Filimonenko et al., 2010). Numbers indicate amino acids. The figure is adapted from Filimonenko et al., 2010. *Lower:* HeLa cells were transfected with Tomato or different Alfy truncations as indicated for 48 hours. Cells were fixed and immunostained for MB^d quantification as described above. The average of two independent experiments is shown. Error bars represent standard deviations.

Based on this, we aim to identify additional NBR1-mediated degradation pathway members and the spatiotemporal mechanism involved in NBR1-mediated MB^d degradation. In this chapter, we present the first proteomics study on the NBR1-interaction network. Our results reveal several new potential cofactors and MB^d substrates for NBR1, as well as modification events that may regulate NBR1 substrate recognition. Together, our results reinforce a primary role for NBR1 in MB^d degradation.

RESULTS AND DISCUSSION

Proteome analysis of NBR1-containing protein complexes reveals potential players involved in MB^d degradation

To identify additional MB proteins that serve as recognition molecules for NBR1, as well as other proteins that cooperate with NBR1 to mediate MB^d degradation, we performed mass spectrometry analyses to identify NBR1 interactions. To purify NBR1-interacting proteins, a fluorescent protein-based tandem affinity purification tag (MAP) that contains His₈, SBP, Flag, and mVenus-tags was used (Ma et al., 2012). The mVenus tag allowed us to confirm that MAP-tagged NBR1, like endogenous NBR1, localizes to cytosolic puncta structures, and can accumulate in the lysosome (data not shown). We purified NBR1-MAP complexes from asynchronous cells or mitotic cells, and then the purified complexes were digested and subjected to two-dimensional liquid-chromatography-tandem mass-spectrometry (2D-LC-MS/MS, MudPIT, in collaboration with Dr. Kathleen Gould's group).

LC-MS/MS of NBR1-MAP purifications identified a large number of potential NBR1 interacting partners that are specifically enriched in asynchronous cells (Table 3-1) or mitotic cells. In addition, we confirmed known interactions between NBR1 and p62, ubiquitin, MAP1B, and Cep55 (chapter II; Kirkin et al., 2009a; Marchbank et al., 2012), suggesting that our LC-MS/MS of NBR1-MAP interactions was robust. To search for factors involved in NBR1-mediated MB^d degradation, we focused on the proteins that are frequently detected from asynchronous cells (n=158, identified by at least 2 unique

Table 3-1.

NBR1-interacting proteins identified in duplicate asynchronous or mitotic NBR1-MAP purifications by LC-MS/MS.

A list of all proteins (>8 TSC) enriched in asynchronous NBR1 purifications by at least fivefold is shown.

Acc ID, Uniprot gene symbol; TSC, total spectral counts for all NBR1-MAP purifications.

AVG, spectral counts divided by total NBR1 spectral counts times 1000; Asyn/Mito Ratio, normalized abundance for asynchronous purification divided by normalized abundance for mitotic purification.

Identified Proteins	Acc ID	TSC	Mito-AVG	Asyn-AVG	Asyn/Mito ratio
Neuroblast differentiation-associated protein AHNAK	AHNK_HUMAN	27	0.21	3.69	17.6
U4/U6 small nuclear ribonucleoprotein Prp31	PRP31_HUMAN	26	0.18	2.80	16.0
Multifunctional protein ADE2	PUR6_HUMAN	24	0.21	3.07	14.7
Zinc-alpha-2-glycoprotein	ZA2G_HUMAN	21	0.18	2.20	12.5
DnaJ homolog subfamily C member 10 (ERdj5)	DJC10_HUMAN	18	0.18	2.02	11.5
L-lactate dehydrogenase B chain	LDHB_HUMAN	16	0.18	2.00	11.4
Clathrin heavy chain 1 (CLTC, CHC17)	CLH1_HUMAN	54	0.59	6.32	10.6
Inosine 5'-monophosphate dehydrogenase 2	IMDH2_HUMAN	20	0.21	2.21	10.6
Importin subunit beta-1	IMB1_HUMAN	48	0.56	5.92	10.6
RB1-inducible coiled-coil protein 1 (FIP200)	RBCC1_HUMAN	13	0.18	1.74	9.9
Myosin-9 (NMMHC II-a)	MYH9_HUMAN	72	1.05	9.46	9.0
Nucleolin	NUCL_HUMAN	12	0.18	1.44	8.2
Bleomycin hydrolase	BLMH_HUMAN	32	0.35	2.87	8.2
Leucine-rich PPR motif-containing protein, mitochondrial	LPPRC_HUMAN	116	1.36	11.04	8.1
Uncharacterized protein (Elongation factor 1-delta)	E9PRY8_HUMAN	14	0.21	1.65	7.9
Dynein light chain 1, cytoplasmic	DYL1_HUMAN	14	0.21	1.59	7.6
Serine/threonine-protein kinase 38 (NDR1 protein kinase)	STK38_HUMAN	14	0.21	1.51	7.2
Fatty acid synthase	FAS_HUMAN	39	0.59	4.07	6.9
cDNA FLJ52712, highly similar to Tubulin beta-6 chain	B4DP54_HUMAN	35	0.59	4.02	6.8
L-lactate dehydrogenase	C9J4M5_HUMAN	13	0.21	1.39	6.6
Kelch-like ECH-associated protein 1	KEAP1_HUMAN	61	1.01	6.62	6.5
Ependymin related protein 1 (Zebrafish), isoform CRA_b (MERP-1, UCC1)	A4D1W8_HUMAN	11	0.18	1.08	6.2
Gasdermin-A	GSDMA_HUMAN	20	0.35	2.15	6.1
CAD protein	PYR1_HUMAN	54	0.98	5.98	6.1
Enhancer of rudimentary homolog	ERH_HUMAN	10	0.18	1.04	5.9
Peptidyl-prolyl cis-trans isomerase A (Cylophilin A)	PPIA_HUMAN	14	0.18	0.98	5.6
Major vault protein (Lung resistance-related protein)	MVP_HUMAN	152	3.25	17.73	5.4
DEAD (Asp-Glu-Ala-Asp) box polypeptide 41, isoform CRA_a	B3KRK2_HUMAN	10	0.21	1.13	5.4
Nucleoside diphosphate kinase, mitochondrial	NDKM_HUMAN	159	3.16	16.76	5.3
Splicing factor 3B subunit 3	SF3B3_HUMAN	8	0.18	0.93	5.3
Protein-glutamine gamma-glutamyltransferase K	TGM1_HUMAN	39	0.70	3.60	5.1

peptides and > 8 total spectral counts), given that MB^d degradation is a post-mitotic event. We compared our identified NBR1 interaction network with reported autophagy-relevant protein networks (networks composed of 409 high-confidence candidate interaction proteins, Behrends et al., 2010). This comparison revealed an overlap of 17 proteins (10.7% of NBR1-binding proteins present in interphase).

Several of these proteins, like NBR1, are known to bind multiple Atg8/LC3 homologues (Behrends et al., 2010), thus are particularly interesting as they could potentially link the MB^d to the autophagosome membrane with NBR1. Among them, RB1CC1, CLTC, and KEAP1 have been implicated in autophagy. RB1CC1 contributes to autophagosome formation through stabilizing the ULK1 kinase complex, while CLTC provides needed membrane from the trans-Golgi network for autophagosome formation (Hara et al., 2008; Guo et al., 2012). KEAP1 is localized to ubiquitinated protein aggregates and appears to facilitate aggregate degradation (Fan et al., 2010). Although the function is unknown, proteins NIPSNAP1 and GBAS have domains similar to the t-SNARE protein SNAP25, suggesting their potential involvement in vesicle transport and fusion (Behrends et al., 2010). Because CLTC, KEAP1, and NIPSNAP1 were detected in the mitotic MB proteome (see below, Skop et al., 2004), they are considered as our primary candidates in mediating MB^d degradation. Besides these autophagy-related proteins, 16 additional candidates (10.1% NBR1-binding proteins) are also associated with intracellular transport pathways, such as GRP78 and Cep57 (Huang et al., 2009a and 2009b). Future analyses are required to validate their participation in MB^d degradation.

So far, the MB protein Cep55 is the only known MB^d-localized autophagy substrate that links the MB^d to autophagy degradation (Fig. 2-7a, d, e). To determine if other MB proteins in addition to Cep55 could be targets for NBR1, we compared the NBR1 interaction network with the mitotic MB proteome (Skop et al., 2004). Strikingly, we found that 28 of the NBR1-binding proteins (17.7% of the 158 interactions) were also detected in the mitotic MB proteome (Table 3-2), including known MB proteins PLK1, MYH9, FLNA, and KIF11 (Wei and Adelstein, 2000; Tsvetkov et al., 2003; Ma et al., 2010; Mondal et al., 2012). PLK1 and MYH9 remain on the MB^d (Fig. 3-3; Hu et al., 2012), suggesting that they may function as additional substrates for NBR1 to mediate MB^d degradation. These proteins may act in concert with Cep55 to recruit NBR1 and/or other potential autophagy-related members to the MB, thereby creating more docking sites for efficient elongation and fusion of the autophagosome precursors around the MB^ds. Overexpression experiments of PLK1 or MYH9 could help to confirm this hypothesis as their overexpression may sequester NBR1 away from the MB thus resulting in increased MB^d level.

Table 3-2 NBR1-interacting proteins that are also present in mitotic midbody proteome (Skop et al., 2004).

Identified Proteins	Acc ID
Clathrin heavy chain 1 (CLTC, CHC17)	CLH1_HUMAN
Inosine-5'-monophosphate dehydrogenase 2	IMDH2_HUMAN
Importin subunit beta-1	IMB1_HUMAN
Myosin-9 (NMMHC II-a)	MYH9_HUMAN
Nucleolin	NUCL_HUMAN
Fatty acid synthase	FAS_HUMAN
Kelch-like ECH-associated protein 1	KEAP1_HUMAN
CAD protein	PYR1_HUMAN
Enhancer of rudimentary homolog	ERH_HUMAN
Peptidyl-prolyl cis-trans isomerase A (Cyclophilin A)	PPIA_HUMAN
Splicing factor 3B subunit 3	SF3B3_HUMAN
Elongation factor 2	EF2_HUMAN
Heat shock protein 105 kDa (HSPH1)	HS105_HUMAN
Filamin-A	FLNA_HUMAN
Nuclear migration protein udC	NUDC_HUMAN
Kinesin-like protein KIF11	KIF11_HUMAN
40S ribosomal protein S3	RS3_HUMAN
Serine/threonine-protein kinase PLK1	PLK1_HUMAN
ADP/ATP translocase 2 (SLC25A5)	ADT2_HUMAN
Leucine-rich PPR motif-containing protein, mitochondrial	LPPRC_HUMAN
Cofilin-1	COF1_HUMAN
Dynein heavy chain 8, axonemal	DYH8_HUMAN
Tubulin alpha-1C chain	TBA1C_HUMAN
Tubulin beta polypeptide	Q5JP53_HUMAN
T-complex protein 1 subunit alpha (TCP1)	TCPA_HUMAN
Protein ipSnap homolog 1	NIPS1_HUMAN
Ubiquitin-40S ribosomal protein S27a	RS27A_HUMAN
Coatomer subunit alpha	COPA_HUMAN

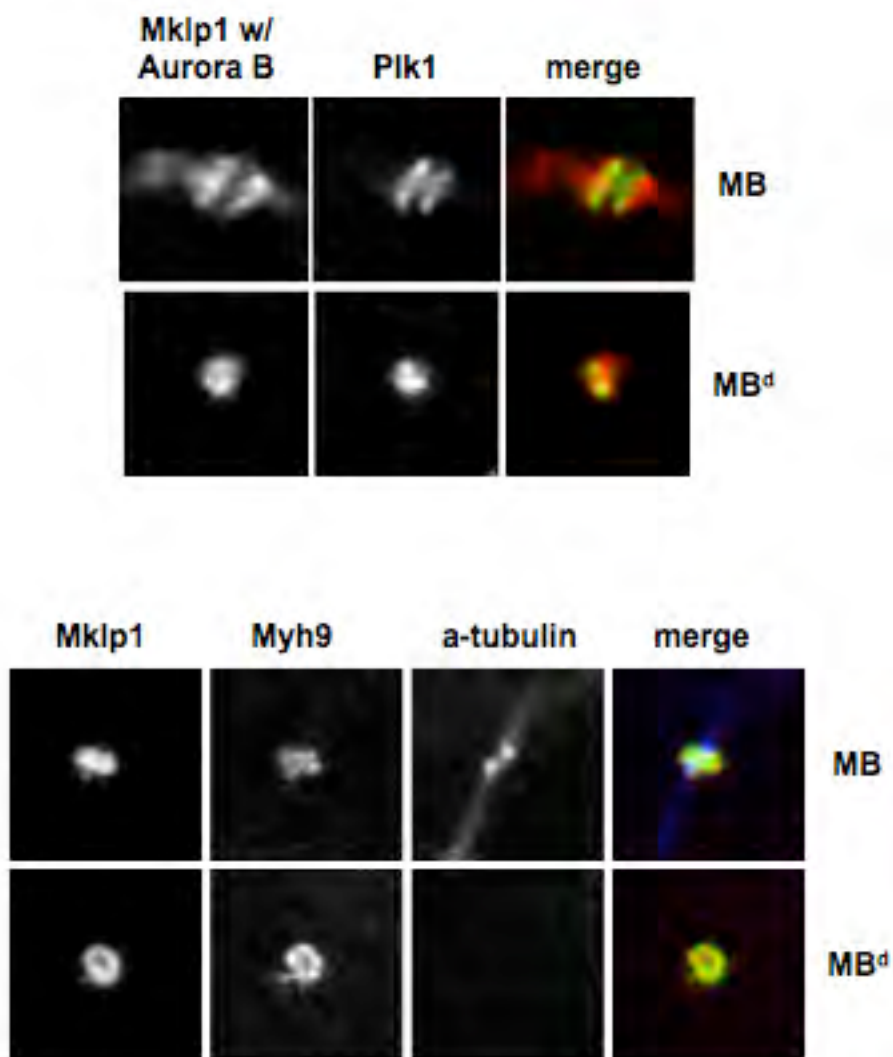


Figure 3-3 Plk1 and Myh9 are localized to both mitotic MB and the MB^d. Single-plane confocal images showing localization of Plk1 (*Upper*) and Myh9 (*Lower*) on both mitotic MB and the MB^d. Mklp1, MB marker; Aurora B and α -tubulin, mitotic MB marker.

Phosphorylation site mapping of NBR1 reveals potential regulatory events for NBR1's function in autophagy

The integrity of the mitotic MB is essential for proper cytokinesis to occur as it serves as a platform to localize factors and orchestrates events required for faithful abscission (reviewed in Hurley and Hanson 2010; Lekomtsev et al., 2012). Therefore, the NBR1-mediated MB^d degradation by autophagy is an event that must be prohibited before (or activated after) abscission. Emerging data have suggested roles for post-translational modifications, particularly phosphorylation events, in regulating selective autophagy (Matsumoto et al., 2011; Wild et al., 2011). Interestingly, we found that NBR1 is phosphorylated in a cell cycle-dependent manner. It is hyperphosphorylated during mitosis, but becomes dephosphorylated after abscission has completed, and remains dephosphorylated throughout interphase (Fig. 3-4). Based on this observation, I propose that NBR1 phosphorylation may serve as a regulatory strategy to limit autophagic cargo recognition and untimely MB degradation.

We performed mass spectrometry analyses to map NBR1's cell cycle stage-specific phosphorylation sites. LC-MS/MS of NBR1-MAP purifications identified a number of NBR1 phosphorylation sites that occur specifically in mitotic or asynchronous cells (Fig. 3-5). We found that several phosphorylation sites are located nearby or within domains that have been implicated for NBR1's function in autophagy: the LC3-interaction region (LIR), the LC3-interaction region 2 (LIR2) and the juxta-ubiquitin

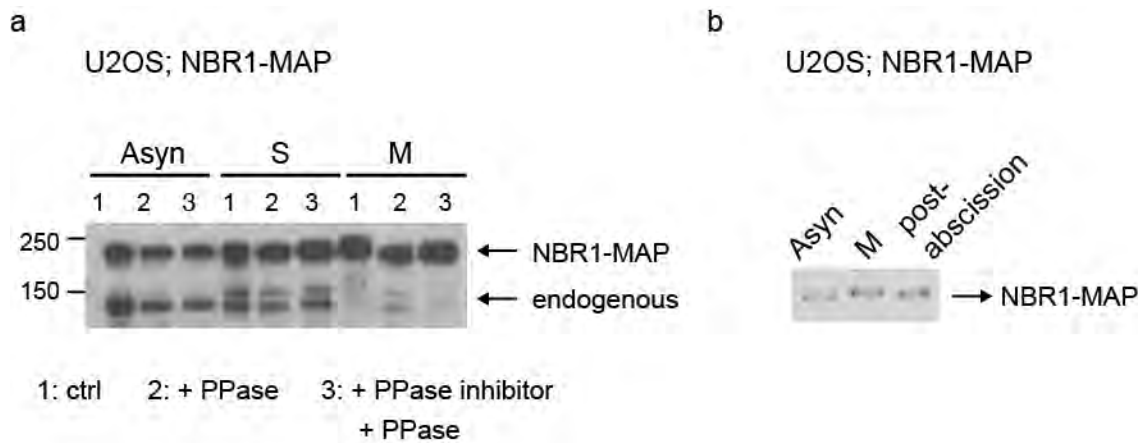


Figure 3-4 NBR1 is hyperphosphorylated in mitosis. *a*: Cell lysates from asynchronous (Asyn), S phase, and mitotic NBR1-MAP expressing U2OS were treated with λ -phosphatase (PPase) or both λ -PPase and PPase inhibitor and immunoblotted with an anti-NBR1 antibody. S phase and mitotic cells were prepared by aphidicolin and nocodazole treatment, respectively. *b*: Cell lysates from asynchronous or mitotic cells were prepared as in *a*. To prepare lysates from post-abscission cells, mitotic cells were first collected by shake-off and then re-plated. Four hours later, when most cells already completed abscission, cell lysates were collected for immunoblotting. NBR1-MAP was detected by either anti-NBR1 or anti-GFP antibodies.

associated domain (JUBA). NBR1 has two LIR domains, both of which can mediate NBR1 binding to LC3 in vitro (Kirkin et al., 2009a). The JUBA region is a novel region preceding the UBA domain and mediates membrane interaction (Mardakheh et al., 2010). Together with the UBA domain, these three regions contribute to the autophagic degradation of ubiquitinated aggregates and peroxisomes (Kirkin et al., 2009a; Deosaran et al., 2012). The phosphorylation sites within these domains likely act as molecular switches that control NBR1 function, as illustrated by other autophagy receptors. For instance, the autophagy receptor required for the clearance of cytosolic *Salmonella*, Optineurin, displays higher binding affinity to LC3 and promotes autophagy of the bacteria when a residue adjacent to its LC3-interacting motif is phosphorylated (Wild et al., 2011). Accordingly, future experiments can be designed to test if the phosphorylation sites enriched in mitosis within these domains function as negative regulators for NBR1's function in autophagy, and furthermore if the phosphorylation sites enriched in interphase act in opposite manner as positive regulators for NBR1's function in autophagy.

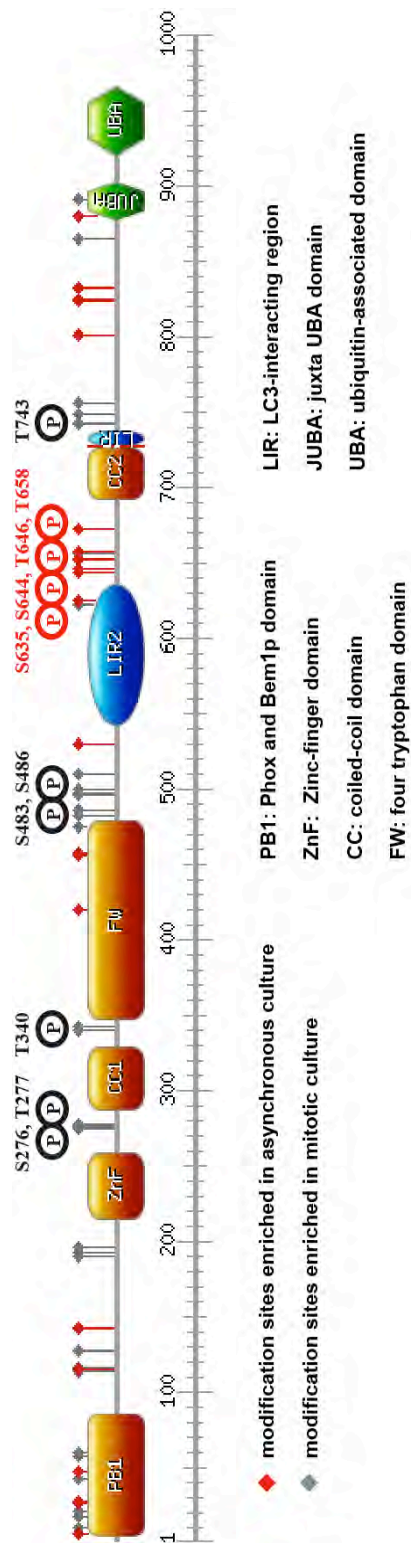


Figure 3-5 Schematic representation of NBR1 showing its functional domains and phosphorylation sites mapped in mitotic cells or asynchronous cultures. The amino acid position of highly-enriched phosphorylated serine or threonine residues (letter P in circle) is shown.

CONCLUSIONS

In this chapter, we reported the first proteomics study on NBR1. Through comparative proteomics and gene ontology analysis, we identified a list of proteins that are potentially involved in NBR1-mediated MB^d degradation (Table 3-1). We also identified a number of phosphorylation sites in NBR1 domains critical for autophagy function (Fig. 3-5). In addition, our findings provided a preliminary understanding of the selectivity of different autophagy pathways (NBR1 vs. p62), based on the extensive difference in associated proteins isolated (Fig. 3-6). Because the role of autophagy receptors in selective autophagy is not well understood, and the exact molecular mechanisms underpinning cargo recognition are still obscure, these initial interaction and phosphorylation profiles of NBR1 can be very useful for the future autophagy research. Our NBR1 profiles are also critical for understanding MB^d function in stem and cancer cells and have implications for cancer research, given the potential importance of MB^d accumulation (chapter II). As more factors and detailed mechanisms modulating MB^d accumulation are revealed, the role(s) of MB^ds can be addressed more sophisticatedly and precisely. Ultimately, strategies that directly and selectively target MB^ds in cancer cells can be developed without affecting normal cells in the body.

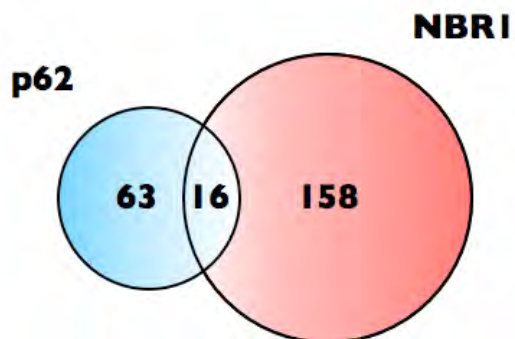


Figure 3-6 Overlap of interacting proteins found between NBR1 and p62 by LC-MS/MS. The list of p62-interacting proteins is from Behrends et al., 2010. All proteins used for comparison were detected with at least 2 unique peptides and 8 total spectral counts.

CHAPTER IV

General Discussion

The midbody (MB), a transient organelle formed between two daughter cells during cell division, is well known for its role in abscission, the last step of cytokinesis. Chapter II outlines the work that myself and colleagues in the Doxsey laboratory performed to determine the fate and function of MB^ds. We found that MB^ds are degraded soon after abscission in normal dividing cells but can accumulate in stem and cancer cells through evasion of NBR1-mediated autophagic degradation. Cells that were enriched with MB^ds through depletion of NBR1 displayed enhanced anchorage-independent growth and cellular reprogramming. In chapter III, we identified additional MB^d substrates for NBR1 and showed that MB^d degradation can only be promoted by NBR1, but not other autophagy factors required for aggregate degradation, like p62 or Alfy. Our proteomics analysis also revealed several potential cofactors as well as post-translational modification events to be involved in NBR1-mediated autophagy. In summary, my thesis research has manifested a role of selective autophagy in regulating MB^d fate and function. My results suggest that NBR1-mediated MB^d degradation is a distinct form of

selective autophagy, and also propose a role for MB^ds in regulating cell fate determination.

p62, a receptor protein that targets ubiquitinated proteins and aggregates for autophagosomal degradation, was previously shown to be involved in MB^d clearance (Pohl and Jentsch, 2009). Our results, however, suggested that MB^d degradation is not mediated by p62, but by the structurally related receptor NBR1. siRNA-mediated p62 silencing using the published siRNA sequence (Pohl and Jentsch, 2009) did not show any detectable effects on MB^d levels in two different cell lines (HeLa and U2OS; Fig. 2-7b and 2-S6). Moreover, we found no changes in MB^d levels in cells where p62 was completely lost by genetic deletion (Fig. 2-7c) or in cells where p62 was ectopically expressed, in contrast to NBR1-overexpressed cells (Fig. 3-1). Furthermore, our mass spectrometry analysis of NBR1-containing complexes identified more than twenty MB-localized proteins, suggesting them as MB^d substrates for NBR1. However, only two of the high-confidence p62 interactions are known to localize to the MB (Skop et al., 2004; Behrends et al., 2010). These results reinforce that NBR1 and p62 can function in different forms of selective autophagy (Kirkin et al., 2009a; Itakura et al., 2011), and also demonstrate that p62 is not a likely receptor for MB^d autophagic degradation, although it is localized to the mitotic MB at the time of MB ubiquitination (Pohl and Jentsch, 2009). Given that Pohl and Jentsch appeared to analyze both mitotic MBs and MB^ds, whereas we focused solely on MB^ds (see MATERIALS AND METHODS), we have been wondering if the discrepancy between studies is due to the difference in the methods of MB^d quantification. A caveat with quantifying both mitotic MBs and MB^ds is that any

increase in mitotic progression or delay will also affect MB^d levels. Interestingly, the transition from mitosis to interphase is slower in cells that have reduced p62 (Linares et al., 2011). In addition to this, a difference in the efficiency of protein depletion could also be a possible explanation for our discrepant results. We feel this later possibility is less likely as p62 depletion was ~95% (Fig. 2-7b) and MB^d analysis was only done in cells negative for p62 immunofluorescence. However, we could not rule out the possibility that residual p62 that was below the detection limit of immunofluorescence microscopy still mediated MB^d degradation. Future studies that utilize the same MB^d quantification method as well as other known p62 substrates as experimental controls to better demonstrate the loss of p62 will hopefully clarify the role of p62 in MB^d degradation. Additionally, since autophagy receptors function to link selective cargoes to autophagosomes (Kim et al., 2008; Kirkin et al., 2009a; Thurston et al., 2009; Ogawa et al., 2011) and loss of NBR1 leads to a decrease in autophagosome localization of the MB^d (Fig. 2-S5). To demonstrate a role of p62 in acting as an autophagy receptor for the MB^d, it will be necessary to determine if p62 loss also causes a deficit in the autophagosomal encapsulation of MB^ds.

A number of autophagy receptors and adaptors have been identified for selective autophagy. In several cases, autophagy receptors and adaptors act cooperatively to target the designated cargo to Atg8/LC3-positive autophagosomal compartments. NBR1 is so far the only known receptor with substantial function in MB^d degradation, other receptors/adaptors, yet to be tested, may also function in MB^d removal. A recent proteomics study revealed a number of proteins to have high-confidence interactions with

the Atg8/LC3 family homologues, suggesting roles for these proteins in autophagy (Behrends et al., 2010). As some of these proteins (e.g., KEAP1, NIPSNAP1, GBAS, CLTC, and RBICC1) were shown to interact with NBR1 (Chapter III), it is tempting to speculate that these proteins act in concert with NBR1 to mediate MB^d degradation through autophagosome recruitment. Other Atg8 homologue-interacting proteins (identified in Behrends et al., 2010) that do not appear to bind NBR1 could be involved in MB^d degradation in an NBR1-independent manner through binding to other yet unidentified receptors. Future candidate characterization will delineate the mechanisms responsible for MB^d degradation.

The trigger that initiates MB^d degradation at the right time and place is currently unknown. Undoubtedly the cell would have to maintain the MB structure during cytokinesis, as the integrity of the mitotic MB is essential for faithful cell separation (Hu et al., 2012; Joseph et al., 2012). Given that NBR1 is localized to both mitotic MBs and MB^ds, NBR1 may be the trigger that recognizes whether a MB is mitotic or a derivative. Along these lines, NBR1 displays mitotic specific phosphorylation (Fig. 3-4). Therefore, several possibilities arise from our NBR1 phosphorylation mapping results (Fig. 3-5). For example, it would be interesting to examine if the mitosis-specific phosphorylation sites near the LC3-binding region of NBR1 (T743, T749, and T756) serve as an inhibitory regulation to prevent NBR1 from binding to LC3, thereby suspending autophagosomal encapsulation of the MB until abscission is completed. In support of this idea, T743 is a predicted phosphorylation site for PLK1, a kinase with roles in several steps of mitosis, including the formation and maintenance of the MB during cytokinesis (Hu et al., 2012).

Conversely, the NBR1 phosphorylation sites near the LC3-binding regions that are enriched in asynchronous cells may positively regulate MB^d degradation. Of these sites, T658 and T673 are particularly interesting, in that these two sites are predicted binding sites for 14-3-3 proteins. When associated with the mitotic MB, 14-3-3 leads to abnormal MB disintegration before abscission (Joseph et al., 2012). Given that protein phosphorylation has been implicated in the regulation of autophagy receptors, and those modifications occur within the domains commonly shared among autophagy receptors (Matsumoto et al., 2011; Wild et al., 2011), a similar mechanism may exist to regulate NBR1 activity.

In addition to post-translational modifications of the receptor, specific modifications in MB proteins could also trigger degradation. During the final stages of cytokinesis, it is known that MB proteins are ubiquitinated (Pohl and Jentsch, 2008). Since autophagy receptors (e.g., p62 and NBR1) localize to the MB, ubiquitin modification has been suggested to serve as an initial trigger for autophagic degradation of the MB^d (Pohl and Jentsch, 2009). However, this potential mechanism for MB^d degradation initiation has yet to be conclusively tested. Interestingly, Cep55 in NBR1 immunoprecipitates does not appear to have a molecular weight shift for ubiquitin modification in Western blotting analysis (Fig. 2-7d and 2-S9), suggesting that the interaction between NBR1 and Cep55 does not require ubiquitin modification of Cep55. Furthermore, although the MB protein MKLP1 is ubiquitinated during cytokinesis (Pohl and Jentsch, 2008), we were not able to detect MKLP1 in NBR1-immunoprecipitates, demonstrating that ubiquitination is not sufficient to trigger NBR1-mediated MB^d

degradation. Due to NBR1's specificity for non-ubiquitinated Cep55 and its p62-independent role in MB^d clearance, I propose that other modifications beside ubiquitination are used for regulating NBR1-mediated MB^d degradation. Further domain analysis of NBR1 and Cep55 would likely provide more information on this subject with regard to the post-translation modifications within the domains required for their interaction. As many MB-localized proteins are identified in NBR1-containing complexes, it would also be interesting to see if a modification common to all of these proteins is involved in mediating their binding to NBR1.

A question that I am always interested in is how MB^ds in stem cells and cancer cells escape recognition by autophagic machinery. Our results suggest MB^d accumulation in these cell types is dictated partly by the level of autophagic activity because these MB^d-high cells possess lower basal autophagic activity compared to MB^d-low cells and MB^d levels are reduced upon autophagy induction (Fig. 2-6). In support of this idea, constitutive activation of the PI3K-Akt-mTOR signaling pathway, which negatively regulates basal autophagy, often occurs in cancer cells (reviewed in Menon & Manning 2008; Laplante & Sabatini, 2012). Additionally, MB^d accumulation is controlled by the amount of autophagy receptor, since exogenous NBR1 can further promote MB^d degradation in autophagy-component cells (Fig. 3-1). The amount of a given protein is determined by the balance between its synthesis and degradation. NBR1 degradation is mediated by autophagy (Kirkin et al., 2009a), therefore NBR1 levels could be higher in autophagy-low stem and cancer cells, compared to autophagy-high normal differentiated cells. However, the synthesis of NBR1 have not been examined in cells with different

differentiation status. It thus will be interesting to test if stem and cancer cells regulate NBR1 synthesis differently compared to normal dividing cells. It's also possible that cancer and stem cells have distinct NBR1 or MB^d modifications that prohibit the MB^d from degradation.

In contrast to the idea that the MB^d fate is passively determined by the cellular autophagy activity, the MB^d itself could regulate its own degradation through recruiting or releasing factors crucial for autophagy induction. Such factors could be mediators involved in the PI3K-Akt-mTOR signaling cascade that negatively regulates autophagy (Fig. 1-1; reviewed in Yang & Klionsky, 2010). Active mTOR associates with the MB during cytokinesis as indicated by its serine2481 autophosphorylation form (Peterson et al., 2000; Copp et al., 2009; Vazquez-Martin et al., 2009 and 2012; Soliman et al., 2010). Moreover, the active form of the mTORC1 upstream effector, Akt, is also localized to the MB (Mao et al., 2012; A. Purohit and S. Doxsey, unpublished results). Furthermore, MB^(d) protein Cep55 is known to interact with the PI3K complex and enhances the kinase's activity (Chen et al., 2007). Collectively, these results indicate active PI3K-Akt-mTOR signaling on the MB and also suggest a possibility of the MB^d in the control of its own fate.

Perhaps the most intriguing question raised by this thesis study is how MB^ds contribute to tumorigenicity and pluripotency. Despite limited information on MB^d composition, several MB^d proteins have been individually associated with stem cell maintenance and cancer progression. For instance, the expression of MgcRacGAP is required for stem cell self-renewal and is declined during differentiation (O'Brien et al.,

2010). Similarly, elevated expression of Cep55 or PLK1 has been found in various tumors and is associated with tumorigenicity (Holtrich et al., 1994; Takai et al., 2005; Chen et al., 2007; Inoda et al., 2009). These results together with the finding that stem cell marker CD133 associates with MB^ds (Fig. 2-2d and 2-S2) suggest a scaffolding role for MB^ds in organizing cell fate determinants. More specifically, given that Cep55 promotes tumorigenicity by enhancing PI3K kinase activity and signaling, and that CD133 represses cell differentiation through p38 MAPK activation (Chen et al., 2007; Takenobu et al., 2011), it is tempting to speculate that MB^ds may serve as a hub to orchestrate various signaling pathways required for maintaining tumorigenicity and pluripotency. Further studies to determine the MB^d proteome will provide more information on associated signaling molecules. Certainly, to establish a role for the MB^d in serving as a signaling hub, investigations are needed to determine if the MB^d localization of aforementioned signaling molecules is essential for their function.

Autophagy is an essential cell makeover process used during mammalian developmental stages (Cecconi and Levine et al., 2008; Mizushima and Levine, et al., 2010). At the cellular level, autophagy induction along with cell differentiation has been observed in several types of stem cells, including embryonic stem cells and adult stem cells (Fig. 2-6g; Vazquez et al., 2012; Zhang et al., 2012). Although the mechanisms by which autophagy participates in these processes are not clear, it is possible that autophagy influences cell fate by removing cell fate molecules and organelles, a hypothesis that is supported by our studies. In line with this idea, autophagic degradation of the oncoprotein PML-RARa is required for poorly-differentiated leukemia cells to differentiate (Isakson

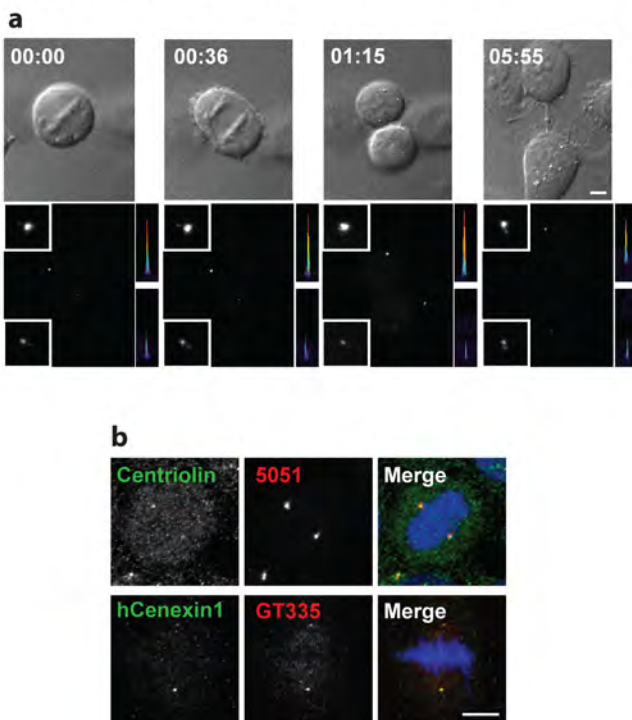
et al., 2010; Wang et al., 2011). Other molecules known to control cell fate decisions, such as Dishevelled in Wnt signaling, have also been identified as targets of selective autophagy (Marson et al., 2008; Gao et al., 2010). Autophagy could therefore act as a transcription-independent mechanism in regulating cell differentiation. A global characterization of autophagy receptors and their substrates during stem cell differentiation and induced pluripotency will provide invaluable information to construct a mechanism for the role of autophagy in cell differentiation.

Several alternative explanations for MB^d accumulation and function remain possible at this stage, as we haven't been able to determine MB^d function by directly removing the MB^d. Given that PI3K protein level can be variable from cell to cell (Yuan et al., 2011), it is possible that autophagy is heterogeneous in a given cell population and that MB^d accumulation simply reflects the heterogeneity of autophagy. Alternatively, since autophagy is required for the homeostasis of various proteins and organelles under basal condition and since several selective autophagy pathways exist, it is not unreasonable to speculate that some selective autophagy pathways are more favorable than others by the cell under low autophagy condition. According to these ideas, the effects we observed from MB^d enrichment represent simply the functions of other autophagy substrates or the importance of their homeostasis. To address these concerns, we could ask if depletion of other known autophagy substrates would totally abolish the effects of MB^d enrichment on cellular reprogramming and tumorigenicity. We could also examine if a block in NBR1-mediated autophagy expedites other selective autophagy pathways, such as the degradation of mitochondria. However, since the identity and

function of autophagy substrates are largely unknown, strategies that attack MB^d function without compromising autophagy are inevitable and essential in order to uncouple the effects of MB^d accumulation from general autophagy. As discussed above, investigation of a unique molecular trigger for MB^d degradation would likely enable the development of methods that specifically manipulate MB^d fate during cell fate changes. Meanwhile, exploring signaling pathways at the MB^d would hopefully shed light on the role of MB^ds in stem and cancer cells.

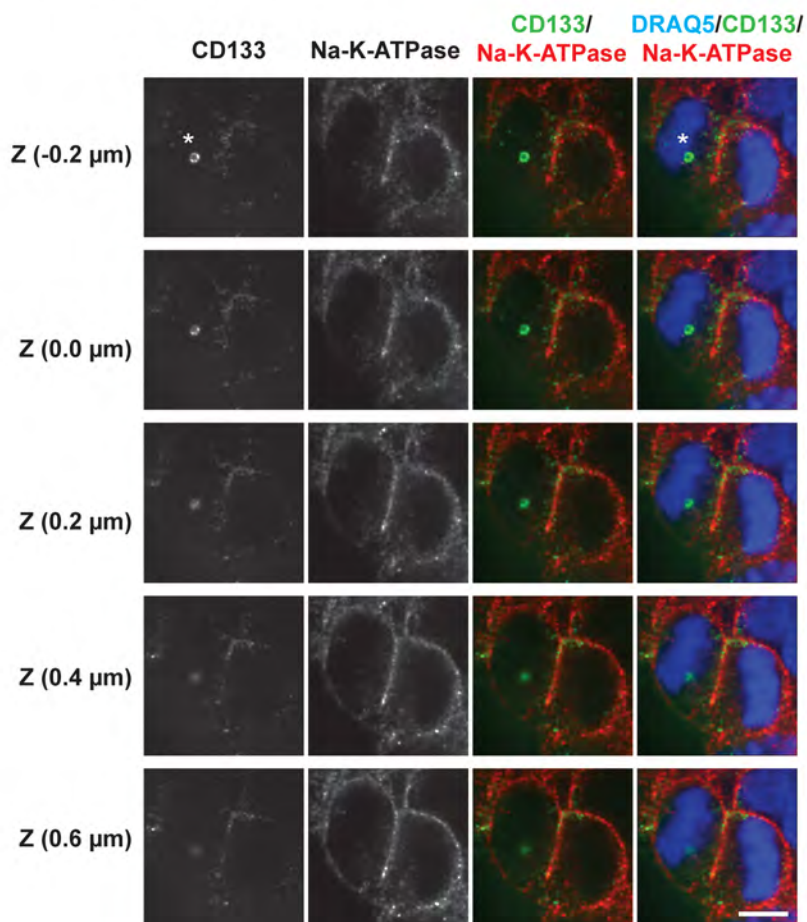
In conclusion, this thesis delineates the molecular mechanism for receptor-mediated autophagic degradation of the post-mitotic midbody. Not only did I identify the MB^d as a cargo for the autophagy receptor NBR1, but also I provided the mechanism for how the MB^d is targeted by autophagy. I also presented evidence identifying the mechanism for MB^d accumulation and the functional consequences of MB^d accumulation in cells with differentiating capabilities. In addition, these findings offer initial understanding of the interplay between selective autophagy and cell differentiation. Although the exact role of MB^ds has yet to be determined, this work certainly opens up many new avenues for future investigation.

Supplementary Figure 2-S1



Supplementary Figure 2-S1 Different-aged centrosomes in dividing cells show differential labeling for the components and modification of centrosomes. (a) Older/more mature centrosome retains the brighter CETN1-GFP signal throughout the mitotic cell cycle. Left to right: metaphase, anaphase, telophase and cytokinesis. **(b)** The centrosome pairs in representative mitotic cells show differential labeling of centriolin (top panel, green), hCenexin1 (bottom panel, green) and glutamylated tubulin (GT335; bottom panel, red). Centriolin and hCenexin1 are markers for centriole maturation, and glutamylated tubulin for tubulin modification at centrioles, respectively. Centrosomes are labeled by human autoimmune antibody 5051 (top panel, red). DAPI stains DNA (blue). Bar, 5 μ m.

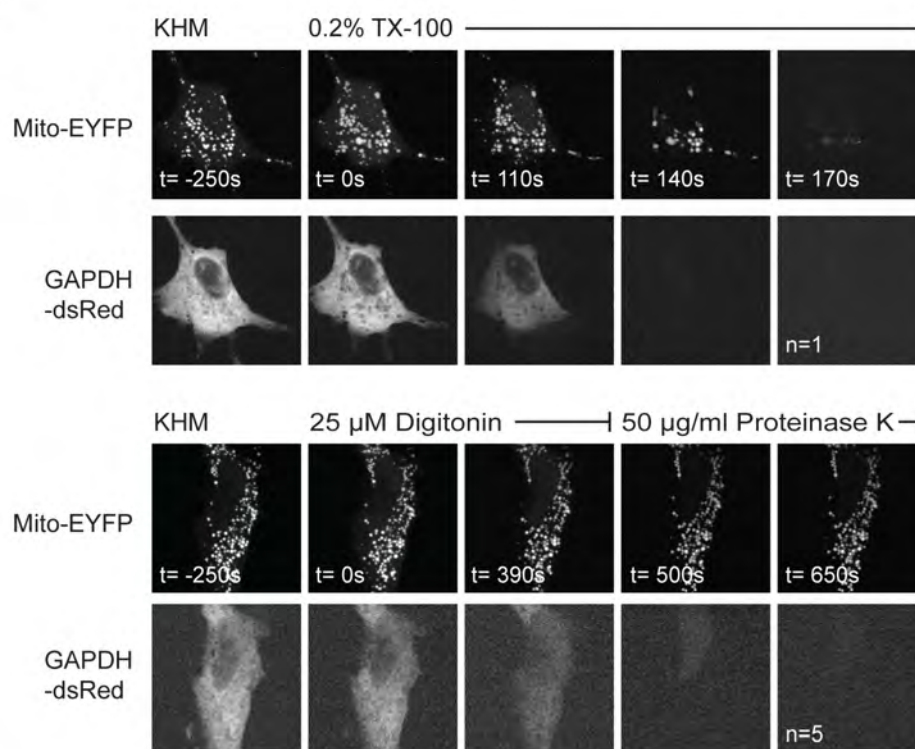
Supplementary Figure 2-S2



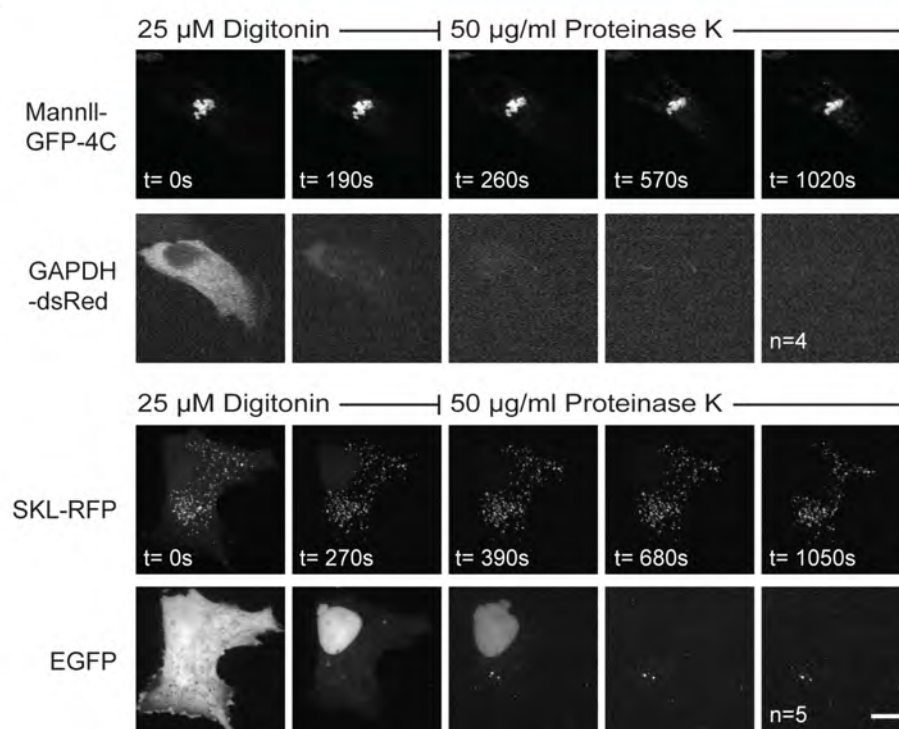
Supplementary Figure 2-S2 Multiple planes of confocal images demonstrate that the MB^d (asterisk) in the ventricle-facing daughter of the dividing neural progenitor is intracellular (also shown in Fig. 2-3d). CD133, MB/MB^d marker (green); Na-K-ATPase, cell-border marker (red); DRAQ5, DNA (blue); Bar, 5 μ m.

Supplementary Figure 2-S3

a

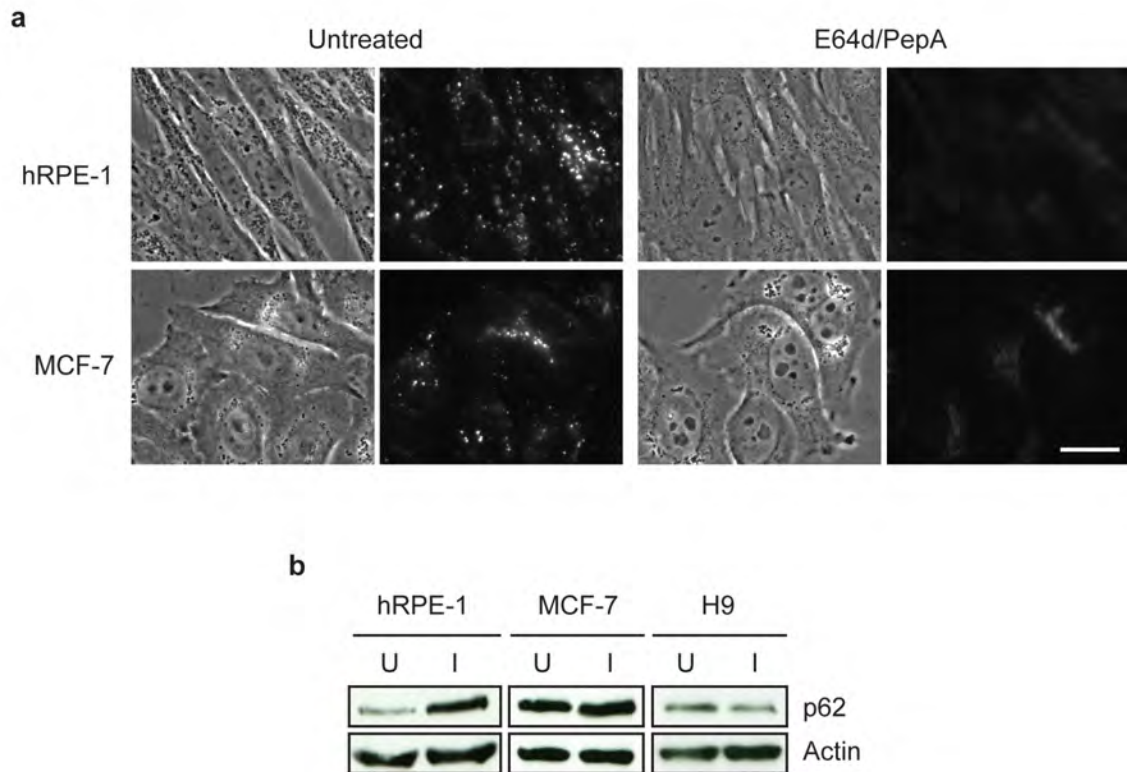


b



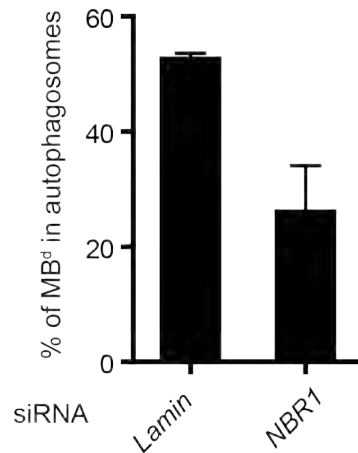
Supplementary Figure 2-S3 Organelles respond to digitonin treatment as expected. (a, b) Membranous organelles are not disrupted during digitonin-mediated permeabilization in FPP assays. (a) hRPE-1 cells expressing Mito-EYFP to label mitochondria, and GAPDH-dsRed to mark cytoplasm, are pre-incubated in KHM buffer (110 mM potassium acetate, 20 mM HEPES, 2 mM MgCl₂), and then treated either with 0.2% TX-100 (top panel) or with 25 μM digitonin (bottom panel). TX-100 releases both GAPDH and Mito-EYFP from cells, whereas digitonin releases only GAPDH and does not disrupt mitochondrial integrity as shown by the retention of Mito-EYFP in the presence of Proteinase K. (b) hRPE-1 cells expressing MannII-GFP-4C, a Golgi complex marker (top panel), or SKL-RFP, a peroxisome marker (bottom panel), are treated with digitonin followed by proteinase K digestion as in (a). The fluorescent proteins in Golgi complex and peroxisomes are resistant to proteinase K digestion after digitonin-mediated permeabilization, showing that the Golgi complex and peroxisomes are intact. Other organelles were also examined to ensure their integrity. Similar results were observed in HeLa cells. Bar, 5 μm.

Supplementary Figure 2-S4



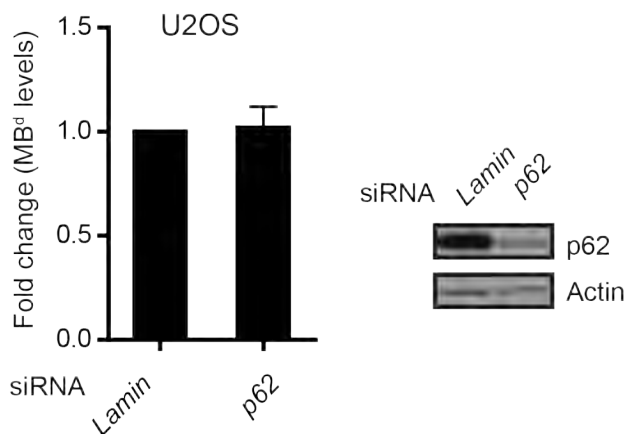
Supplementary Figure 2-S4 Effects of lysosomal inhibition. (a) Lysosomal activity is visualized by fluorescent DQ-BSA. DQ-BSA substrates fluoresce when degraded in lysosomes (left, untreated) but not when lysosomal enzymes are blocked (right panels), confirming function of inhibitors. Bar, 20 μ m. (b) Use of p62, another protein degraded by autophagy, as an indicator of autophagic flux confirms LC3-II results (Fig. 2-6d). I, inhibited by lysosomal inhibitors as in Fig. 2-6d. U, uninhibited. Actin, loading control.

Supplementary Figure 2-S5



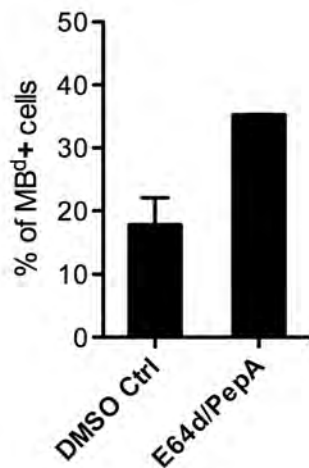
Supplementary Figure 2-S5 NBR1 depletion impedes autophagosome capturing of MB^ds. HeLa cells were transfected with siRNA against Lamin or NBR1 as indicated for 24 hours before bafilomycin A1 was added to block the fusion of autophagosomes with lysosomes. Twenty-two hours after bafilomycin A1 treatment, cells were fixed and immunostained for autophagosome marker LC3, midbody marker MKLP1, and α -tubulin, mitotic MB and cell boundary marker. The percent of MB^ds in autophagosomes is evidently decreased following NBR1 depletion. The average of two independent experiments is shown. Error bars represent standard deviations.

Supplementary Figure 2-S6



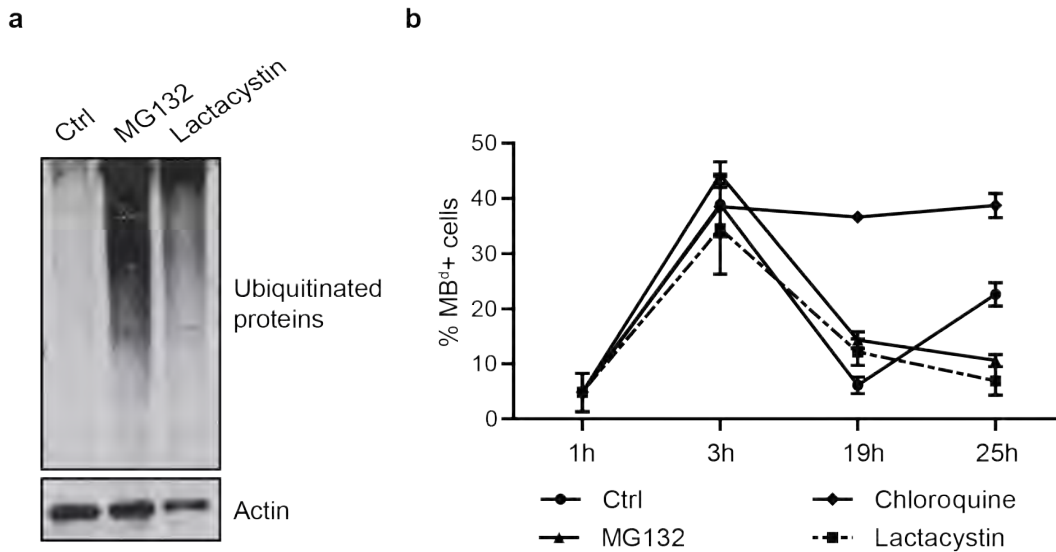
Supplementary Figure 2-S6 p62 depletion does not affect MB^ds in U2OS cells. U2OS cells were transfected with siRNA against Lamin or p62 as indicated for 48 hours. Cells were then fixed and immunostained for p62, midbody marker MKLP1, and α -tubulin, mitotic MB and cell boundary marker. In cells transfected with p62 siRNA, only cells negative for p62 immunofluorescence were analyzed. MB^d levels (percent of MB^d-containing cells) are not affected by p62 depletion. The average of two independent experiments is shown. Error bars represent standard deviations.

Supplementary Figure 2-S7

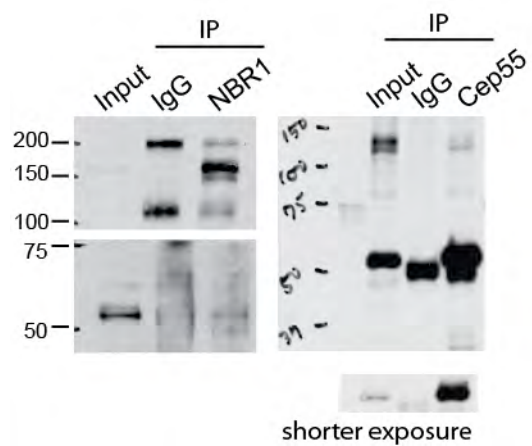


Supplementary Figure 2-S7 An unidentified lysosomal degradation pathway compensates for autophagy deficiency. Lysosomal inhibitor E64d/PepA treatments further increase the percent of MB^d+ cells in atg5 knockout cells where autophagy is deficient, suggesting a yet identified lysosomal degradation pathway compensates for autophagy deficiency (p=0.0099, n=3).

Supplementary Figure 2-S8



Supplementary Figure 2-S8 The proteasome does not play a role in MB^d degradation. (a) Ubiquitinated protein levels, assessed by anti-ubiquitin antibody, increase in cells treated with proteasome inhibitors (MG132, lactacystin) as indicated, confirming proteasome inhibition. (b) Proteasome inhibition has no significant effect on MB^d degradation in hRPE-1 cells compared with the lysosomal inhibitor chloroquine. It only slightly slows the process of MB^d clearance, as control cells have removed most MB^ds by 19 hours. They reenter mitosis and begin to make additional MB^ds from 19-25 hours. Assays were performed by collecting mitotic cells after mitotic shake-off and treating cells with drugs 1 hour after re-plating, when most cells were in cytokinesis. This is to avoid arresting cells in mitosis and thus blocking MB formation. MB^d levels (the percent of MB^d+ cells) are determined as described above.



Supplementary Figure 2-S9 Full scan data of immunoblots in Fig. 2-7d.

Supplementary Table 2-S1

	1	2	3	4	5	6	7	8	9
dH1f									
experiment	1	2	3	4	5	6	7	8	9
shNT	137	466	250	9	11	20	88	78	120
shNBR1	242	708	703	56	96	91	160	280	210
dH1f-continued									
experiment	10	11	12	13	14	15			
shNT	21	27	24	39	47	27			
shNBR1	71	26	70	84	72	56			
IMR90									
experiment	1	2	3						
shNT	14	49	125						
shNBR1	59	199	222						
hFib2									
experiment	1	2	3	4	5	6			
shNT	27	51	28	423	411	501			
shNBR1	39	64	69	662	771	656			

Supplementary Table 2-S1 Reprogramming is more efficient following an increase in MB^d levels by NBR1 depletion. Fibroblast-like cells differentiated from H1-OGN (dH1f), human embryonic fibroblasts (IMR90), and human adult fibroblasts (hFib2) selected for stable expression of NBR1-specific (shNBR1) or non-targeting shRNA (shNT) are reprogrammed (Fig. 2-8a, b). The numbers of iPSC colonies in each reprogramming experiment are summarized in the table.

Supplementary Table 2-S2

MB protein (Homo sapiens)	Position (amino acid)	sequence	Representation
MKLP1	85 - 89	QKELF	Q + - Φ Φ
	352 - 356	NRLRE	
	554 - 558	QKLEI	
Cep55	85 - 89	QRLRD	Q + Φ + +
	305 - 309	QKLRE	
	418 - 422	NREKV	
MgcRacGAP	101 - 106	QLIRE	Q Φ Φ + +
	519 - 523	QDIKR	

Supplementary Table 2-S2 MB^d proteins contain KFERQ-like motif. Protein substrates for chaperone-mediated autophagy contain in their amino-acid sequence a pentapeptide KFERQ-like motif, which is recognized by Hsc70, the cytosolic chaperone of 70 kDa. Hsc70 unfolds substrates for translocation into the lysosome by lysosome-associated membrane glycoprotein 2A (LAMP-2A), which results in substrate degradation (Majeski and Dice, 2004). Basic amino acid (K, R; +); Acidic (D, E; -); Bulky hydrophobic (F, I, L, V; Φ).

MATERIALS AND METHODS

Chapter II:

Cell lines. hESC and iPSC lines include H1 (WA01), H9 (WA09), H1-OGN (Oct4-EGFP knock-in H1, Zwaka and Thomson, 2003), and dH1f-iPS (Park, et al., 2008), which is reprogrammed from dH1f cells differentiated from H1-OGN (HSCI at Children's Hospital Boston). Differentiated lines include hRPE-1 (Clontech), MCF-10A, adult human fibroblasts (PCS-201-012, ATCC), hFib2 (Zwaka and Thomson, 2003), IMR90 (CCL-186, ATCC), *ex vivo* C57BL/6 MEFs, GFP-LC3-expressing *Atg5*^{-/-} and *Atg5*^{+/+} MEFs (Kuma et al., 2004), and *p62*^{-/-} and *p62*^{+/+} MEFs (Komatsu et al., 2007). Cancer cell lines include DLD-1, HeLa, NCC-IT, PC-3, U2OS, SAOS-2, 134-4, MCF-7, MCF-10AT, and MCF-10CA1a. Mouse skeletal muscle progenitors (SMPs; Conboy et al., 2010) and *in vitro* activated T cells were isolated and stimulated following standard protocols. Cells were used within 4 (primary cultures) or 10 (established cell lines, hESCs, and iPSCs) passages. Cells expressing MKLP1-GFP, monomeric RFP and CETN1-GFP were created in the present study or in Piel et al., 2000.

Immunofluorescence and Immunohistochemistry. Immunofluorescence was carried out as described (Gromley et al., 2005; Marzesco et al., 2005; Xu et al., 2010). To label lysosomes and autophagosomes, cells were permeabilized with 0.05% saponin in blocking buffer (10% goat serum/PBS). Preparations for immunohistochemistry were fixed with 4% paraformaldehyde/0.5% glutaraldehyde via perfusion. Testes were processed and stained following 2-4hr post-fixation with 4% paraformaldehyde. MB-

derived rings between spermatocyte syncytia (Greenbaum et al., 2007) were observed if stained longer. Images were taken on a Zeiss Axioskop 2 microscope, a Zeiss Axiovert 200 microscope with PerkinElmer UltraView LAS spinning disc, or an Olympus BX-51 microscope. Images were processed and analyzed with MetaMorph (Molecular Devices) and Imaris (Bitplane Inc.).

Electron Microscopy. *Conventional EM:* Mouse tissue, fixed with 5% glutaraldehyde in 50 mM sodium cacodylate buffer (pH=7.4) for 30 min via perfusion, was diced into 1-mm cubes for 1-hr post-fixation at 4°C. Cubes were washed with cacodylate buffer, stained and embedded in Spi-pon/Araldite, and sectioned at 70-500 nm before staining with 25% uranyl acetate and Reynold's lead citrate. Images were taken on a Philips CM12 electron microscope with an Erlangshen CCD Camera (Gatan).

Immunogold EM: MCF-7 cells on coverslips were permeabilized for 60 sec with permeabilization buffer (80 mM PIPES, pH6.8, 0.5 mM EGTA, 1 mM MgCl₂, 0.5% Triton X-100), fixed with 4% paraformaldehyde for 10 min, labeled for MKLP1 for 1 hour, processed as described (Mitchison, et al., 1986) using 12-nm gold-conjugated goat anti-rabbit IgG (Jackson ImmunoResearch) and embedded in Spi-pon/Araldite. 80-nm sections were cut, stained and viewed as above.

Time-lapse imaging. CETN1-GFP-expressing lines were grown on 35-mm MatTek dishes (MatTek Corp.) or coverslips before imaging (Gromley et al., 2005). H9 hESCs were seeded on matrigel-coated dishes overnight, then transduced with CETN1-GFP, and grown for >72 hours in complete mTeSR1 medium (Stemcell Technologies). The

transduced cells were imaged every 15 min in phenol red-free D-MEM/F12 medium (Invitrogen) with mTeSR1 supplement and 10 mM HEPES, and stained to confirm MB^d inheritance. Duplicate dishes of transduced cells were stained for stem-cell markers to ensure cell quality.

MB^d quantification. Quantification was based on the markers that: 1) labeled both mitotic MBs and MB^ds (MKLP1, mgcRACGAP, or Cep55); 2) labeled MBs differently than MB^ds (α-tubulin or Aurora B); 3) defined cell boundaries (α-tubulin or ZO-1). Because Cep55, MKLP1, and mgcRACGAP also label centrioles and spindle midzones, cells were co-stained with centrosome antibody (e.g. 5051), and a size threshold for MB/MB^ds (1 μm) was introduced to exclude non-MB^d structures. Structures with MB-specific or non-MB/MB^d labeling were excluded from MB^d counts. Cell counts: For hESCs, 5-11 colonies were imaged from triplicates in each experiment. For other cell types, random fields were imaged until $n > 500$ cells. Each dividing cell was considered one cell.

Doubling time calculations. Cells were seeded ($1-1.5 \times 10^5$ per 60-mm dish), and total cell counts were taken by hemocytometer every 24 hours for 4 days. Alternatively, cells were seeded ($2.5-5.0 \times 10^3$ per well, 96-well plates), and the absorbance from an MTS-based colorimetric assay (#G3582; Promega Corp.) was used to estimate cell counts every 24 hours. Timepoints vs. Log_{10} (average cell counts or absorbance at that time) was plotted and the slope ascertained. $T_{1/2} = \text{Log}_{10}(2) / \text{slope}$. For some cell lines, both methods were used and gave similar results.

MB^d localization assays. *Extracellular trypsin treatment:* MKLP1-GFP-expressing HeLa cells grown in MatTek dishes were imaged every 3 min, and underwent no morphological changes upon replacement of media with PBS. After trypsin addition, GFP+ MB^ds were monitored for 60-90 min for intensity reduction (degradation) or detachment from cells (dissociation).

Co-culture assay: Equal numbers of monomeric RFP- or MKLP-GFP-expressing cells were seeded and co-cultured in 60-mm dishes with coverslips. Cells were stained 2 days later, and the percentage of GFP+ MB^ds associated with RFP+ cells was determined.

FPP assay: The FPP assay was carried out as reported (Lorenzet al., 2006) except cells were plated in MatTek dishes 24 hours before co-transfection of MKLP1-GFP and GAPDH-dsRed (Lipofectamine 2000, Invitrogen). Cells were permeabilized and then digested with proteinase K (50 $\mu\text{g ml}^{-1}$). Constructs labeling mitochondria, peroxisomes, endoplasmic reticulum and Golgi were used as controls.

Lysosome and proteasome assays. Cells at 70% confluency were incubated with chloroquine (200 μM /PBS; Sigma), E64d + pepstatin A (E64d/PepA) (10 $\mu\text{g ml}^{-1}$ /DMSO each; Sigma; Komatsu et al., 2007; Klionsky et al., 2008) or solvents alone (controls) for 22 hours before fixation. Lysosome inhibition was confirmed and visualized after 12-hour DQ-Red BSA (10 $\mu\text{l ml}^{-1}$; Invitrogen) incubation. Mitotic hRPE-1 cells were treated with proteasome inhibitors, MG132 (1 μM ; Sigma) or lactacystin (50 μM ; Sigma) 1 hour after replating.

Autophagy manipulation assays. MB^ds were quantified in more than 500 cells in triplicate unless otherwise noted.

Protein depletion: siRNAs targeting human Atg7 (Yu et al., 2004), p62 (Pohl and Jentsch, 2009), NBR1 (Kirkin et al., 2009; 2503-2521 base pairs, GenBank NM 005899), Lamin A/C (Gromley et al., 2005), and GFP (5'-NNCAUGAAGCAGCAGCAGACUUC-3') were from Dharmacon. MB^d levels were analyzed 48 hours after 1 nmol siRNA transfection (Oligofectamine, Invitrogen) in HeLa cells, whereas in U2OS cells MB^d levels were analyzed 30 hours after 100 nM siRNA transfection (Nucleofector, Amaxa) as previously described (Pohl and Jentsch, 2009). For NBR1 and p62 experiments, only cells negative for p62 and/or NBR1 immunofluorescence were analyzed.

Beclin1 (BECN1) overexpression: MB^d levels were analyzed in 265 Flag+ and 2200 control MCF-7 cells 48 hours after Flag-BECN1 (4 µg) or mock nucleofection (Amaxa).

LiCl + rapamycin treatment: MB^d levels in HeLa cells were examined 24 hours after treatment with LiCl (10 mM; Sigma) and rapamycin (200 nM; Calbiochem), or with DMSO.

CEP55-EGFP overexpression: MB^d levels and its NBR1-association were assessed in hRPE-1 cells (1X10⁵ per well, six-well plates) 48 hours after CEP55-EGFP (1 µg), EGFP (1 µg), or mock transfection.

Bafilomycin A1 treatment: HeLa cells were transfected with siRNA against Lamin or NBR1 as described above for 24 hours before bafilomycin A1 (100 nM; Sigma) was added to block the fusion of autophagosomes with lysosomes. Twenty-two hours after bafilomycin A1 treatment,

cells were fixed and immunostained.

Biochemical assays. Protease and phosphatase inhibitors, cell lysates, SDS-PAGE and immunoblotting were purchased or carried out as described (Gromley et al., 2005) unless specified.

Autophagy activity: The activity of autophagy was determined by measuring autophagy flux: the amount of autophagic cargo that is delivered to lysosomes for degradation (i.e. the amount of autophagic cargo that is accumulated upon lysosomal inhibition in a given time period). E64d/PepA treatment was used to block lysosomal enzyme activity and lipidated LC3 (LC3-II), an autophagic cargo, was used to assess autophagic flux (Bjorkoy et al., 2005; Komatsu et al., 2007; Mizushima and Yoshimori, 2007; Klionsky et al., 2008). Lysates of E64d/PepA and DMSO treated cells were blotted for α -tubulin and LC3. LC3-II levels were then determined and normalized to α -tubulin using ImageJ. Autophagic flux = 100 [1– (LC3-II level in control lysates/ LC3-II level in E64d/PepA treated lysates)].

Immunoprecipitation: hRPE-1 cell lysates (50 mM Tris-HCl pH 7.5, 150 mM NaCl, 2 mM EDTA, 1 mM EGTA, 1% Triton X-100, 10% glycerol, 4°C) were pre-cleared for 1 hour with protein G-plus conjugated agarose beads (Santa Cruz) at 4°C, incubated with 2 μ g normal IgG, anti-Cep55 or anti-NBR1 antibodies for 3 hours at 4°C, and incubated overnight at 4°C with 25 μ l protein G-plus beads. Following washes with lysis buffer and elution, immunoprecipitated proteins were analyzed by SDS-PAGE and immunoblotting.

Assays for MB^d function. *Cellular reprogramming:* Viral production, transduction and reprogramming were performed as described (Yu et al., 2007; Park et al., 2008, Chan et al., 2009, Loewer et al., 2010). Commercially-available shRNA against NBR1 (pSM2c-shNBR1, V2MM_36901; 4-22bp, GenBank NM 005899) was cloned into pGIPZ lentiviral vector (Open Biosystems). Embryonic fibroblasts (IMR90), adult fibroblasts (hFib2) and dH1f cells were transduced with either NBR1-specific or non-targeting shRNA vector, and puromycin-selected to establish NBR1-depleted (shNBR1) and control (shNT) lines. dH1f (2.5×10^4 per assay) were reprogrammed with lentiviral vectors (Yu et al., 2009; Addgene #21162 and 21164) expressing *OCT4*, *SOX2*, *KLF4* and *c-MYC* (Park et al., 2008, Chan et al., 2009, Loewer et al., 2010) whereas the reprogramming of IMR90 and hFib2 cells (5×10^4 per assay) also included lentiviral vectors expressing Nanog and Lin28 (Yu et al., 2007, 2009; Addgene #21163). iPSC colonies were quantified on day 21 based on Tra-1-60 expression using ImageJ, as reported (Chan et al., 2009; Loewer et al., 2010) and with parameters: ≥ 148 (threshold), 0.5-1 (circularity), and either 10-infinity or 30-infinity (size).

Side Population (SP) assay: The assays were carried out as previously described (Engelmann et al., 2008) in MCF-7 cells. The MB^d levels in SP and non-SP populations were determined as described above.

Soft-agar assays: “MB^d high” and “MB^d low” subpopulations of MKLP1-GFP-expressing HeLa cells were separated by FACS, and plated in soft-agar (2.5×10^4 per well, 6-well plates). The MB^d levels were determined 12-15 hours after plating aliquots

of subpopulations onto coverslips. For the NBR1-silencing soft-agar assay, NBR1-depleted (shNBR1) and control (shNT) cells (1×10^5 per 100-mm dish) were plated. For both assays, cells were grown for ~3 weeks at 37°C, and stained as described (Sachdev et al., 2009). Colonies were quantified microscopically, and the average from triplicate wells or plates presented.

Antibodies. Antibodies to the following proteins/tags were used in this study: Atg5 (1:2000, Cosmo Bio, CAC-TMD-PH-ATG); Atg7 (1:1000, ProSci, 3617); Actin (1:300, Sigma, AC-40); Aurora B (1:100, BD Trans Lab, 611082); CD13 (1:50, BioLegend, 301707); CD133 (1:200, eBioscience, 14-1331); Cep55 (1:50, 1:100 and 1:1000 for immunofluorescence, Abnova #H00055165-B01, Abnova #H00055165-A01, and the gift from K. Kurtche, respectively; 1:500 for immunoblotting, Genetax #GTX112190); hCenexin1 (1:100, a gift from K.S. Lee); Centriolin (1:200, ref. 9); Flag (1:200, Sigma, F7425); GAPDH (1:8000; Santa Cruz, SC-32233); GFP (1:1000; Abcam, ab6556 and Santa Cruz, sc-9996); GT335 (1:100; a gift from P. Denoulet); b1-Integrin (1:50; BD Phramingen); K15 (1:100; Lab Vision, MS-1068-P); LC3 (1:10 for immunofluorescence, Nano Tools, LC3-5F10; 1:300 for immunoblotting, Novus Bio NB100-2331); LAMP2 (1:50, H4B4 from DSHB); mgcRACGAP (1:500, Abcam, ab2270); MKLP1 (1:1000 for immunofluorescence, 1:200 for immunohistochemistry, 1:10 for immuno-EM, Santa Cruz, sc-867); NBR1 (1:500, Abnova, H00004077-B01P); p62, human samples (1:500, BD Trans Lab, 610833); p62, mouse samples (1:1000, Progen, GP62-C); RFP (1:200, Clontech, 632496); Na-K-ATPase (1:15, a6F from DSHB); α -tubulin (1:100 for immunofluorescence, 1:400 for immunoblotting, Sigma, T9026a; 1:100 for

immunofluorescence, Millipore, CBL270); α -tubulin-FITC (1:300, Sigma, F2168); Tra-1-60-biotin (1:200, eBioscience, 13-8863); Ubiquitin (1:2000, BD BioSci, #550944); WGA-Alexa Fluor 555 (1:200, Molecular Probes, W32464); ZO-1-FITC (1:50, Zymed, 33-9111).

Statistics. Data was analyzed by Student's one-tailed paired *t*-test or unpaired with Welch's correction unless specified. One-way ANOVA was used in conjunction with Tukey's test for comparisons among multiple groups. For the EdU-labeling assay, the EdU intensity was first logarithmically transformed for the use of one-way ANOVA. Statistically analyzed experiments were completed at least 3 times.

Chapter III:

Cell lines and plasmids. MAP vector was kindly provided by Dr. Dannel McCollum (University of Massachusetts Medical School; Ma et al., 2012). Plasmid pEGFP-p62 was a gift from Dr. Terje Johansen (University of Tromsø, Tromsø, Norway; Lamark et al., 2003). Alf_y truncations (pDEST-Tomato-Alf_y) were described previously (Filimonenko et al., 2010) and were kindly provided by Dr. Anne Simonsen (University of Oslo, Oslo, Norway). Establishment and cell synchronization of U2OS cells expressing NBR1-MAP or MAP were performed based on Ma et al., 2012.

NBR1, p62, or Alf_y overexpression. MB^d levels were assessed in HeLa cells (1X10⁵ per well, 6-well plates) 48 hours after plasmid cDNA transfection (1 µg for all plasmids). Transfection was carried out using Fugene 6 (Roche).

Comparative Proteomics. The protein set for the p62 interactions was obtained from Behrends et al., 2010. For proteins identified in this study, the unique UniProt accessions were mapped to gene names using UniProt KB. Accessions that didn't map successfully in UniProt KB were manually analyzed. These lists of proteins were then compared in Microsoft Excel 2011 using PivotTable.

Antibodies. Antibodies to the following proteins were used in this chapter: MKLP1 (1:1000 for immunofluorescence, Santa Cruz, sc-867); MYH9 (1:50 for immunofluorescence, Santa Cruz, sc-47199); NBR1 (1:50, Abnova, H00004077-B01P); PLK1 (1:500, 05-844, EMD Millipore); α-tubulin (1:100 for immunofluorescence, Millipore, CBL270).

REFERENCES

- Anderson, C.T. and Stearns, T. (2009). Centriole age underlies asynchronous primary cilium growth in mammalian cells. *Curr. Biol.* 19, 1498-502.
- Barr, F.A. and Gruneberg, U. (2007). Cytokinesis: placing and making the final cut. *Cell*, 131, 847-60.
- Barroca, V. et al. (2009). Mouse differentiating spermatogonia can generate germinal stem cells in vivo. *Nat. Cell Biol.* 11, 190-6.
- Behrends, C., Sowa, M. E., Gygi, S. P., & Harper, J. W. (2010). Network organization of the human autophagy system. *Nature*, 466(7302), 68–76.
- Berry, D. L., & Baehrecke, E. H. (2007). Growth Arrest and Autophagy Are Required for Salivary Gland Cell Degradation in *Drosophila*. *Cell*, 131(6), 1137–1148.
- Bilgüvar, K. et al., (2010). Whole-exome sequencing identifies recessive WDR62 mutations in severe brain malformations. *Nature* 467, 207-10.
- Bjorkoy, G. et al. (2005). p62/SQSTM1 forms protein aggregates degraded by autophagy and has a protective effect on huntingtin-induced cell death. *J. Cell Biol.* 171, 603-14.
- Carlton, J.G., and Martin-Serrano, J. (2007). Parallels between cytokinesis and retroviral budding: a role for the ESCRT machinery. *Science* 316, 1908–1912.
- Cecconi, F. and Levine, B. (2008). The role of autophagy in mammalian development: cell makeover rather than cell death. *Dev. Cell* 15, 344-57.
- Cemma, M., Kim, P. K., & Brumell, J. H. (2011). The ubiquitin-binding adaptor proteins p62/SQSTM1 and NDP52 are recruited independently to bacteria-associated microdomains to target *Salmonella* to the autophagy pathway. *Autophagy*, 7(3), 341–345.
- Chai, Y., Tian, D., Yang, Y., Feng, G., Cheng, Z., Li, W., & Ou, G. (2012). Apoptotic regulators promote cytokinetic midbody degradation in *C. elegans*. *J Cell Biol.* 199 (7):1047-55.
- Chan, E.M. et al. (2009). Live cell imaging distinguishes bona fide human iPS cells from partially reprogrammed cells. *Nat. Biotechnol.* 27, 1033-7.
- Chen, C.-H., Lu, P.-J., Chen, Y.-C., Fu, S.-L., Wu, K.-J., Tsou, A.-P., et al. (2007). FLJ10540-elicited cell transformation is through the activation of PI3-kinase/AKT pathway. *Oncogene*, 26(29), 4272–4283.

- Clausen, T. H., Lamark, T., Isakson, P., Finley, K., Larsen, K. B., Brech, A., et al. (2010). p62/SQSTM1 and ALFY interact to facilitate the formation of p62 bodies/ALIS and their degradation by autophagy. *Autophagy*, 6(3), 330–344.
- Conboy, M.J., Cerletti, M., Wagers, A.J. and Conboy, I.M. (2010). Immuno-analysis and FACS sorting of adult muscle fiber-associated stem/precursor cells. *Methods Mol. Biol.* 621, 165-73.
- Copp, J., Manning, G., & Hunter, T. (2009). TORC-specific phosphorylation of mammalian target of rapamycin (mTOR): phospho-Ser2481 is a marker for intact mTOR signaling complex 2. *Cancer research*, 69(5), 1821–1827.
- Doxsey, S., McCollum, D. and Theurkauf, W. (2005). Centrosomes in cellular regulation. *Annu. Rev. Cell Dev. Biol.* 21, 411-34.
- Dubreuil, V. et al. (2007). Midbody and primary cilium of neural progenitors release extracellular membrane particles enriched in the stem cell marker prominin-1. *J. Cell Biol.* 176, 483-95.
- Eggert, U.S., Mitchison, T.J. and Field, C.M. (2006). Animal cytokinesis: from parts list to mechanisms. *Annu. Rev. Biochem.* 75, 543-66.
- Elizabeth Deosaran, Kenneth B Larsen, Rong Hua, Graeme Sargent, Yuqing Wang, Sarah Kim, Trond Lamark, Miluska Jauregui, Kelsey Law, Jennifer Lippincott-Schwartz, Andreas Brech, Terje Johansen, and Peter K Kim. (2012) NBR1 acts as an autophagy receptor for peroxisomes. *JCS* online publication date 13 December 2012.
- Engelmann, K., Shen, H., and Finn, O.J. (2008). MCF7 side population cells with characteristics of cancer stem/progenitor cells express the tumor antigen MUC1. *Cancer Res.* 68, 2419-26.
- Eskelinen, E.L., Tanaka, Y. and Saftig, P. (2003). At the acidic edge: emerging functions for lysosomal membrane proteins. *Trends Cell Biol.* 13, 137-45.
- Fan, W., Tang, Z., Chen, D., Moughon, D., Ding, X., Chen, S., et al. (2010). Keap1 facilitates p62-mediated ubiquitin aggregate clearance via autophagy. *Autophagy*, 6(5), 614–621.
- Fededa, J. P. & Gerlich, D. W. (2012). Molecular control of animal cell cytokinesis. *Nature Cell Biol.* 14, 440–447.

Fielding, A.B. et al. (2005) Rab11–FIP3 and FIP4 interact with Arf6 and the exocyst to control membrane traffic in cytokinesis. *EMBO J.* 24, 3389–3399.

Filimonenko, M., Isakson, P., Finley, K. D., Anderson, M., Jeong, H., Melia, T. J., et al. (2010). The selective macroautophagic degradation of aggregated proteins requires the PI3P-binding protein Alfy. *Molecular Cell*, 38(2), 265–279.

Fimia, G.M. et al. (2007). Ambra1 regulates autophagy and development of the nervous system. *Nature* 447, 1121-5.

Fuchs, E. (2009). The tortoise and the hair: slow-cycling cells in the stem cell race. *Cell* 137, 811-9.

Furuya, T., Kim, M., Lipinski, M., Li, J., Kim, D., Lu, T., et al. (2010). Negative regulation of Vps34 by Cdk mediated phosphorylation. *Molecular Cell*, 38(4), 500–511.

Gamerding M, Hajieva P, Kaya AM, Wolfrum U, Hartl FU, Behl C. (2009). Protein quality control during aging involves recruitment of the macroautophagy pathway by BAG3. *Embo J*; 28: 889–901.

Gal, J., Ström, A.-L., Kwinter, D. M., Kilty, R., Zhang, J., Shi, P., et al. (2009). Sequestosome 1/p62 links familial ALS mutant SOD1 to LC3 via an ubiquitin-independent mechanism. *Journal of Neurochemistry*, 111(4), 1062–1073.

Gao, C., Cao, W., Bao, L., Zuo, W., Xie, G., Cai, T., et al. (2010). Autophagy negatively regulates Wnt signalling by promoting Dishevelled degradation. *Nature Cell Biology*, 12(8), 781–790.

Geir Bjørkøy, Trond Lamark, Andreas Brech, Heidi Outzen, Maria Perander, Aud Overvatn, Harald Stenmark, and Terje Johansen. (2005). p62/SQSTM1 forms protein aggregates degraded by autophagy and has a protective effect on huntingtin-induced cell death., 171(4), 603–614.

Green, R. A., Paluch, E. & Oegema, K. (2012). Cytokinesis in animal cells. *Annu. Rev. Cell Dev. Biol.* 28, 29–58.

Greenbaum, M.P., Ma, L., and Matzuk, M.M. (2007). Conversion of midbodies into germ cell intercellular bridges. *Dev. Biol.* 305, 389-96.

Gromley, A. et al. (2005). Centriolin anchoring of exocyst and SNARE complexes at the midbody is required for secretory-vesicle-mediated abscission. *Cell* 123, 75-87.

- Goss, J.W. and Toomre, D.K. (2008). Both daughter cells traffic and exocytose membrane at the cleavage furrow during mammalian cytokinesis. *J. Cell Biol.* 181, 1047-54.
- Guo, Y., Chang, C., Huang, R., Liu, B., Bao, L., & Liu, W. (2012). AP1 is essential for generation of autophagosomes from the trans-Golgi network. *Journal of cell science*, 125(Pt 7), 1706–1715.
- Hara, T. et al. (2006). Suppression of basal autophagy in neural cells causes neurodegenerative disease in mice. *Nature* 441, 885-9.
- Hara, T., Takamura, A., Kishi, C., Iemura, S.-I., Natsume, T., Guan, J.-L., & Mizushima, N. (2008). FIP200, a ULK-interacting protein, is required for autophagosome formation in mammalian cells. *The Journal of cell biology*, 181(3), 497–510.
- Holtrich, U., Wolf, G., Bräuninger, A., Karn, T., Böhme, B., Rübsamen-Waigmann, H., & Strebhardt, K. (1994). Induction and down-regulation of PLK, a human serine/threonine kinase expressed in proliferating cells and tumors. *Proceedings of the National Academy of Sciences of the United States of America*, 91(5), 1736–1740.
- Hu, C.-K., Ozlü, N., Coughlin, M., Steen, J. J., & Mitchison, T. J. (2012). Plk1 negatively regulates PRC1 to prevent premature midzone formation before cytokinesis. *Molecular biology of the cell*, 23(14), 2702–2711.
- Hu, C.-K., Coughlin, M., & Mitchison, T. J. (2012). Midbody Assembly and its Regulation during Cytokinesis. *Molecular biology of the cell*.
- Huang DW, Sherman BT, Lempicki RA. (2009). Systematic and integrative analysis of large gene lists using DAVID Bioinformatics Resources. *Nature Protoc.* 4(1):44-57.
- Huang DW, Sherman BT, Lempicki RA. (2009). Bioinformatics enrichment tools: paths toward the comprehensive functional analysis of large gene lists. *Nucleic Acids Res.* 37(1):1-13.
- Hurley, J. H. and Hanson, P. I. (2010). Membrane budding and scission by the ESCRT machinery: it's all in the neck. *Nat. Rev. Mol. Cell Biol.* 11, 556-566.
- Inoda, S., Hirohashi, Y., Torigoe, T., Nakatsugawa, M., Kiriya, K., Nakazawa, E., Harada, K., Takasu, H., Tamura, Y., Kamiguchi, K., Asanuma, H., Tsuruma, T., Terui, T., Ishitani, K., Ohmura, T., Wang, Q., Greene, M. I., Hasegawa, T., Hirata, K., and Sato, N. (2009). Cep55/c10orf3, a tumor antigen derived from a centrosome-residing protein in breast carcinoma. *J. Immunother.* 32, 474 – 485

Isakson, P., Bjørås, M., Bøe, S. O., & Simonsen, A. (2010). Autophagy contributes to therapy-induced degradation of the PML/RARA oncoprotein. *Blood*, 116(13), 2324–2331.

Itakura E, Mizushima N. (2010). Characterization of autophagosome formation site by a hierarchical analysis of mammalian Atg proteins. *Autophagy* 6:764–76

Johnston, J.A., Illing, M.E. and Kopito, R.R. (2002). Cytoplasmic dynein/dynactin mediates the assembly of aggresomes. *Cell Motil. Cytoskeleton* 53, 26-38.

Joseph, N., Hutterer, A., Poser, I., & Mishima, M. (2012). ARF6 GTPase protects the post-mitotic midbody from 14-3-3-mediated disintegration. *The EMBO Journal*, 31(11), 2604–2614.

Kaushik et al., (2008). Constitutive Activation of Chaperone-mediated Autophagy in Cells with Impaired Macroautophagy. *Mol. Biol. Cell* 19, 2179-92.

Kim, P. K., Hailey, D. W., Mullen, R. T., & Lippincott-Schwartz, J. (2008). Ubiquitin signals autophagic degradation of cytosolic proteins and peroxisomes. *Proceedings of the National Academy of Sciences of the United States of America*, 105(52), 20567–20574.

Kirkin, V., Lamark, T., Sou, Y.-S., Bjørkøy, G., Nunn, J. L., Bruun, J.-A., et al. (2009a). A role for NBR1 in autophagosomal degradation of ubiquitinated substrates. *Molecular cell*, 33(4), 505–516.

Kirkin, V., McEwan, D. G., Novak, I., & Dikic, I. (2009b). A role for ubiquitin in selective autophagy. *Molecular cell*, 34(3), 259–269.

Klionsky, D.J. et al. (2008). Guidelines for the use and interpretation of assays for monitoring autophagy in higher eukaryotes. *Autophagy* 4, 151-75.

Komatsu, M. et al. (2005). Impairment of starvation-induced and constitutive autophagy in Atg7-deficient mice. *J. Cell Biol.* 169, 425-34.

Komatsu, M. et al. (2007). Homeostatic levels of p62 control cytoplasmic inclusion body formation in autophagy-deficient mice. *Cell* 131, 1149-63.

Kraft, C., Deplazes, A., Sohrmann, M., and Peter, M. (2008). Mature ribosomes are selectively degraded upon starvation by an autophagy pathway requiring the Ubp3p/Bre5p ubiquitin protease. *Nat. Cell Biol.* 10, 602– 610.

- Kristensen, A. R., Schandorff, S., Høyer-Hansen, M., Nielsen, M. O., Jäättelä, M., Dengjel, J., & Andersen, J. S. (2008). Ordered organelle degradation during starvation-induced autophagy. *Molecular & Cellular Proteomics : MCP*, 7(12), 2419–2428.
- Kuma, A., Hatano, M., Matsui, M., Yamamoto, A., Nakaya, H., Yoshimori, T., et al. (2004). The role of autophagy during the early neonatal starvation period. *Nature*, 432(7020), 1032–1036.
- Lamark, T., Perander, M., Outzen, H., Kristiansen, K., Øvervatn, A., Michael- sen, E., Bjørkøy, G., and Johansen, T. (2003). Interaction codes within the family of mammalian Phox and Bem1p domain-containing proteins. *J. Biol. Chem.* 278, 34568-81.
- Laplante, M., & Sabatini, D. M. (2012). mTOR signaling in growth control and disease. *Cell*, 149(2), 274–293.
- Lee, C., Fotovati, A., Triscott, J., Chen, J., Venugopal, C., Singhal, A., et al. (2012). Polo-like kinase 1 inhibition kills glioblastoma multiforme brain tumor cells in part through loss of SOX2 and delays tumor progression in mice. *Stem Cells (Dayton, Ohio)*, 30(6), 1064–1075.
- Lee, H. H., Elia, N., Ghirlando, R., Lippincott-Schwartz, J., & Hurley, J. H. (2008). Midbody targeting of the ESCRT machinery by a noncanonical coiled coil in CEP55. *Science (New York, NY)*, 322(5901), 576–580.
- Lekomtsev, S., Su, K.-C., Pye, V. E., Blight, K., Sundaramoorthy, S., Takaki, T., et al. (2012). Centralspindlin links the mitotic spindle to the plasma membrane during cytokinesis. *Nature*, 492(7428), 276–279.
- Levine, B. and Kroemer, G. (2008). Autophagy in the pathogenesis of disease. *Cell* 132, 27-42.
- Liang, X.H. et al. (1999). Induction of autophagy and inhibition of tumorigenesis by beclin 1. *Nature* 402, 672-6.
- Linares, J. F., Amanchy, R., Diaz-Meco, M. T., & Moscat, J. (2011). Phosphorylation of p62 by cdk1 controls the timely transit of cells through mitosis and tumor cell proliferation. *Molecular and cellular biology*, 31(1), 105–117.
- Lipinski, M. M., Hoffman, G., Ng, A., Zhou, W., Py, B. F., Hsu, E., et al. (2010). A genome-wide siRNA screen reveals multiple mTORC1 independent signaling pathways regulating autophagy under normal nutritional conditions. *Developmental Cell*, 18(6), 1041–1052.

- Loewer, S. et al., (2010). Large intergenic non-coding RNA-RoR modulates reprogramming of human induced pluripotent stem cells. *Nat. Genet.* 42, 1113-7.
- Lorenz, H., Hailey, D.W. and Lippincott-Schwartz, J. (2006). Fluorescence protease protection of GFP chimeras to reveal protein topology and subcellular localization. *Nat. Methods* 3, 205-10.
- Ma, H., McLean, J. R., Chao, L. F.-I., Mana-Capelli, S., Paramasivam, M., Hagstrom, K. A., et al. (2012). A highly efficient multifunctional tandem affinity purification approach applicable to diverse organisms. *Molecular & Cellular Proteomics : MCP*, 11(8), 501–511.
- Ma, N., Tulu, U. S., Ferenz, N. P., Fagerstrom, C., Wilde, A., & Wadsworth, P. (2010). Poleward transport of TPX2 in the mammalian mitotic spindle requires dynein, Eg5, and microtubule flux. *Molecular biology of the cell*, 21(6), 979–988. doi:10.1091/mbc.E09-07-0601
- Majeski, A.E. and Dice, J.F. (2004). Mechanisms of chaperone-mediated autophagy. *Int. J. Biochem. Cell Biol.* 36, 2435-44.
- Mao, J.-Z., Jiang, P., Cui, S.-P., Ren, Y.-L., Zhao, J., Yin, X.-H., et al. (2012). Girdin locates in centrosome and midbody and plays an important role in cell division. *Cancer science*, 103(10), 1780–1787.
- Marchbank, K., Waters, S., Roberts, R. G., Solomon, E., & Whitehouse, C. A. (2012). MAP1B Interaction with the FW Domain of the Autophagic Receptor Nbr1 Facilitates Its Association to the Microtubule Network. *International Journal of Cell Biology*, 2012, 208014.
- Mardakheh, F. K., Auciello, G., Dafforn, T. R., Rappoport, J. Z., & Heath, J. K. (2010). Nbr1 is a novel inhibitor of ligand-mediated receptor tyrosine kinase degradation. *Molecular and Cellular Biology*, 30(24), 5672–5685.
- Marson, A., Foreman, R., Chevalier, B., Bilodeau, S., Kahn, M., Young, R. A., & Jaenisch, R. (2008). Wnt signaling promotes reprogramming of somatic cells to pluripotency. *Cell stem cell*, 3(2), 132–135.
- Marzesco, A.M. et al. (2005). Release of extracellular membrane particles carrying the stem cell marker prominin-1 (CD133) from neural progenitors and other epithelial cells. *J. Cell Sci.* 118, 2849-58.

- Matsumoto, G., Wada, K., Okuno, M., Kurosawa, M., & Nukina, N. (2011). Serine 403 Phosphorylation of p62/SQSTM1 Regulates Selective Autophagic Clearance of Ubiquitinated Proteins. *Molecular Cell*, 44(2), 279–289.
- Matsunaga K, Morita E, Saitoh T, Akira S, Ktistakis NT, et al. (2010). Autophagy requires endoplasmic reticulum targeting of the PI3-kinase complex via Atg14L. *J. Cell Biol.* 190:511–21
- Menon, S., & Manning, B. D. (2008). Common corruption of the mTOR signaling network in human tumors. *Oncogene*, 27 Suppl 2, S43–51.
- Mishima, M., Kaitna, S. & Glotzer, M. (2002). Central spindle assembly and cytokinesis require a kinesin-like protein/RhoGAP complex with microtubule bundling activity. *Dev. Cell* 2, 41–54.
- Mitchison, T., Evans, L., Schulze, E. and Kirschner, M. (1986). Sites of microtubule assembly and disassembly in the mitotic spindle. *Cell* 45, 515-27.
- Mizushima, N., and Klionsky, D. (2007). Protein turnover via autophagy: implications for metabolism. *Annu. Rev. Nutr.* 27, 19–40.
- Mizushima, N., & Levine, B. (2010). Autophagy in mammalian development and differentiation. *Nature cell biology*, 12(9), 823–830.
- Mizushima, N., Levine, B., Cuervo, A.M. and Klionsky, D.J. (2008). Autophagy fights disease through cellular self-digestion. *Nature* 451, 1069-75.
- Mizushima, N. and Yoshimori, T. (2007). How to interpret LC3 immunoblotting. *Autophagy* 3, 542-5.
- Mizushima, N., & Yoshimori, T. (2011). The Role of Atg Proteins in Autophagosome Formation - Annual Review of Cell and Developmental Biology, 27(1):107. Annual Review of Cell
- Mondal, G., Rowley, M., Guidugli, L., Wu, J., Pankratz, V. S., & Couch, F. J. (2012). BRCA2 localization to the midbody by filamin A regulates cep55 signaling and completion of cytokinesis. *Developmental cell*, 23(1), 137–152.
- Morita, E. et al. (2007). Human ESCRT and ALIX proteins interact with proteins of the midbody and function in cytokinesis. *EMBO J.* 26, 4215–4227.
- Morris, R.J. et al. (2004). Capturing and profiling adult hair follicle stem cells. *Nat. Biotechnol.* 22, 411-7.

Mukai, A., Mizuno, E., Kobayashi, K., Matsumoto, M., Nakayama, K. I., Kitamura, N., & Komada, M. (2008). Dynamic regulation of ubiquitylation and deubiquitylation at the central spindle during cytokinesis. *Journal of Cell Science*, 121(Pt 8), 1325–1333.

Mullins, J.M. and Biesele, J.J. (1977). Terminal phase of cytokinesis in D-98s cells. *J. Cell Biol.* 73, 672-84.

Nedelsky, N. et al. (2008). Autophagy and the ubiquitin-proteasome system: collaborators in neuroprotection. *Biochim. Biophys. Acta.* 1782, 691-9.

Neumüller, R.A. and Knoblich, J.A. (2009). Dividing cellular asymmetry: asymmetric cell division and its implications for stem cells and cancer. *Genes Dev.* 23, 2675-99.

Oatley, J.M. and Brinster, R.L. (2008). Regulation of spermatogonial stem cell self-renewal in mammals. *Annu. Rev. Cell Dev. Biol.* 24, 263-86.

O'Brien, C.A., Pollett, A., Gallinger, S. and Dick, J.E. (2007). A human colon cancer cell capable of initiating tumour growth in immunodeficient mice. *Nature* 445, 106-10.

O'Brien, R. N., Shen, Z., Tachikawa, K., Lee, P. A., & Briggs, S. P. (2010). Quantitative proteome analysis of pluripotent cells by iTRAQ mass tagging reveals post-transcriptional regulation of proteins required for ES cell self-renewal. *Molecular & Cellular Proteomics : MCP*, 9(10), 2238–2251.

Ogawa M, Yoshikawa Y, Kobayashi T, Mimuro H, Fukumatsu M, Kiga K et al. (2011). A Tecpr1- dependent selective autophagy pathway targets bacterial pathogens. *Cell Host Microbe.* 9: 376–389.

Orenstein, S. J., & Cuervo, A. M. (2010). Chaperone-mediated autophagy: molecular mechanisms and physiological relevance. *Seminars in Cell & Developmental Biology*, 21(7), 719–726.

Orvedahl, A., MacPherson, S., Sumpter, R., Tallóczy, Z., Zou, Z., & Levine, B. (2010). Autophagy protects against Sindbis virus infection of the central nervous system. *Cell Host & Microbe*, 7(2), 115–127.

Pankiv, S. et al. (2007). p62/SQSTM1 binds directly to Atg8/LC3 to facilitate degradation of ubiquitinated protein aggregates by autophagy. *J. Biol. Chem.* 282, 24131-45.

Pardal, R., Clarke, M.F. and Morrison, S.J. (2003). Applying the principles of stem-cell biology to cancer. *Nat. Rev. Cancer* 3, 895-902.

- Park, I.H. et al. (2008). Reprogramming of human somatic cells to pluripotency with defined factors. *Nature* 451, 141-6.
- Pavicic-Kaltenbrunner, V., Mishima, M. & Glotzer, M. (2007). Cooperative assembly of CYK-4/MgcRacGAP and ZEN-4/MKLP1 to form the centralspindlin complex. *Mol. Biol. Cell* 18, 4992–5003.
- Pece, S. et al. (2010). Biological and molecular heterogeneity of breast cancers correlates with their cancer stem cell content. *Cell* 140, 62-73.
- Peterson, R. T., Beal, P. A., Comb, M. J., & Schreiber, S. L. (2000). FKBP12-rapamycin-associated protein (FRAP) autophosphorylates at serine 2481 under translationally repressive conditions. *The Journal of biological chemistry*, 275(10), 7416–7423.
- Piel, M., Meyer, P., Khodjakov, A., Rieder, C.L. and Bornens, M. (2000). The respective contributions of the mother and daughter centrioles to centrosome activity and behavior in vertebrate cells. *J. Cell Biol.* 149, 317-30.
- Pohl, C., & Jentsch, S. (2008). Final stages of cytokinesis and midbody ring formation are controlled by BRUCE. *Cell*, 132(5), 832–845.
- Pohl, C. and Jentsch, S. (2009). Midbody ring disposal by autophagy is a post-abscission event of cytokinesis. *Nat. Cell Biol.* 11, 65-70.
- Rawi, Al, S., Louvet-Vallée, S., Djeddi, A., Sachse, M., Culetto, E., Hajjar, C., et al. (2011). Postfertilization autophagy of sperm organelles prevents paternal mitochondrial DNA transmission. *Science (New York, NY)*, 334(6059), 1144–1147.
- Rujano, M.A. et al. (2006). Polarised asymmetric inheritance of accumulated protein damage in higher eukaryotes. *PLoS Biol.* 4, 2325-2335.
- Sachdev, S., Bu, Y., and Gelman, I.H. (2009). Paxillin-Y118 phosphorylation contributes to the control of Src-induced anchorage-independent growth by FAK and adhesion. *BMC Cancer* 12, 9:12.
- Sahu, R., Kaushik, S., Clement, C. C., Cannizzo, E. S., Scharf, B., Follenzi, A., et al. (2011). Microautophagy of cytosolic proteins by late endosomes. *Developmental Cell*, 20(1), 131–139.
- Salic, A. and Mitchison, T.J. (2008). A chemical method for fast and sensitive detection of DNA synthesis in vivo. *Proc. Natl. Acad. Sci. U.S.A.* 105, 2415-20.

- Sarkar, S. et al. (2005). Lithium induces autophagy by inhibiting inositol monophosphatase. *J. Cell Biol.* 170, 1101-11.
- Sarkar, S. et al. (2008). A rational mechanism for combination treatment of Huntington's disease using lithium and rapamycin. *Hum. Mol. Genet.* 17, 170-8.
- Sato, K. et al. (2007). Autophagy is activated in colorectal cancer cells and contributes to the tolerance to nutrient deprivation. *Cancer Res.* 67, 9677-84.
- Sato, M., & Sato, K. (2011). Degradation of paternal mitochondria by fertilization-triggered autophagy in *C. elegans* embryos. *Science (New York, NY)*, 334(6059), 1141–1144.
- Sandilands E, Serrels B, McEwan DG, Morton JP, Macagno JP, McLeod K et al. (2011). Autophagic targeting of Src promotes cancer cell survival following reduced FAK signalling. *Nat Cell Biol.* 14: 51–60.
- Simonsen A, Birkeland HC, Gillooly DJ, Mizushima N, Kuma A, Yoshimori T, et al. (2004). Alfy, a novel FYVE- domain-containing protein associated with protein granules and autophagic membranes. *J Cell Sci.* 117:4239-51.
- Skop, A. R., Liu, H., Yates, J., Meyer, B. J., & Heald, R. (2004). Dissection of the mammalian midbody proteome reveals conserved cytokinesis mechanisms. *Science (New York, NY)*, 305(5680), 61–66.
- Soliman, G. A., Acosta-Jaquez, H. A., Dunlop, E. A., Ekim, B., Maj, N. E., Tee, A. R., & Fingar, D. C. (2010). mTOR Ser-2481 Autophosphorylation Monitors mTORC-specific Catalytic Activity and Clarifies Rapamycin Mechanism of Action. *The Journal of biological chemistry*, 285(11), 7866–7879.
- Steigemann, P. et al. (2009). Aurora B-mediated abscission checkpoint protects against tetraploidization. *Cell* 136, 473-84.
- Strome, S. (2005). Specification of the germ line. *WormBook* 28, 1-10.
- Strebhardt, K., & Ullrich, A. (2006). Targeting polo-like kinase 1 for cancer therapy. *Nature Reviews Cancer*, 6(4), 321–330.
- Takai, N., Hamanaka, R., Yoshimatsu, J., & Miyakawa, I. (2005). Polo-like kinases (Plks) and cancer. *Oncogene*, 24(2), 287–291.

- Takaki, T., Trenz, K., Costanzo, V., & Petronczki, M. (2008). Polo-like kinase 1 reaches beyond mitosis--cytokinesis, DNA damage response, and development. *Current Opinion in Cell Biology*, 20(6), 650–660.
- Takenobu, H., Shimozato, O., Nakamura, T., Ochiai, H., Yamaguchi, Y., Ohira, M., et al. (2011). CD133 suppresses neuroblastoma cell differentiation via signal pathway modification. *Oncogene*, 30(1), 97–105.
- Tan, J. M. M., Wong, E. S. P., Kirkpatrick, D. S., Pletnikova, O., Ko, H. S., Tay, S.-P., et al. (2008). Lysine 63-linked ubiquitination promotes the formation and autophagic clearance of protein inclusions associated with neurodegenerative diseases. *Human Molecular Genetics*, 17(3), 431–439.
- Thurston TL, Ryzhakov G, Bloor S, von Muhlinen N, Randow F. (2009). The TBK1 adaptor and autophagy receptor NDP52 restricts the proliferation of ubiquitin-coated bacteria. *Nat Immunol*. 10: 1215–1221.
- Tsukamoto, S., Kuma, A., Murakami, M., Kishi, C., Yamamoto, A., & Mizushima, N. (2008). Autophagy is essential for preimplantation development of mouse embryos. *Science (New York, NY)*, 321(5885), 117–120.
- Tsvetkov, L., Xu, X., Li, J., & Stern, D. F. (2003). Polo-like kinase 1 and Chk2 interact and co-localize to centrosomes and the midbody. *The Journal of biological chemistry*, 278(10), 8468–8475.
- Van der Horst, A., Simmons, J., & Khanna, K. K. (2009). Cep55 stabilization is required for normal execution of cytokinesis. *Cell Cycle (Georgetown, Tex)*, 8(22), 3742–3749.
- Vazquez-Martin, A., Oliveras-Ferraros, C., Bernadó, L., López-Bonet, E., & Menendez, J. A. (2009). The serine 2481-autophosphorylated form of mammalian Target Of Rapamycin (mTOR) is localized to midzone and midbody in dividing cancer cells. *Biochemical and biophysical research communications*, 380(3), 638–643.
- Vazquez-Martin, A., Sauri-Nadal, T., Menendez, O. J., Oliveras-Ferraros, C., Cufí, S., Corominas-Faja, B., et al. (2012). Ser2481-autophosphorylated mTOR colocalizes with chromosomal passenger proteins during mammalian cell cytokinesis. *Cell cycle (Georgetown, Tex)*, 11(22), 4211–4221.
- Vazquez P, Arroba AI, Cecconi F, de la Rosa EJ, Boya P, de Pablo F. (2012). Atg5 and Ambra1 differentially modulate neurogenesis in neural stem cells. *Autophagy* 8: 187-199.

- Visvader, J.E. and Lindeman, G.J. (2008). Cancer stem cells in solid tumours: accumulating evidence and unresolved questions. *Nat. Rev. Cancer* 8, 755-68.
- Wang, X. et al. (2009). Asymmetric centrosome inheritance maintains neural progenitors in the neocortex. *Nature* 461, 947-55.
- Wang, Z., Cao, L., Kang, R., Yang, M., Liu, L., Zhao, Y., et al. (2011). Autophagy regulates myeloid cell differentiation by p62/SQSTM1-mediated degradation of PML-RAR α oncoprotein. *Autophagy*, 7(4), 401–411.
- Watanabe, Y., & Tanaka, M. (2011). p62/SQSTM1 in autophagic clearance of a non-ubiquitylated substrate. *Journal of Cell Science*, 124(Pt 16), 2692–2701.
- Waters, S. et al., (2009). Interactions with LC3 and polyubiquitin chains link nbr1 to autophagic protein turnover. *FEBS Lett.* 583, 1846-52.
- Wei, Q., & Adelstein, R. S. (2000). Conditional expression of a truncated fragment of nonmuscle myosin II-A alters cell shape but not cytokinesis in HeLa cells. *Molecular biology of the cell*, 11(10), 3617–3627.
- Wild, P., Farhan, H., McEwan, D. G., Wagner, S., Rogov, V. V., Brady, N. R., et al. (2011). Phosphorylation of the autophagy receptor optineurin restricts Salmonella growth. *Science (New York, NY)*, 333(6039), 228–233.
- Wilson, G.M. et al. (2005) The FIP3–Rab11 protein complex regulates recycling endosome targeting to the cleavage furrow during late cytokinesis. *Mol. Biol. Cell* 16, 849–860.
- Xu, P., and Davis, R.J. (2010). c-Jun NH2-terminal kinase is required for lineage-specific differentiation but not stem cell self-renewal. *Mol. Cell Biol.* 30, 1329-40.
- Yamashita, Y.M., Jones, D.L. and Fuller, M.T. (2003). Orientation of asymmetric stem cell division by the APC tumor suppressor and centrosome. *Science* 301, 1547-50.
- Yamashita, Y.M., Mahowald, A.P., Perlin, J.R. and Fuller, M.T. (2007). Asymmetric inheritance of mother versus daughter centrosome in stem cell division. *Science* 315, 518-21.
- Yorimitsu, T. and Klionsky, D.J. (2007). Eating the endoplasmic reticulum: quality control by autophagy. *Trends Cell Biol.* 17, 279-85.
- Yu, J. et al., (2007). Induced pluripotent stem cell lines derived from human somatic cells. *Science* 318, 1917-20.

- Yu, J. et al., (2009). Human induced pluripotent stem cells free of vector and transgene sequences. *Science* 324, 797-801.
- Yu, L. et al., (2004). Regulation of an ATG7-beclin 1 program of autophagic cell death by caspase-8. *Science* 304, 1500-2.
- Zhang, Y., Yan, L., Zhou, Z., Yang, P., Tian, E., Zhang, K., et al. (2009). SEPA-1 mediates the specific recognition and degradation of P granule components by autophagy in *C. elegans*. *Cell*, 136(2), 308–321.
- Zhang J, Liu J, Huang Y, Chang JY, Liu L, McKeehan WL, Martin JF, Wang F (2012a) FRS2alpha- mediated FGF signals suppress premature differentiation of cardiac stem cells through regulating autophagy activity. *Circ Res* 110: e29-e39.
- Zhang J, Liu J, Liu L, McKeehan WL, Wang F (2012b) The fibroblast growth factor signaling axis controls cardiac stem cell differentiation through regulating autophagy. *Autophagy* 8: 690-691.
- Zhao, W.-M., Seki, A., & Fang, G. (2006). Cep55, a microtubule-bundling protein, associates with centralspindlin to control the midbody integrity and cell abscission during cytokinesis. *Molecular Biology of the Cell*, 17(9), 3881–3896.
- Zheng YT, Shahnazari S, Brech A, Lamark T, Johansen T, Brumell JH. The adaptor protein p62/SQSTM1 targets invading bacteria to the autophagy pathway. *J Immunol* 2009; 183: 5909–5916.
- Zwaka, T.P. and Thomson, J.A. (2003). Homologous recombination in human embryonic stem cells. *Nat. Biotechnol.* 21, 319-21.
- Yang, Z., & Klionsky, D. J. (2010). Mammalian autophagy: core molecular machinery and signaling regulation. *Current opinion in cell biology*, 22(2), 124–131.
- Yuan, T. L., Wulf, G., Burga, L., & Cantley, L. C. (2011). Cell-to-cell variability in PI3K protein level regulates PI3K-AKT pathway activity in cell populations. *Current biology* : CB, 21(3), 173–183.